2014

Novel techniques for estimation and tracking of radioactive sources

Henry Ernest Baidoo-Williams
University of Iowa

NOVEL TECHNIQUES FOR ESTIMATION AND TRACKING OF RADIOACTIVE SOURCES

by

Henry Ernest Baidoo-Williams

A thesis submitted in partial fulfillment of the
requirements for the Doctor of Philosophy
degree in Electrical and Computer Engineering
in the Graduate College of
The University of Iowa

May 2015

Thesis Supervisor: Assistant Professor Raghu Mudumbai

Graduate College
The University of Iowa
Iowa City, Iowa

CERTIFICATE OF APPROVAL

PH.D. THESIS

This is to certify that the Ph.D. thesis of

Henry Ernest Baidoo-Williams

has been approved by the Examining Committee for the thesis requirement for the Doctor of Philosophy degree in Electrical and Computer Engineering at the May 2015 graduation.

Thesis Committee: _____
Raghu Mudumbai, Thesis Supervisor

_____
Soura Dasgupta, Thesis Co-Advisor

_____
Er-Wei Bai, Thesis Co-Advisor

_____
Weiyu Xu

_____
Tonya Peeples

To my wife Adwoa and my son Ethan.

A little sleep, a little slumber, and you my learned friend, put all mankind in *a* stone age.

ACKNOWLEDGEMENTS

I would like to thank my advisors, Professors Raghuraman Mudumbai, Soura Dasgupta and Er-Wei Bai, for their immense input to bring this dissertation to fruition. I am indebted for their insights and enthusiasm which carried my research to logical conclusions. I am grateful to Cathy Kern, without whom I may not have been to Iowa and Dina Blanc for all the help I got navigating the ECE Department.

I extend my profound gratitude to Joseph Baah-Agyepong for his brotherly love during my time in graduate school. I also thank the Etseys, Edudzi and Janetta Dromi(JD), for all the help I got during my stay in Iowa. My appreciation also goes to Keith Plate(MD) and his wife Carol for being there always. I appreciate the help of my dad Joseph Baidoo Williams(deceased), mum Mary S. Williams and siblings, Frank Baidoo-Williams(MD), Joseph Baidoo-Williams and Mary Mensah, for their encouragement from grade school till now. I also appreciate the valuable time I had with all my lab mates, notably Hema Achanta. I couldn't have come this far without you all.

Finally I will like to thank my wife Adwoa and son Ethan for their patience and support during this critical point in my education.

ABSTRACT

Radioactive source signal measurements are Poisson distributed due to the underlying radiation process. This fact, coupled with the ubiquitous normally occurring radioactive materials (NORM), makes it challenging to localize or track a radioactive source or target accurately. This leads to the necessity to either use highly accurate sensors to minimize measurement noise or many less accurate sensors whose measurements are averaged to minimize the noise. The cost associated with highly accurate sensors places a bound on the number that can realistically be deployed. Similarly, the degree of inaccuracy in cheap sensors also places a lower bound on the number of sensors needed to achieve realistic estimates of location or trajectory of a radioactive source in order to achieve reasonable error margins.

We first consider the use of the smallest number of highly accurate sensors to localize radioactive sources. The novel ideas and algorithms we develop use no more than the minimum number of sensors required by triangulation based algorithms but avoid all the pitfalls manifest with triangulation based algorithms such as multiple local minima and slow convergence rate from algorithm reinitialization. Under the general assumption that we have a priori knowledge of the statistics of the intensity of the source, we show that if the source or target is known to be in one open half plane, then N sensors are enough to guarantee a unique solution, N being the dimension of the search space. If the assumptions are tightened such that the source or target lies in the open convex hull of the sensors, then $N + 1$ sensors are required. Suppose we

do not have knowledge of the statistics of the intensity of the source, we show that $N+1$ sensors is still the minimum number of sensors required to guarantee a unique solution if the source is in the open convex hull of the sensors.

Second, we present tracking of a radioactive source using cheap low sensitivity binary proximity sensors under some general assumptions. Suppose a source or target moves in a straight line, and suppose we have a priori knowledge of the radiation intensity of the source, we show that three binary sensors and their binary measurements depicting the presence or absence of a source within their nominal sensing range suffices to localize the linear trajectory. If we do not have knowledge of the intensity of the source or target, then a minimum of four sensors suffices to localize the trajectory of the source.

Finally we present some fundamental limits on the estimation accuracy of a stationary radioactive source using ideal mobile measurement sensors and provide a robust algorithm which achieves the estimation accuracy bounds asymptotically as the expected radiation count increases.

PUBLIC ABSTRACT

The purpose of this research is to study and develop robust algorithms for detection, estimation, localization and tracking of radioactive materials. Unlike other signal propagation models, the recorded signals from a radioactive source or target is itself stochastic, even in the absence of any background or propagation channel noise. This is due to the number of radioactive particles leaving the source or target following a Poisson process. The measurement at the sensors also follow a Poisson arrival process. These facts make detection, estimation, localization and tracking of radioactive materials highly challenging.

The research in this thesis presents novel approaches to detection, estimation, localization and tracking of radioactive materials . First, we show, under some general assumptions on the placement of measurement sensors, that a minimum number of highly accurate sensors will yield a unique solution for the location of the source or target. Our approach is superior to conventional triangulation based algorithms in the sense that it avoids the problem of multiple local minima and persistent reinitialization while utilizing no more than the number of sensors required for triangulation. We also present results on tracking of a mobile source or target on a linear trajectory using cheap binary proximity sensors. We show that three generically placed cheap binary proximity sensors suffice to localize a linear trajectory if we have a priori knowledge of the statistics of the radiation source intensity . In the absence of knowledge of the radiation source intensity , four generically placed sensors suffice.

Finally, we explore the fundamental limits of estimating the location and radiation intensity of a source or target using a single mobile ideal detector moving on a straight line with uniform speed. We show that the maximum likelihood estimate achieves the fundamental accuracy limit asymptotically as the total radiation count at the receiver increases.

Our results are relevant in the effort for proactive protection against nuclear and radiological threats of public events and areas. Currently, there does not exist a reliable and efficient system to detect the presence of nuclear or radioactive materials in a relatively large area. What is needed is a system integrating nuclear and radioactive material detection and localization of weak and possibly shielded radioactive materials so that public and law enforcement officials can respond accordingly to the situation in a timely manner. Our algorithms and results are a major step in this direction.

TABLE OF CONTENTS

LIST OF FIGURES

Figure

LIST OF ALGORITHMS

CHAPTER 1
INTRODUCTION

1.1 Motivation

We are interested in estimation and tracking of radioactive sources using a network of radiation sensors. Source estimation and tracking are classical problems in fields such as wireless communication and navigation. Radioactive sources, however, present a unique challenge in terms of uncertainties and the detection or estimation process. Our research interest is in developing novel ideas and algorithms to deal with this challenge.

1.2 Background

Over the years, the problem of localizing and tracking of radioactive sources has become an area of intense research due to its obvious implications to security and public safety[1, 2, 3, 4, 5, 6]. Fundamentally, these problems involve estimation of the position and trajectory of objects of interest using the observations of a network of sensors, [7, 8]. With projections estimating that 80% of the population will reside within city limits by 2025 in the USA [9], there is an expected astronomical increase in the effects of any radioactive material leakage within city limits. Timely estimation and tracking of radioactive sources is thus critical to forestall any future catastrophe in this regard. The technical challenges of this problem are compounded by the fact that nuclear materials vary widely in their concentrations and compositions [6], and are often concealed by shielding material, and submerged in ever present background

radiation that varies widely in strength and spectrum over time and space [10]. Likewise, there are also many types of detectors [11] and sensors used in practical tracking systems, and these too vary widely in their quality and sensitivity.

The accuracy of radioactive source estimation or tracking relies on the received signal strength at the sensor from the target [12]. This in turn depends on proximity of the sensor to their target. This proximity requirement is especially stringent for sensing applications where signal absorption by the medium is large. For example, the strength of gamma rays emanated by a radioactive source, in the presence of structures that act as shielding material [13], exponentially decline with distance. In such a setting a wide coverage area requires a network of many sensors. Deploying expensive sensors, in such instances, become cost prohibitive.

Many existing studies for estimation of radioactive sources rely on using a large number of low-cost radiation sensors [9]. These techniques perform poorly when the number of sensors is reduced to the barest minimum. This is because the averaging effect of the large number of sensors is lost. Other studies which use the fewest number of expensive sensors have the problem of false minima which increase computational time of their algorithms. Our approach, using fewest number of expensive sensors, avoids the pitfalls of false minima and long computation time. We describe our novel approaches to estimation of radioactive sources in details in Chapter 2 using the minimum number of sensors under some general assumptions. We first deal with the case where we have an idea of the volume, shape and size of the radioactive. Then we consider the case where the volume, shape and size of the radioactive is unknown.

Similarly, many of the existing studies on tracking of radioactive sources rely on the density of the sensors being large enough to essentially guarantee blanket coverage of the region of interest [14, 15]. The idea is that if the density is high enough, every movement of the object lies in the sensing range of several sensors and the object's position and trajectory can be pinned down with a higher degree of accuracy because the intersection of sensing ranges of multiple sensors is much smaller than the sensing area of any single sensor. Clearly, a higher density implies that the sensing ranges of more sensors intersect which results in a smaller intersecting area or a more accurate estimate. In fact, as shown in [14] the estimation accuracy is of the order $1/\rho$, where ρ is the sensor density, if each sensor has a fixed sensing range.

Instead of a blanket coverage of the region of interest for tracking, we consider a unique approach in Chapter 3. The sensors we consider are cheap binary proximity sensors, that can only detect if an object is in their sensing radius. Effectively, this is a case of one-bit signal quantization. Each sensor can only record instances at which a moving object enters or leaves its sensing range. Such sensors represent a convenient and powerful abstraction for a variety of physical sensors, and have been widely studied in the literature on localization and tracking [16, 17, 18, 19, 20, 21, 22, 23, 24, 25, 14, 15]. One type of binary sensor network tries to use the geometry of the network [16] and considers the network as a connected graph to aid detection. The work in [20] considers heterogeneous binary sensors with different performance and cost. The purpose is to analyze the best proportion of sensors in each class to tradeoff performance with cost. Some assume probabilistic models

for object movement and/or for the received signal strength [18, 19, 21, 23, 24] and develop detection algorithms based on these models. Others additionally assume that each sensor has the ability to sense if the object is approaching or moving away [16]. We consider two approaches in Chapter 3. First we assume that we have an idea of the volume, shape and size of the radioactive source. This translates to having knowledge of some nominal radius from the measurement sensor within which the source can be detected. We then consider the case where the characteristics of the source is unknown. We still use binary sensors that can only detect if an object is in their unknown but fixed nominal sensing radius.

Finally, in Chapter 4, we consider the achievable error bounds on estimation of weak radioactive sources using a cheap mobile measurement sensor. We develop bounds for an ideal mobile measurement sensor over an infinite time horizon and generalize it for the finite horizon case. We develop an efficient algorithm which attains the Cramer-Rao bounds asymptotically as the expectation of the received signal strength grows.

1.3 Challenges in detecting, estimating and tracking radioactive sources

There are several challenges that underlie the detection, estimation and tracking of radioactive materials. To set the stage, let us first understand how such detection is effected. The principal instruments used are Geiger counters that record the radiation count per second. The signal model for this count at a sensor i is:

$$s_i = Poisson\left(\frac{Ae^{-\alpha d_i}}{d_i^2}\right) + Poisson(w_i) \tag{1.1}$$

where s_i is the received signal at the i^{th} sensor, d_i the distance between the source and the i^{th} sensor, α is the attenuation coefficient and depends on the shielding material's density and the absorption of the propagation channel. The attenuation coefficients are known and available in public domain for various common shielding materials [6]. A is the expectation of the signal strength at a unit distance, zero shielding coefficient and no background noise whilst w_i is the expectation of the background noise at the i^{th} sensor.

First, background radiation generated by NORM, the w_i which is modeled as a Poisson random variable, is large. There is also substantial uncertainty in $\frac{Ae^{-\alpha d_i}}{d_i^2}$, which too is modeled as a Poisson random variable. Similar uncertainty manifests in α. Consequently, accurate localization is a particular challenge. Large accurate sensors are expensive. Given that they must often be deployed in crowded public places, one is confronted with one of two alternatives. Either deploy a few expensive sensors, or use a network of cheap sensors. Indeed this thesis addresses two complementary problems: How to accurately localize with the fewest possible expensive sensors? How to track a mobile source using a network of *cheap sensors*? By cheap sensors we mean sensors that are only capable of detecting whether a source is in their sensing range,and will be referred to as *binary sensors*. We also consider the fundamental limits to the estimation accuracy of possibly weak sources using ideal mobile sensors.

1.4 Deploying fewest possible sensors for radioactive source estimation

Referring to (1.1), the signal strength s_i in principle provides a measure of distance. In N-dimensions, distances between the source and $N+1$ sensors that avoid an N-dimensional hyperplane theoretically suffice to localize. Indeed linear triangulation algorithms can be used to effect such localization.

As argued in [26], accurate source estimation is a fundamentally nonlinear problem. Accordingly, papers like [26] cast it as a non-convex optimization problem, involving cost functions manifested with multiple local minima. This causes algorithms such as gradient descent optimization to potentially get captured by local minima. The repeated reinitialization this requires impedes time critical localization. A related issue is the number of sensors that can be deployed. Accurate sensors for detecting radioactive materials are expensive. Thus it is highly desirable to deploy as few sensors as is possible.

Motivated by these considerations, in Chapter 2 we consider localization of radioactive sources using the fewest sensors under some assumptions, and propose novel approaches that while involving non-convex minimization avoids the pitfalls of convergence to local minima. First, a feasible assumption is made that the source lies in the open convex hull of $N+1$ sensors in $\mathbb{R}^N, N \in \{2,3\}$. Here we assume that A in (1.1) is known. We then consider a situation where we can use precisely N sensors in $\mathbb{R}^N, N \in \{2,3\}$ by relaxing the assumption of the source in the open convex hull of the measurement sensors. Here we consider that the centers of the N sensors in $\mathbb{R}^N, N \in \{2,3\}$ define a separating $N-1$ dimensional hyperplane which separates

the domain into two open half planes. Suppose that we know which open half plane contains the source, then precisely N sensors in $\mathbb{R}^N, N \in \{2, 3\}$ suffice to localize the source if the orthonormal projection of the source unto the separating hyperplane lies in the convex hull of the measurement sensors. Here again we assume that A in (1.1) is known. We finally consider the case where A in (1.1) is unknown. We show that using precisely $N + 1$ sensors in $\mathbb{R}^N, N \in \{2, 3\}$, the source can be uniquely determined under the assumption that the source is in the open convex hull of the sensors. In all these scenarios, our main motivation is using the minimum number of sensors, and our approaches rely on using precisely the minimum number of sensors required.

1.5 Tracking of radioactive sources with binary sensors

We consider the tracking of radioactive sources moving on piece-wise linear trajectories with constant speed through a field of cheap binary proximity sensors with "*on*" and "*off*" time stamps indicating the source entering and leaving a sensors range respectively. The assumption of piece-wise linear trajectories is reasonable and practical since radioactive sources are carried by persons or vehicles whose movement are well approximated by piece-wise linear joins over short intervals. The assumption of constant speed is also reasonable because over short intervals a person or a vehicle does not change speed drastically. We only require a constant speed spanning the number of sensors used for estimating a segment of the piecewise linear trajectory being tracked.

Consider a non stationary radioactive source instantaneously located at $y^* \in \mathbb{R}^2$, and binary proximity sensors located at $x_i \in \mathbb{R}^2, i \in \{1, ..., n\}$. Define $d_i = \|x_i - y^*\|$ where $\|\cdot\|$ denotes the 2-norm. The i^{th} sensor, which can be a portable or non-portable gamma-ray spectrometer [6, 5], produces an indicator signal I_i, dependent on the total gamma-ray counts received:

$$I_i = \begin{cases} 1, & \text{if } Poisson\left(\frac{Ae^{-\alpha d_i}}{d_i^2} + w_i\right) \geq T_d \\ 0, & \text{if } Poisson\left(\frac{Ae^{-\alpha d_i}}{d_i^2} + w_i\right) < T_d \end{cases} \tag{1.2}$$

where A_i, α, w_i and d_i are as defined in (1.1), T_d is a predetermined threshold above the expectation of the background noise to trigger sensor measurements. The transitions 0-1 and 1-0 define the "*on*" and "*off*" times of the binary proximity sensor. We are interested in the following; suppose we have "*on*" and "*off*"' time stamps from a number of sensors, indicating that a source entered and left their sensing ranges, and suppose we are given the centers of the location of the sensors, can we estimate the trajectory of the source uniquely?

In Chapter 3, we first assume that we know the "*noise free*" nominal sensing range required to trigger the sensor. Here we define "*noise free*" as the expectation of (1.1) in the absence of NORM. Knowledge of the nominal sensing range inherently assumes that we have knowledge of A or the characteristics of the source. We devise a linear approach to estimate each piece of the piece-wise linear trajectory and present analysis of the performance in the presence of noise. Second, we tackle the case where we do not know A or the characteristics of the source. We formulate an algorithm to estimate the piece-wise linear trajectory and analyze the performance in the presence

of noise.

1.6 Performance bounds on localization with cheap mobile sensors

We consider the achievable limits on estimation of a possibly weak stationary radioactive source using ideal measurement sensors in Chapter 4. We consider an ideal mobile detector making perfect, noiseless measurements and formulate a general problem of maximum likelihood estimation of a radioactive using such measurements. For the case of a stationary source and a mobile detector moving with constant velocity, we derive closed form solutions to the maximum likelihood estimate as well as the corresponding Cramer-Rao bounds. We present simulations showing that the maximum likelihood estimate achieves the Cramer-Rao bounds asymptotically.

1.7 Main contributions

Our main contributions are summarized as follows:

Estimation of radioactive sources with the minimum number of sensors: We consider a class of natural, non-convex cost functions, applicable to general observation models under some general assumptions.

First we assume that we know A and the source is in the open convex hull of the sensors. The assumption of the source in the open convex hull can be easily satisfied following a crude initial detection. Under these conditions, we show that when the number of sensors is precisely $N + 1$, $N \in \{2, 3\}$-dimensional space, the gradient descent minimization of such cost functions has no false stationary points inside the convex hull of the sensors.

Then we assume that we again know A but the source is in an open half plane separated by an $N-1$ dimensional hyperplane that contains the known centers of N radiation sensors. The assumption of the source in an open half plane can also be easily satisfied following a crude initial detection. Under these conditions, we show that when the number of sensors is precisely N, $N \in \{2,3\}$-dimensional space, the gradient descent minimization of such cost functions with projections has no false stationary points inside the domain of all points whose projection unto the separating hyperplane lie in the convex hull of the N sensors.

Finally, we consider the case where we have no idea of A. We however assume that the source is in the open convex hull of the sensors. The assumption of the source in the open convex hull can be easily satisfied following a crude initial detection. Under these conditions, we show that when the number of sensors is precisely $N+1$, $N \in \{2,3\}$-dimensional space, the gradient descent minimization of such cost functions has no false stationary points inside the convex hull of the sensors. Note that the number of radiation sensors is the same as that for the known A.

Tracking of radioactive sources using binary proximity sensors:

We consider a moving target in a field of binary proximity sensors with "*on*" and "*off*" timestamps correlating to the source entering and leaving the sensing range of a sensor and assume that (1) the source is moving with a constant speed and (2) the source trajectory is well approximated by piecewise linear joins. Under these two conditions, we show that with probability 1, a minimum of 3 and 4 sensors are sufficient to track the a segment of the piece-wise linear trajectory of the source for the

known and unknown nominal sensing ranges of the measurement sensors respectively.

First we consider the case where we know the nominal sensing range, meaning we know A. We show that this problem can be converted into a linear parameter estimation. Our approach works even with arbitrarily small sensor densities. Second, we consider the case where we do not know the nominal sensing range. We develop a non-convex function and use a Newton based algorithmic approach to estimate the trajectory of the radioactive source.

Performance bounds on estimation accuracy of radioactive sources: We consider a moving ideal measurement sensor and a stationary radioactive source and derive the performance accuracy bounds on source estimation. We show that the maximum likelihood estimate achieves the bound for the infinite time horizon case. We generalize our results for the finite horizon case.

1.8 Organization

The rest of this thesis is organized as follows. Chapter 2 describe the localization of radioactive sources using the minimum number of sources under some general assumptions. Chapter 3 describes the tracking of radioactive sources using binary proximity sensors with known and unknown nominal sensing ranges. Chapter 4 describes the achievable performance bounds of estimation of possibly weak radioactive sources using cheap mobile sensors. Chapter 5 describes possible future work and concludes.

CHAPTER 2
ESTIMATION OF RADIOACTIVE SOURCES USING THE LEAST NUMBER OF SENSORS

2.1 Introduction

In this chapter, we provide novel approaches to estimating radioactive sources using the minimum number of sensors under some general assumptions. Though the results are motivated by the radioactive sources and their estimation, the signal models used are in fact quite general and apply to a broader class of non-convex optimization. In particular, consider a source located at $y^* \in \mathbb{R}^N$, $N \in \{2, 3\}$, and n sensors located at $x_i \in \mathbb{R}^N$, $i \in \{1, ..., n\}$. Define

$$d_i = \|x_i - y^*\| \tag{2.1}$$

where $\|\cdot\|$ denotes the 2-norm. The received signal strength (RSS) at the i^{th} sensor is:

$$s_i \sim Poisson\left(\lambda_i = \frac{Ae^{-\alpha d_i}}{d_i^2}\right) + w_i \tag{2.2}$$

In principle knowledge of A and α, and the s_i measurements provide a noisy estimate of d_i; $N + 1$ such distances from non-collinear x_i, when $N = 2$, and non-coplanar x_i, when $N = 3$, suffice to estimate y^*. Indeed there are simple linear triangulation algorithms that permit localization from distances, [27].

However, the following compelling example shows the pitfalls that accompany such algorithms: $x_1 = [0, 0]^\top$, $x_2 = [43, 7]^\top$, $x_3 = [47, 0]^\top$ and $y^* = [18, -29]^\top$. The true distances are: $d_1 = 34$, $d_2 = 43$ and $d_3 = 41$. Now, suppose $\alpha = 0$ and

the measured distances are respectively, 35, 42 and 43. The linear triangulation algorithm of [27] yields: $y = [16.9, -6.5]^\top$. Observe, the dramatic inaccuracy in the second element despite the modest errors in the measured distances. As noted in [26], the difficulty lies in the fact that source estimation is a fundamentally nonlinear problem. Figure 2.1 illustrates graphically the behavior in this example.

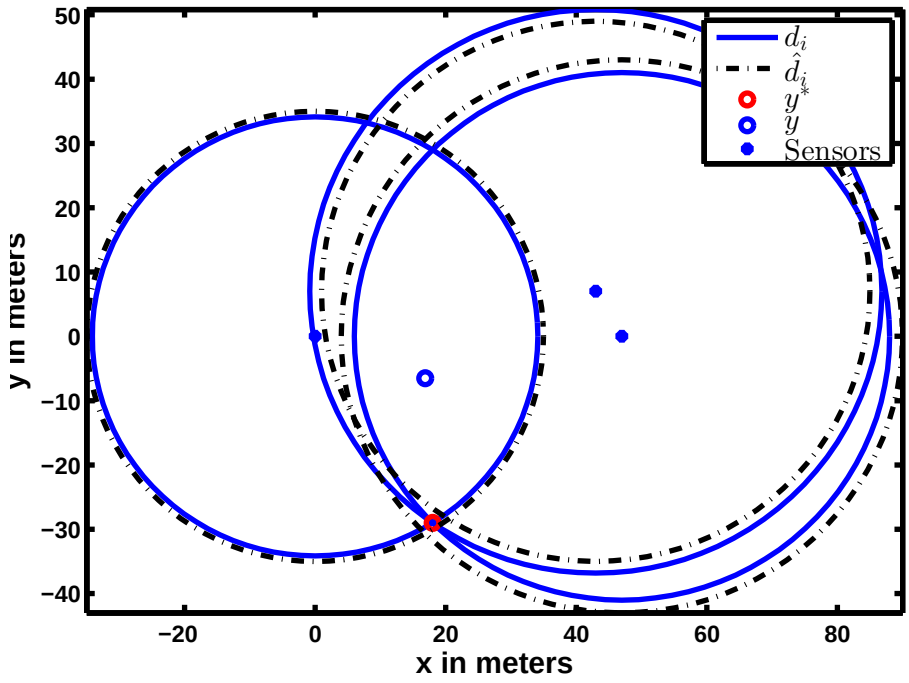

Figure 2.1: Illustration of non robustness of triangulation

We propose alternative gradient descent minimizations of the non-convex cost function, (2.2). Standard stability theory, [28, 29] shows that should the gradient descent minimization of such a cost function be uniformly convergent under the ideal

conditions of perfectly known A and zero noise, then the algorithm will be robust to uncertainties in the A and noise. Our approaches all avoid false stationary points.

2.2 Summary of our contributions

We consider a natural, non-convex cost function of (2.2), and assume that:

1. The source strength A is known and the source is in the convex hull of the sensors. We show that when the number of sensors is precisely $N+1$, $N \in \{2, 3\}$-dimensional space, (2.6) under mild assumptions gives a corresponding gradient descent algorithm which converges uniformly to a stationary point, false or otherwise. We also derive the main result under very general conditions, and discuss its implications. We argue that the gradient descent algorithm with random projections, if needed, will uniformly converge in probability.

2. The source strength A is known and the orthonormal projection of the source unto a separating hyperplane containing all the measurement sensors is in the convex hull of the measurement sensors which avoid an $N-1$-dimensional hyperplane. We show that when the number of sensors is precisely N, $N \in \{2, 3\}$-dimensional space, (2.6) under mild assumptions gives a corresponding gradient descent algorithm which converges uniformly to a stationary point, false or otherwise. We also derive the main result under very general conditions, and discuss its implications. We argue that the gradient descent algorithm with random projections, if needed, will uniformly converge in probability.

3. The source strength A is unknown and the source is in the convex hull of the

sensors. We show that when the number of sensors is precisely $N+1$, $N \in \{2, 3\}$-dimensional space, (2.6) under mild assumptions gives a corresponding gradient descent algorithm which converges uniformly to a stationary point, false or otherwise. We also derive the main result under very general conditions, and discuss its implications. We argue that the gradient descent algorithm with random projections, if needed, will uniformly converge in probability.

2.3 Estimation of known radioactive sources using precisely $N+1$ sensors

Consider arbitrary $N \geq 2$ and a fairly general observation model that in the noise free case obeys

$$z_i = g(d_i) \tag{2.3}$$

with d_i as in (2.1). In the sequel, the $g(\cdot)$ will satisfy the following assumption.

Assumption 2.3.1. *For $d > 0$, $i \in \{1, \cdots, n\}$, $g(d)$ is strictly decreasing and analytic. Further for every $\rho_1, \rho_2 > 0$, there exists $M(\rho_1, \rho_2)$ such that the $g(d_i)$ and their first two derivatives are all bounded in magnitude by $M(\rho_1, \rho_2)$ whenever $\rho_1 \leq d \leq \rho_2$.*

It is readily seen that with $A, \alpha > 0$, both

$$g(d_i) = \frac{Ae^{-\alpha d_i}}{d_i^2} \Rightarrow \frac{\partial g(d_i)}{\partial d_i} = -g(d_i)\left(\alpha + \frac{2}{d_i}\right) \tag{2.4}$$

and

$$g(d_i) = \ln A - \alpha d_i - 2\ln d_i \Rightarrow \frac{\partial g(d_i)}{\partial d_i} = -\left(\alpha + \frac{2}{d_i}\right) \tag{2.5}$$

obey Assumption 2.3.1, as does the standard RSS model where $\alpha = 0$. Observe the right hand side of (2.5) is just the logarithm of the right side of (2.4).

Now consider the cost function:

$$J(y) = \sum_{i=1}^{n} \left(z_i - g(\|y - x_i\|)\right)^2. \tag{2.6}$$

Suppose the $x_i \in \mathbb{R}^N$ avoid an $(N-1)$-dimensional hyperplane. Then clearly the only global minimum of (2.6) is $y = y^*$. Consequently, the gradient descent minimization of (2.6) is a candidate localization algorithm. Specifically, with $y[k]$ the current estimate of y^*, and sufficiently small $\mu > 0$, such an algorithm will proceed as:

$$y[k+1] = y[k] - \mu \left.\frac{\partial J(y)}{\partial y}\right|_{y=y[k]} \quad \forall k \geq k_0. \tag{2.7}$$

For either (2.4) or (2.5) the knowledge of the A, α and z_i ensures that (2.7) is implementable. Indeed define $g'(\cdot)$ as the derivative of $g(\cdot)$. Observe:

$$\frac{\partial J(y)}{\partial y} = 2\sum_{i=1}^{n} \frac{\left(z_i - g(\|y - x_i\|)\right) g'(\|y - x_i\|)(x_i - y)}{\|y - x_i\|}. \tag{2.8}$$

We also note that with $g(\cdot)$ as in (2.4) the estimate minimizing (2.6) would be the maximum likelihood estimate, if w_i in (2.2) were Gaussian. Though in practice it is modeled as poisson, high variance poisson distributions are well approximated by Gaussian ones. In the event we have the following Theorem.

Theorem 2.1. *Consider (2.7) under (2.3), (2.6) and Assumption 2.3.1. Suppose neither y^* nor $y[k_0]$ are coincident with any of the x_i. Then for every such pair of $y[k_0]$ and y^*, there exists a $\mu^*(y^*, y[k_0])$ such that for all $0 < \mu \leq \mu^*$, the following hold:*

(A) For all $k \geq k_0$ $J\left(y[k]\right) \leq J\left(y[k_0]\right)$.

(B) The following occurs uniformly in the initial time k_0:

$$\lim_{k\to\infty} \left.\frac{\partial J(y)}{\partial y}\right|_{y=y[k]} = 0. \tag{2.9}$$

Further, suppose there exist a $k_1 \geq k_0$ and a compact set $S \subset \mathbb{R}^N$ containing y^*, with boundary ∂S, having the following properties: (I) When $y \in S \setminus \partial S$

$$\frac{\partial J(y)}{\partial y} = 0 \Leftrightarrow J(y) = 0. \tag{2.10}$$

(II)

$$J(y[k_1]) < \min_{y\in\partial S} J(y) \text{ and } y[k_1] \in \{S \setminus \partial S\}.$$

Then the following holds uniformly in k_1

$$\lim_{k\to\infty} J(y[k]) = 0. \tag{2.11}$$

Proof. First observe that as neither y^* nor $y[k_0]$ are coincident with any of the x_i, because of Assumption 2.3.1, for some finite $K > 0$, $J(y[k_0]) = K$. Consider the compact set $\mathcal{J}(K) = \left\{y \in \mathbb{R}^N \,|J(y) \leq K\right\}$. Because of (2.6) and Assumption 2.3.1 there exists an $M_1 > 0$ such that all first and second order derivatives of $J(y)$ with respect to the elements of y are bounded by M_1 for all $y \in \mathcal{J}(K)$. Thus, as because from (2.7),

$$\|y[k+1] - y[k]\| \leq \mu \left\| \left.\frac{\partial J(y)}{\partial y}\right|_{y=y[k]} \right\|, \tag{2.12}$$

there exists a μ_1 and an M_2 such that for all $y[k] \in \mathcal{J}(K)$, and $0 < \mu < \mu_1$, the first and second order derivatives of $J(y)$ on the line segment joining $y[k]$ and $y[k+1]$ are bounded by M_2. From the multivariable Taylor's Theorem there thus exists an

$M_3(\mu)$, determined by M_2 and μ for which:

$$\begin{aligned} J\left(y[k+1]\right) &= J\left(y[k] - \mu \left.\frac{\partial J(y)}{\partial y}\right|_{y=y[k]}\right) \\ &\leq J\left(y[k]\right) - \mu \left\| \left.\frac{\partial J(y)}{\partial y}\right|_{y=y[k]} \right\|^2 (1 - \mu^2 M_3(\mu)). \end{aligned}$$

In particular,

$$\lim_{\mu \to 0} M_3(\mu) = 0.$$

Thus, for any $y[k] \in \mathcal{J}(K)$, there exists a μ_2 depending on K, and an $0 < \epsilon < 1$ such that for all $0 < \mu < \mu_2$, $\mu M_3 < 1 - \epsilon$. For any such μ, this in turn ensures that whenever $y[k] \in \mathcal{J}(K)$, $J(y[k+1]) \leq J(y[k])$, proving (A) through an obvious induction. Further with any such μ, and ϵ as defined there holds:

$$J\left(y[k+1]\right) \leq J\left(y[k]\right) - (1-\epsilon) \left\| \left.\frac{\partial J(y)}{\partial y}\right|_{y=y[k]} \right\|^2 .$$

As $J(\cdot)$ is nonnegative, standard arguments prove (2.9). Uniformity in k_0 follows by the lack of explicit dependence in (2.7) on k. Finally under (II), because of (A), for all $k \geq k_1$, $y[k] \in \{S \setminus \partial S\}$. Then (2.11) occurs because of (I), (2.9), $y^* \in S$ and $J(y^*) = 0$. □

Remark 2.1. This theorem holds even if we replace the strict decreasing requirement on *all* the $g(.)$ by a strict increasing requirement on all of them.

We note that any value of y for which the gradient is zero is a stationary point of (2.7). It is a false stationary point if this y does not equal y^*. Figure 2.2 illustrates graphically the convergence to false stationary points for our cost function.

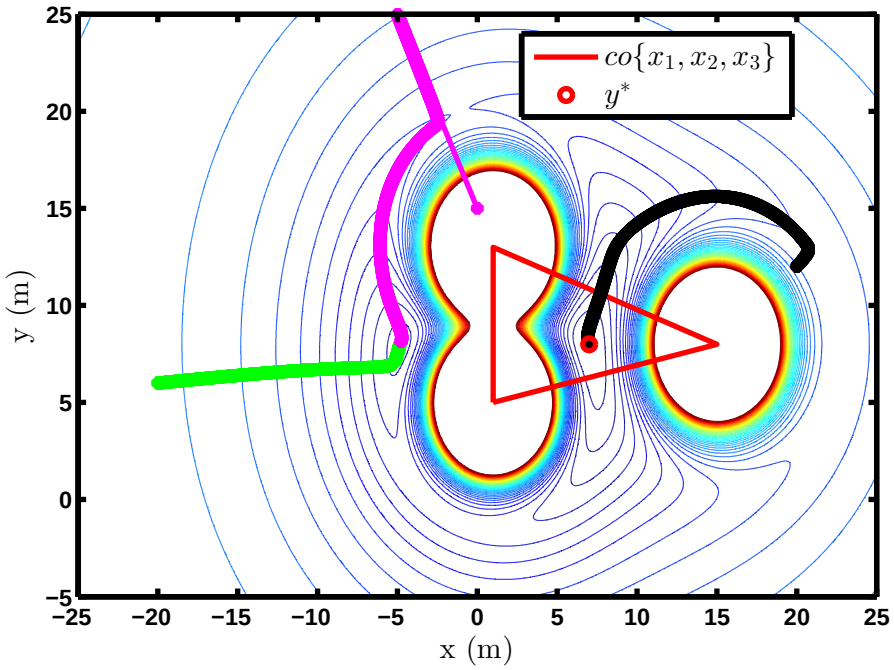

Figure 2.2: Illustration of false stationary points

If the x_i do not lie on an $(N-1)$-dimensional hyperplane, uniform convergence of $y[k]$ to y^* then simply requires that (I) and (II) hold for some k_1. The next section explores how to ensure this.

2.3.1 The main result

We now make two further assumptions.

Assumption 2.3.2. *The number of sensors n, precisely equals $N+1$ and the sensors located at $x_i \in \mathbb{R}^N$ do not lie on an $(N-1)$-dimensional hyperplane.*

Recall this is the minimum number of sensors needed to achieve localization from the z_i in (2.3). The second assumption below is eminently sensible. It presumes

that a very crude detection of the source has occurred and the sensors have been placed so that the source is in their convex hull. In the sequel the notation, $co\{x_1, \cdots, x_{N+1}\}$ denotes the *open* convex hull of the x_i.

Assumption 2.3.3. *The source location $y^* \in \mathbb{R}^N$ is in $co\{x_1, \cdots, x_{N+1}\}$.*

Before presenting our main result, we first provide a Lemma.

Lemma 2.2. *Under assumptions 2.3.2 and 2.3.3 suppose $y \in \mathbb{R}^N$ obeys: (a) $y \neq y^*$ and (b) $y \in co\{x_1, \cdots, x_{N+1}\}$. Then there exist $i, j \in \{1, \cdots, N+1\}$ such that: $\|x_i - y\| < \|x_i - y^*\|$, and $\|x_j - y\| > \|x_j - y^*\|$.*

Proof. As $y \neq y^*$, there exists an $(N-1)$-dimensional hyperplane H that separates $\mathbb{R}^N$ into two open half planes, $\mathcal{H}$ and $\mathcal{H}^*$, such that $\mathcal{H} = \left\{\eta \in \mathbb{R}^N \,|\, \|\eta - y\| < \|\eta - y^*\|\right\}$ and $\mathcal{H}^* = \left\{\eta \in \mathbb{R}^N \,|\, \|\eta - y\| > \|\eta - y^*\|\right\}$.

Further, $H = \left\{\eta \in \mathbb{R}^N \,|\, \|\eta - y\| = \|\eta - y^*\|\right\}$. For the Lemma to be false either for all $i \in \{1, \cdots, N+1\}$

$$x_i \in \mathcal{H}^* \bigcup H \tag{2.13}$$

or for all $i \in \{1, \cdots, N+1\}$

$$x_i \in \mathcal{H} \bigcup H. \tag{2.14}$$

By the separating hyperplane theorem in case of (2.13), $y \notin co\{x_1, \cdots, x_{N+1}\}$ and in case of (2.14), $y^* \notin co\{x_1, \cdots, x_{N+1}\}$. The contradiction proves the result. □

We now present our main result that shows that should the source lie in the open convex hull of the sensors, and should there be precisely the minimum number

of sensors required for localization, then the open convex hull of the sensors is bereft of false stationary points.

Theorem 2.3. *Consider (2.6) under assumptions 2.3.1, 2.3.2 and 2.3.3. Consider* $y \in co\{x_1, \cdots, x_{N+1}\}$. *Then there holds:*

$$\frac{\partial J(y)}{\partial y} = 0 \Leftrightarrow J(y) = 0.$$

Proof. Since $y \in co\{x_1, \cdots, x_{N+1}\}$, there exist $\beta_i > 0$, such that

$$\sum_{i=1}^{N+1} \beta_i = 1 \tag{2.15}$$

and

$$\sum_{i=1}^{N+1} \beta_i x_i = y. \tag{2.16}$$

From (2.15) and (2.16) we obtain:

$$\sum_{i=1}^{N+1} \beta_i x_i = \left(\sum_{i=1}^{N+1} \beta_i \right) y \Leftrightarrow \sum_{i=1}^{N+1} \beta_i (x_i - y) = 0.$$

In other words $\beta = [\beta_1, \cdots, \beta_{N+1}]^\top$ is in the right nullspace of the matrix: $\mathcal{X}(y) = \begin{bmatrix} x_1 - y & \cdots & x_{N+1} - y \end{bmatrix}$. As the x_i do not lie on an $(N-1)$-dimensional hyperplane $\mathcal{X}(y)$ has rank N for all $y \in \mathbb{R}^N$. Thus its nullspace has dimension 1, and as $\beta_i > 0$, all its non-zero null vectors have elements that are either all positive, or are all negative.

Now suppose

$$\frac{\partial J(y)}{\partial y} = 0. \tag{2.17}$$

Define:

$$\xi_i = \frac{(g(\|y^* - x_i\|) - g(\|y - x_i\|))\, g'(\|y - x_i\|)}{\|y - x_i\|} \tag{2.18}$$

From (2.8), $\xi = [\xi_1, \cdots, \xi_{N+1}]^\top$ is in the null space of $\mathcal{X}(y)$. Now suppose $\xi \neq 0$. Then every ξ_i is either positive or every one of them is negative. From Assumption 2.3.1, $g_i'(\|y - x_i\|) < 0$ for all i. Thus, the strict monotonicity of the g_i ensures that either for all i, $\|y^* - x_i\| > \|y - x_i\|$ or for all i, $\|y^* - x_i\| < \|y - x_i\|$. As both y and y^* are in $co\{x_1, \cdots, x_{N+1}\}$, Lemma 2.2 precludes either possibility. Thus $\eta = 0$, and from (2.18) and (2.6), $J(y) = 0$. On the other hand if $J(y) = 0$, then clearly from (2.7), (2.17) holds. □

Remark 2.2. We observe that this theorem too holds if the strictly decreasing nature of all the $g(.)$ is replaced by their being strictly increasing.

Thus should the source be in the open convex hull of $N + 1$ sensors avoiding any $N-1$-dimensional hyperplane, then source estimation is guaranteed provided the location estimate never leaves the convex hull.

In practice however, it may leave the convex hull, even if the initial estimate is in the convex hull. To combat this, consider the following augmented gradient descent algorithm. If in (2.7), $y[k+1] \notin co\{x_1, \cdots, x_{N+1}\}$, then choose $y[k+1]$ to be a randomly chosen point inside the open convex hull. We now argue that such a projection based algorithm will converge in probability as long as the source is inside the open convex hull. Define $\bar{J}$ to be minimum value of $J(y)$ at the boundary of $co\{x_1, \cdots, x_{N+1}\}$, and

$$S = \left\{ y \in \mathbb{R}^N \,\middle|\, J(y) < \bar{J} \right\} \bigcap co\{x_1, \cdots, x_{N+1}\}.$$

This set has nontrivial extent as $y^* \in co\{x_1, \cdots, x_{N+1}\}$, and $J(y^*) = 0$. Thus with

probability 1, there exists k_1 such that a projected estimate at k_1 will enter this set. As $S \subset co\{x_1, \cdots, x_{N+1}\}$ in view of Theorem 2.3, S satisfies (I) and (II) of Theorem 2.1 and convergence in probability follows. In practice simulations presented in the next section show, that estimates leave the convex hull very rarely, and that too only at very low SNR values.

2.3.2 Simulation results

We consider two simulation examples one with $N = 2$, the other with $N = 3$. In both cases we use $n = N+1$. In (2.2) we use: $w_i \sim \text{poisson}(\lambda_{w_i})$ as the background noise. We also use $A = 10^4$. The noise power in evaluating the SNR is the empirical noise power, i.e. computed by averaging the actual difference between s_i and

$$\frac{Ae^{-\alpha d_i}}{d_i^2}.$$

In all cases $\alpha = 0.05$, $\mu = 0.0002$. The mean squared error (MSE) is averaged over 1000 random initial start points all within the convex hull of the sensors, and the algorithm is run for 200 iterations for each initial point. Also, for each iteration of each run, s_i are generated independently. A projection augmented gradient descent minimization of (2.6) under (2.4) is performed. The algorithm uses $\frac{Ae^{-\alpha d_i}}{d_i}$ in computing the gradient and the effect of the uncertainty in A *is thus subsumed in the noise power computation.*

Figure 2.3 depicts performance when $N = 2$. The sensors are at (1,5), (1,13) and (15,8), the source at (7,8), in their convex hull. Figure 2.4 presents the map of the average location estimate provided by our algorithm for various SNR values, as

well as the actual source location. Figure 2.5 is for gauging the convergence speed. For an SNR of 47dB it plots the MSE as a function of the iteration index k. The MSE at each value of k is obtained by averaging over the random runs described above. The fast rate of convergence is self-evident.

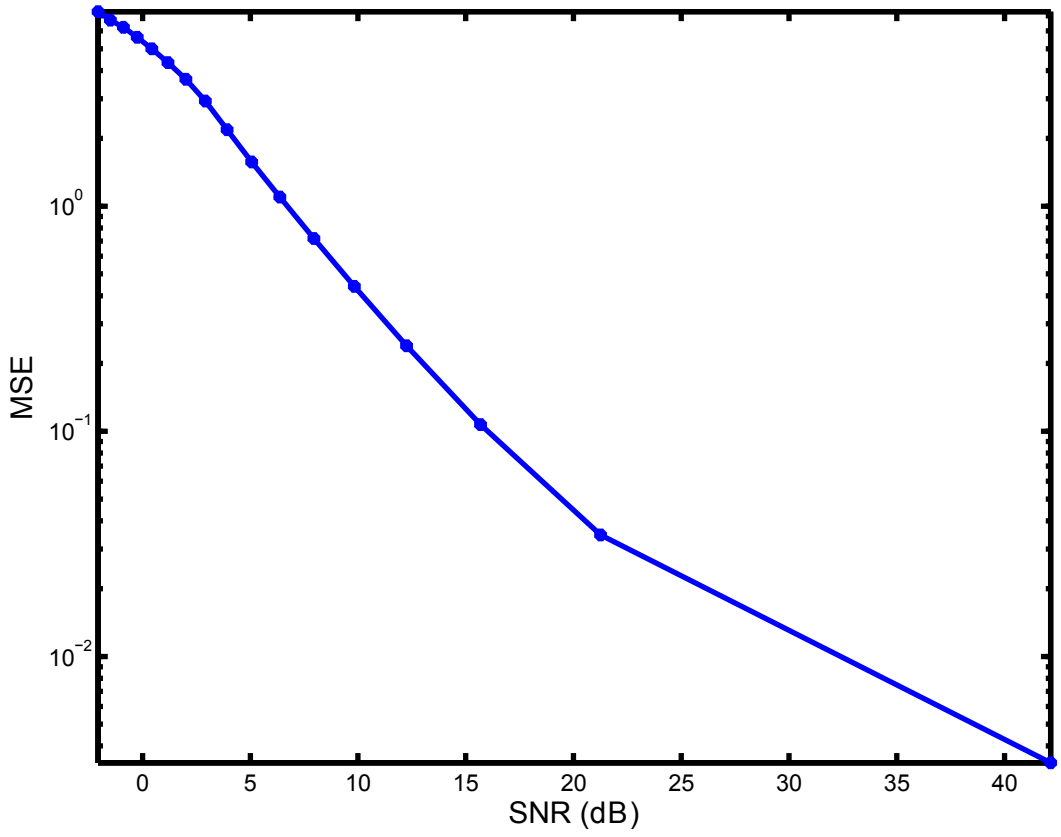

Figure 2.3: MSE against SNR in dB with $N = 2$.

The 3-dimensional counterpart of Figure 2.3 is depicted in Figure 2.6. The sensors are at (1,5,2), (1,13,2), (15,8,2) and (3,4,12) and the source is at (7,8,4). The

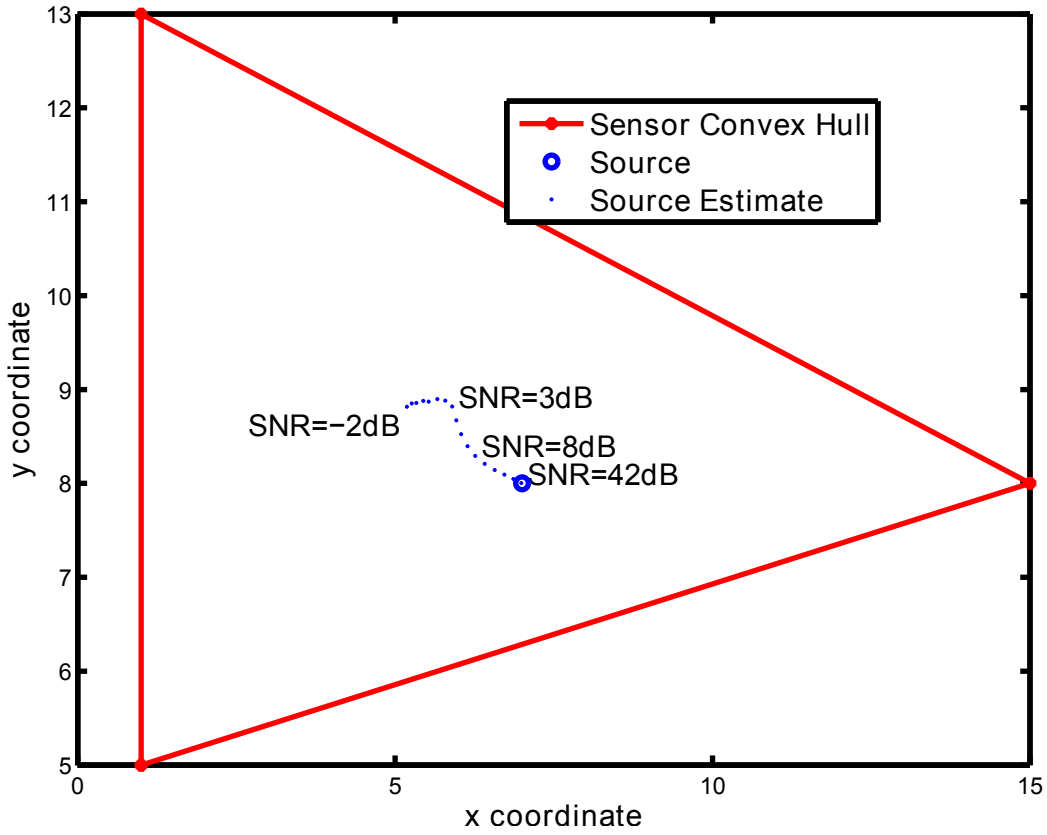

Figure 2.4: The map of the average source location estimate for various SNRs and the true source location.

performance is depicted in figure 2.6.

A noteworthy fact about all these simulations is that except in low SNR regimes, the estimates do not leave the convex hull. Even with low SNRs they leave the convex hull only about 1% of times.

2.4 Estimation of known radioactive sources using precisely N sensors

Consider arbitrary $N \geq 2$ and a fairly general observation model that in the noise free case obeys (2.3) and satisfies assumption 2.3.1. Observe that the gradient

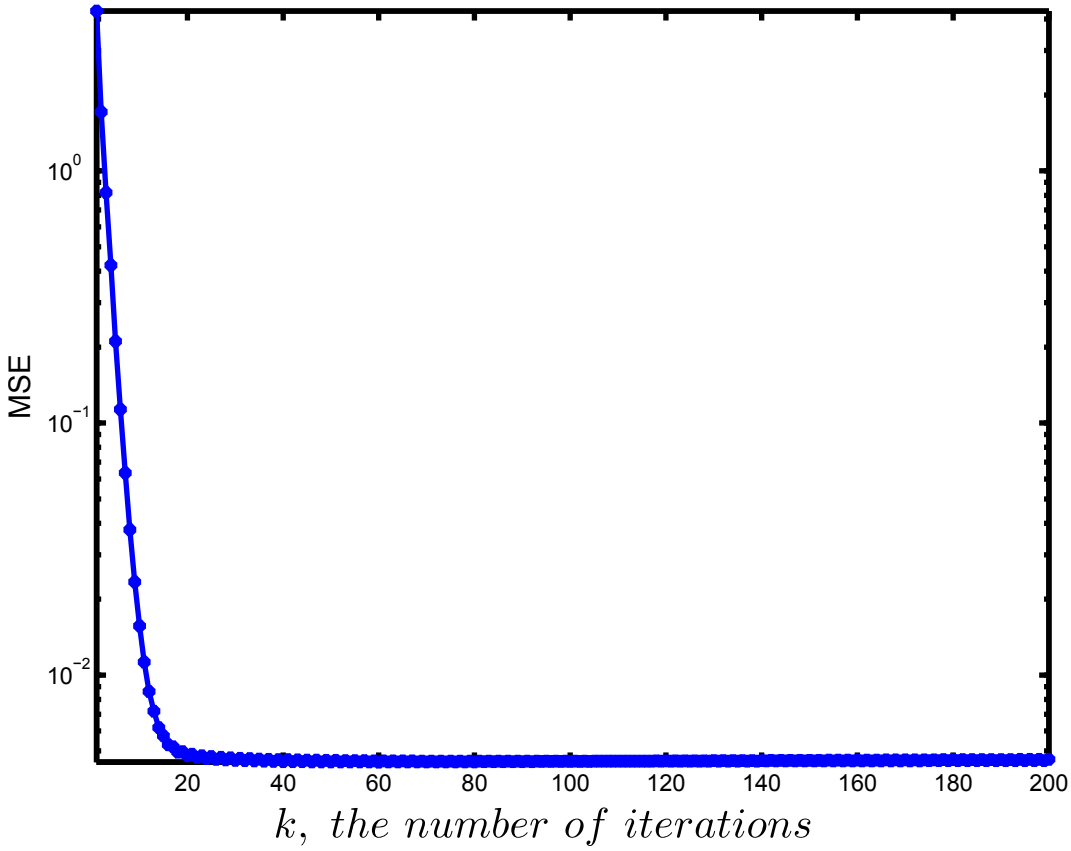

Figure 2.5: MSE vs k for SNR 47 dB.

of (2.4) is:

$$g'(d_i) = -g(d_i)\left(\frac{2}{d_i} + \alpha\right) \tag{2.19}$$

which is negative for $\alpha \geq 0$. Therefore $g(d_i)$ is strictly decreasing for $\alpha \geq 0, i \in \{1, \cdots, N\}$.

Now consider the cost function (2.6). Suppose the $x_i \in \mathbb{R}^N$ avoid an $(N-2)$-dimensional hyperplane. Then clearly the global minima of (2.6) is a finite set including $y = y^*$. Consequently, the gradient descent minimization of (2.6) is a

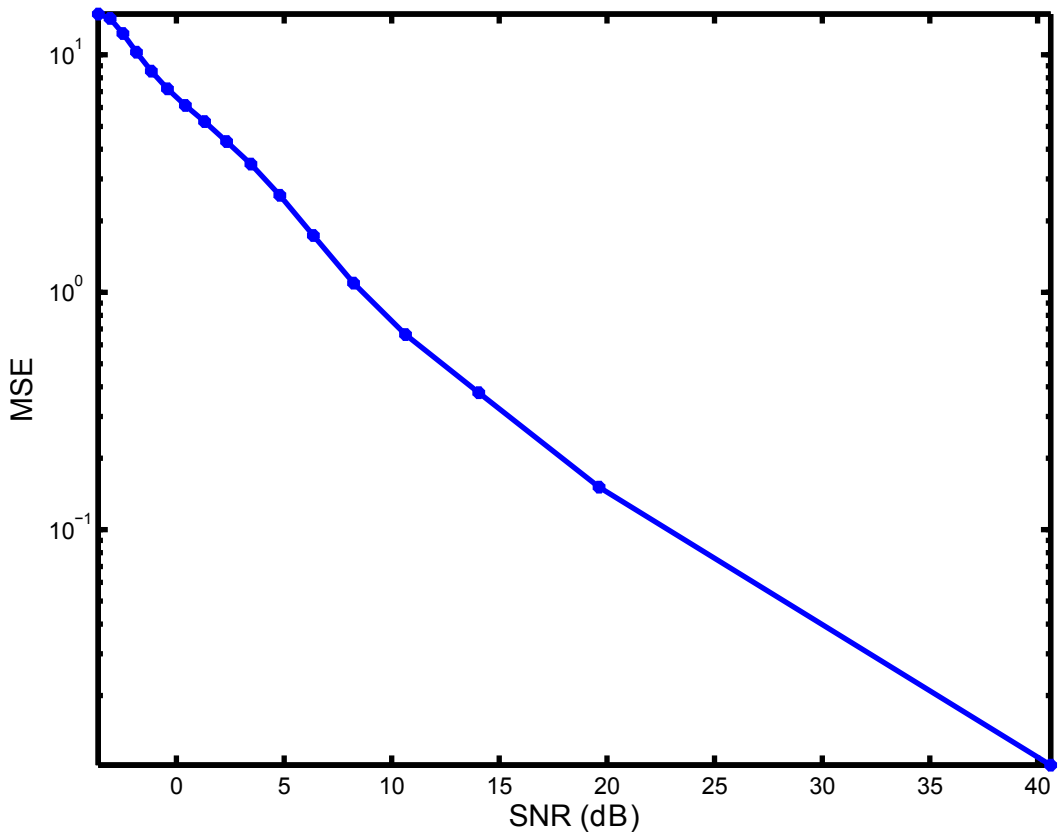

Figure 2.6: MSE against SNR, all in dB with $N = 3$.

candidate localization algorithm. Specifically, with $y[k]$ the current estimate of y^*, and sufficiently small $\mu > 0$, such an algorithm will proceed as (2.7). The knowledge of the α and z_i in (2.4) ensures that (2.7) is implementable. Whether we can get $y = y^*$ uniquely is the subject of our main results in section 2.4.1. Recall the gradient of the cost function in (2.8). We also note that with $g(\cdot)$ as in (2.4), the estimate minimizing (2.6) would be the maximum likelihood estimate, if w_i in (2.2) were Gaussian. Though in practice w_i is modeled as poisson, high variance poisson distributions are well approximated by Gaussian ones.

2.4.1 The main result

We now make two assumptions.

Assumption 2.4.1. *The number of sensors n, precisely equals N and the sensors located at $x_i \in \mathbb{R}^N, N \in \{2,3\}$ do not lie on an $(N-2)$-dimensional hyperplane.*

Recall this is one less than the minimum number of sensors needed to achieve localization from the z_i in (2.3). Before we state the second assumption, define:

$$H_v = \left\{ \psi \in \mathbb{R}^N | \psi = x_1 + \sum_{i=2}^{N} a_i e_{i-1} \, , \forall a_i \in \mathbb{R} \right\} \tag{2.20}$$

where

$$e_i = \frac{(x_i - x_1) - \sum_{k=1}^{i-1} \frac{(x_k - x_1)\cdot(x_i - x_1)}{(x_k - x_1)\cdot(x_k - x_1)}(x_k - x_1)}{\|(x_i - x_1) - \sum_{k=1}^{i-1} \frac{(x_k - x_1)\cdot(x_i - x_1)}{(x_k - x_1)\cdot(x_k - x_1)}(x_k - x_1)\|} \tag{2.21}$$

Also define $\forall z \in \mathbb{R}^N$

$$\hat{z} = \sum_{i=1}^{N-1}(z \cdot e_i)e_i - \frac{\left\| \sum_{i=1}^{N-1}(x_1 \cdot e_i)e_i - x_1 \right\| \left(\sum_{i=1}^{N-1}(z \cdot e_i)e_i - z \right)}{\left\| \sum_{i=1}^{N-1}(z \cdot e_i)e_i - z \right\|}. \tag{2.22}$$

Here $x_i \cdot e_i$ is the scalar dot product. Notice that (2.20) is an (N-1)-dimensional hyperplane containing all the x_i's and (2.22) is an orthonormal projection of all points in $\mathbb{R}^N$ unto H_v. The second assumption presumes that a very crude detection of the source has occurred and x_i's have been placed so that $\hat{y}^*$ is in their convex hull.

Assumption 2.4.2. *$y^* \in \mathbb{R}^N, N \in \{2,3\}$ is in one open half plane separated by H_v and $\hat{y}^* \in \mathbb{R}^N, N \in \{2,3\}$ is in $co\{x_1, \cdots, x_N\}$.*

Before presenting our main result, we first provide a Lemma.

Lemma 2.4. *Under assumptions 2.4.1 and 2.4.2 suppose* $\hat{y} \in \mathbb{R}^N, N \in \{2,3\}$ *obeys: (a)* $\hat{y} \neq \hat{y}^*$ *and (b)* $\hat{y} \in co\{x_1, \cdots, x_N\}$. *Then (I) there exist* $i, j \in \{1, \cdots, N\}$ *such that:* $\|x_i - \hat{y}\| < \|x_i - \hat{y}^*\|$, *and* $\|x_j - \hat{y}\| > \|x_j - \hat{y}^*\|$. *(II) for such* i, j *in (I), if* $\|y - \hat{y}\|^2 < \|y^* - \hat{y}\|^2 + 2\|x_i - \hat{y}\|\|\hat{y} - \hat{y}^*\|$, *then* $\|x_i - y\| < \|x_i - y^*\|$, *and* $\|x_j - y\| > \|x_j - y^*\|$.

Proof. As $\hat{y} \neq \hat{y}^* \Rightarrow y \neq y^*$, there exists an $(N-1)$-dimensional hyperplane H that separates $\mathbb{R}^N$ into two open half planes, $\mathcal{H}$ and $\mathcal{H}^*$, such that:
$\mathcal{H} = \left\{\eta \in \mathbb{R}^N \,|\|\eta - \hat{y}\| < \|\eta - \hat{y}^*\|\right\}$ and $\mathcal{H}^* = \left\{\eta \in \mathbb{R}^N \,|\|\eta - \hat{y}\| > \|\eta - \hat{y}^*\|\right\}$. Further, $H = \left\{\eta \in \mathbb{R}^N \,|\|\eta - \hat{y}\| = \|\eta - \hat{y}^*\|\right\}$. For (I) of the Lemma to be false either for all $i \in \{1, \cdots, N\}$

$$x_i \in \mathcal{H}^* \bigcup H \tag{2.23}$$

or for all $i \in \{1, \cdots, N\}$

$$x_i \in \mathcal{H} \bigcup H. \tag{2.24}$$

By the separating hyperplane theorem in case of (2.23), $\hat{y} \notin co\{x_1, \cdots, x_N\}$ and in case of (2.24), $\hat{y}^* \notin co\{x_1, \cdots, x_N\}$. The contradiction proves (I). Since $\{\hat{y}^*, \hat{y}\}$ are projections of $\{y^*, y\}$ along two distinct parallel hyperplanes orthonormal to H_v, if $\|x_i - \hat{y}\| < \|x_i - \hat{y}^*\|$, and $\|y - \hat{y}\|^2 < \|y^* - \hat{y}\|^2 + 2\|x_i - \hat{y}\|\|\hat{y} - \hat{y}^*\|$ then $\|x_i - y\| < \|x_i - y^*\|$. Similarly if $\|x_j - \hat{y}\| > \|x_j - \hat{y}^*\|$, then $\|x_j - y\| > \|x_j - y^*\|$. This proves (II). □

We now present our main result that shows that should $\hat{y}^*$ lie in $co\{x_1, \cdots, x_N\}$, and should there be precisely N sensors in $\mathbb{R}^N$, then each open half plane of $\mathbb{R}^N$ sepa-

rated by H_v has exactly one minimum whose orthonormal projection unto H_v lies in $co\{x_1, \cdots, x_N\}$ and no false stationary points. Knowledge of which open half plane contains the source suffices to estimate the radioactive source.

Theorem 2.5. *Consider (2.6) under assumptions 2.3.1, 2.4.1 and 2.4.2. Consider* $\hat{y} \in co\{x_1, \cdots, x_N\}$. *Then there holds:*

$$\frac{\partial J(y)}{\partial y} = 0 \Leftrightarrow J(y) = 0.$$

Proof. Since $\hat{y} \in co\{x_1, \cdots, x_N\}$, there exist $\beta_i > 0$, such that from (2.15) and (2.16) we obtain:

$$\sum_{i=1}^{N} \beta_i x_i = \left(\sum_{i=1}^{N} \beta_i \right) \hat{y} \Leftrightarrow \sum_{i=1}^{N} \beta_i (x_i - \hat{y}) = 0. \tag{2.25}$$

In other words $\beta = [\beta_1, \cdots, \beta_N]^\top$ is in the right null space of the matrix: $\mathcal{X}(\hat{y}) = \begin{bmatrix} x_1 - \hat{y} & \cdots & x_N - \hat{y} \end{bmatrix}$. As the x_i's do not lie on an $(N-2)$-dimensional hyperplane $\mathcal{X}(\hat{y})$ has rank $N-1$ for all $\hat{y} \in \mathbb{R}^N$. Thus its nullspace has dimension 1, and as $\beta_i > 0$, all its non-zero null vectors have elements that are either all positive, or are all negative. Without loss of generality, suppose $x_1 = 0$. This is easily attained through translation. We abuse notation by maintaining x_i's and $\{y, y^*\}$ after translation to preserve clarity. Then (2.22) becomes

$$\hat{z} = \sum_{i=1}^{N-1} (z \cdot e_i) e_i. \tag{2.26}$$

Now suppose

$$\frac{\partial J(y)}{\partial y} = 0. \tag{2.27}$$

This means

$$2\sum_{i=1}^{N}\frac{\left(z_i-g\left(d_i\right)\right)g'\left(d_i\right)}{d_i}(x_i-y)=0 \tag{2.28}$$

Define:

$$\xi_i=\frac{\left(z_i-g_i(d_i)\right)g_i'(d_i)}{d_i} \tag{2.29}$$

Then (2.28) becomes

$$\begin{aligned}
2\sum_{i=1}^{N}\xi_i(x_i-y)=0 \Leftrightarrow\\
\sum_{k=1}^{N-1}\left(\left(2\sum_{i=1}^{N}\xi_i(x_i-y)\right)\cdot e_k\right)e_k=0\\
2\sum_{k=1}^{N-1}\sum_{i=1}^{N}\xi_i((x_i\cdot e_k)e_k-(y\cdot e_k)e_k)=0\\
2\sum_{i=1}^{N}\xi_i\sum_{k=1}^{N-1}((x_i\cdot e_k)e_k-(y\cdot e_k)e_k)=0\\
2\sum_{i=1}^{N}\xi_i(\hat{x_i}-\hat{y_i})=0
\end{aligned} \tag{2.30}$$

Now, since the x_i's are on H_v, $\hat{x}_i=x_i\forall i$. Therefore (2.30) becomes

$$2\sum_{i=1}^{N}\xi_i(x_i-\hat{y_i})=0 \tag{2.31}$$

$\xi=[\xi_1,\cdots,\xi_N]^\top$ is in the null space of $\mathcal{X}(\hat{y})$ from (2.31) and (2.25) . Now suppose $\xi\neq 0$. Then every ξ_i is either positive or every one of them is negative. From Assumption 2.3.1, $g_i'(\|y-x_i\|)<0$ for all i. Thus, the strict monotonicity of the g_i ensures that either for all i, $\|y^*-x_i\|>\|y-x_i\|$ or for all i, $\|y^*-x_i\|<\|y-x_i\|$. As both $\hat{y}$ and $\hat{y}^*$ are in $co\{x_1,\cdots,x_N\}$, Lemma 2.4 precludes either possibility. Thus $\xi=0$ meaning that $\|y^*-x_i\|=\|y-x_i\|,\forall i$. Since we know which open half plane

contains y^*, there is exactly 1 solution of $\|y^* - x_i\| = \|y - x_i\|, \forall i \Rightarrow y = y^*$. From (2.29) and (2.6), $J(y) = 0$. On the other hand if $J(y) = 0$, then clearly from (2.7), (2.27) holds. □

A critical procedure in this technique is the initial crude estimate to gauge the location of the source. How do we know that the projection of the source unto H_v lies in $co\{x_1, \cdots, x_N\}$? And how do we know which open half plane, using H_v as the separating hyperplane contains the source? This turns out to be very simple. Consider Figure 2.7 with two sensors at $\{x_1, x_2\}$ and the source at y^* for the 2-dimension case. The hyperplane H_v separates $\mathbb{R}^2$ into two open half planes. Using two sets of perturbations of $\{x_1, x_2\}$ by $\{\delta_1, \delta_2\}$ and $\{\xi_1, \xi_2\}$ along H_v and orthogonal to H_v respectively both decrease the measurements of sensors 1 and 2 ideally and show crudely that the projection of y unto H_v is in $co\{x_1, x_2\}$ and y^* is above H_v. Taking a number or measurements and averaging will approach the ideal situation using the law of large numbers. This clearly scales to $\mathbb{R}^N$.

In practice however, the projection of the estimate may leave $co\{x_1, \cdots, x_N\}$, even if the projection of the initial estimate is in the convex hull. To combat this consider the following augmented gradient descent algorithm. If in (2.7), $\hat{y}[k+1] \notin co\{x_1, \cdots, x_N\}$, then choose $y[k+1]$ to be a randomly chosen point such that $\hat{y}[k+1] \in co\{x_1, \cdots, x_N\}$. We now argue that such a projection based algorithm will converge in probability as long as the orthonormal projection of the source unto H_v lies in $co\{x_1, \cdots, x_N\}$. Define $\bar{J}$ to be minimum value of $J(y)$ at the boundary of

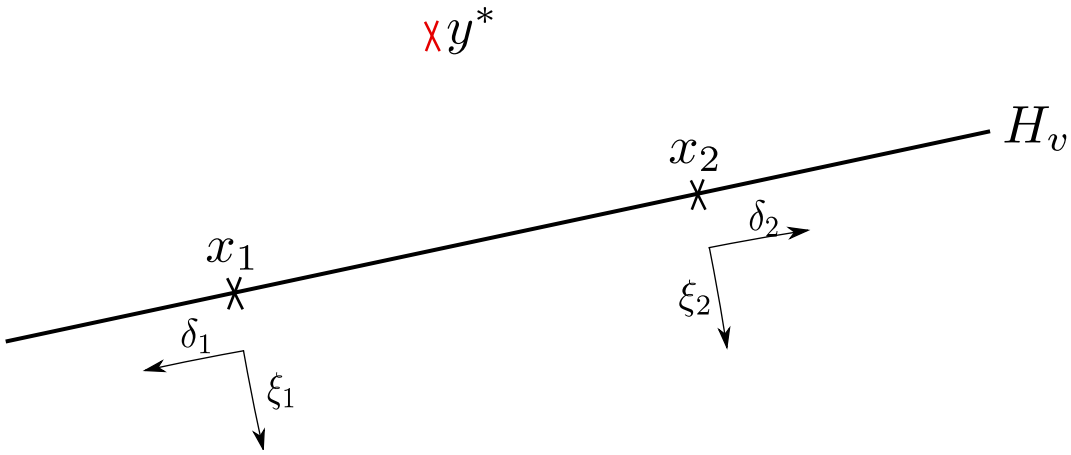

Figure 2.7: 2-Dimensions example for estimating which open half plane contains y^*

$co\{x_1, \cdots, x_N\}$, and

$$S = \left\{ y \in \mathbb{R}^N \,\middle|\, J(y) < \bar{J} \right\} \bigcap \{\hat{y} \in co\{x_1, \cdots, x_N\}\}.$$

This set has nontrivial extent as $\hat{y}^* \in co\{x_1, \cdots, x_N\}$, and $J(y^* | \hat{y}^* \in co\{x_1, \cdots, x_N\}) = 0$. Thus with probability 1, there exists k_1 such that a projected estimate at k_1 will enter this set. As $S \subset \{x | \hat{x} \in co\{x_1, \cdots, x_N\}\}$ in view of Theorem 2.5, S satisfies (I) and (II) of Theorem 2.1 and convergence in probability follows. In practice, simulations presented in the next section show, that orthonormal projections of the estimate unto H_v leaves $co\{x_1, \cdots, x_N\}$ very rarely, and that too only at very low SNR values when the estimate approaches to the separating hyperplane H_v.

2.4.2 Simulation results

We consider simulations with $N = 2$ using exactly 2 sensors. The received signal at sensor i is: $s_i \sim$ poisson $\left(\frac{A}{d_i^2} e^{-\alpha d_i} + w \right)$ and w is the background noise. The

SNR is computed as:

$$SNR = 10\log_{10}\left(\frac{\sum_{i=1}^{N}\frac{Ae^{-\alpha d_i}}{d_i^2}}{\sum_{i=1}^{N+1} w}\right).$$

In all cases $\alpha = 0.0068$, $A = 2\times 10^7$ and $\mu = 0.0005$. The mean squared error (MSE) is averaged over 100 random initial start points $\in \{z|\hat{z} \in co\{x_1, x_2\}\}$ and in the known open half space separated by H_v. The algorithm runs for 20000 iterations. Also, for each iteration of each run, the s_i's are Poisson and generated independently. A projection augmented gradient descent minimization of (2.6) under (2.4) is performed. The fact that the actual s_i differ from the value used in generating the gradient, confirms the robustness of the algorithm to uncertainties in the s_i.

Figure 2.8 depicts performance when $N = 2$. The sensors are at $(-100, 0)$ and $(100, 0)$, the source is at $y^* = (40, 100)$, $\hat{y}^* \in co\{x_1, \cdots, x_{N+1}\}$. Figure 2.9 presents the map of the average location estimate provided by our algorithm for various SNR values, as well as the actual source location. Figure 2.10 is for gauging the convergence speed. For an SNR of 6dB it plots the MSE as a function of the iteration index k. The MSE at each value of k is obtained by averaging over the 100 random runs described above. The fast rate of convergence is self-evident.

A noteworthy fact about all these simulations is that except in low SNR regimes, the estimates do not leave the convex hull. Even with low SNRs they leave the convex hull only about 1% of times. Further, the expectation of the received signal at the sensors in the absence of noise are very small, $[210, 665]^T$. The simulations show the robustness of our algorithm. It is also noticeable that the MSE saturates around 10^4 for low SNR. This is approximately the square of the distance of the

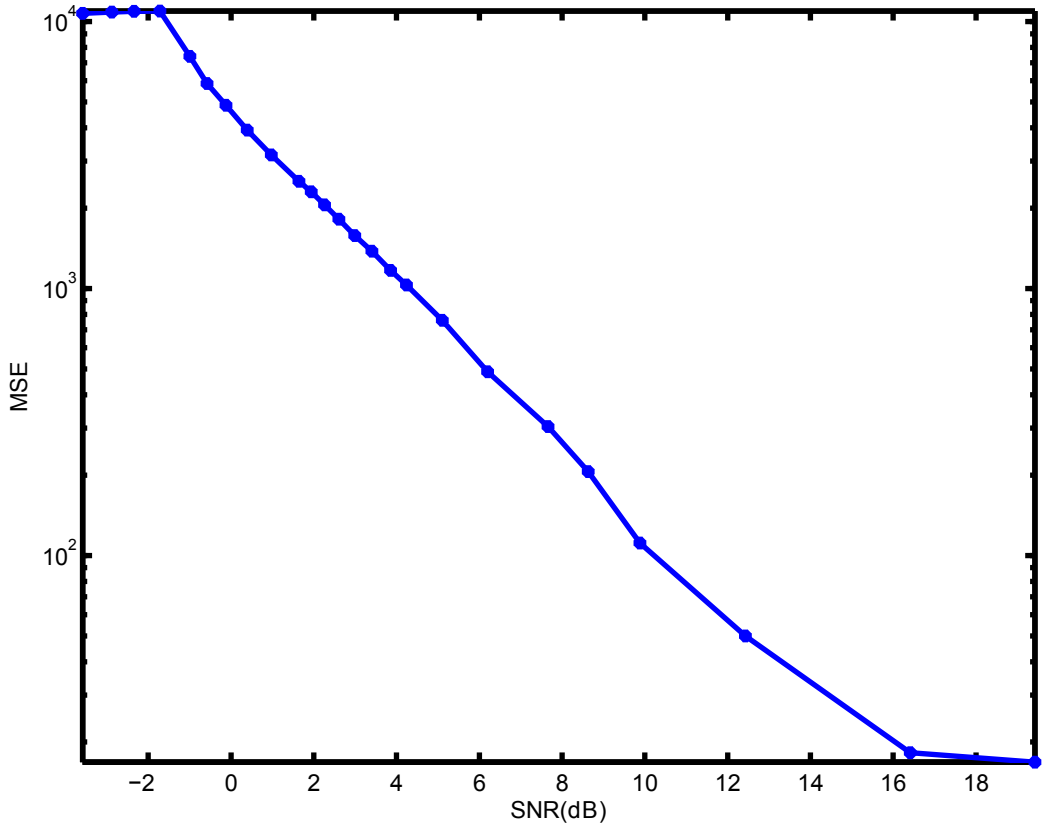

Figure 2.8: MSE against SNR with $N = 2$.

source from the hyperplane H_v. Thus, making H_v close to the source will reduce the measurement error proportionately.

2.5 Estimation of unknown radioactive sources using precisely $N + 1$ sensors

We provide a novel approach to localizing unknown radioactive sources using precisely $N + 1$ sensors in N-dimensions. We make an assumption that the source is in the convex hull of the $N + 1$ sensors.

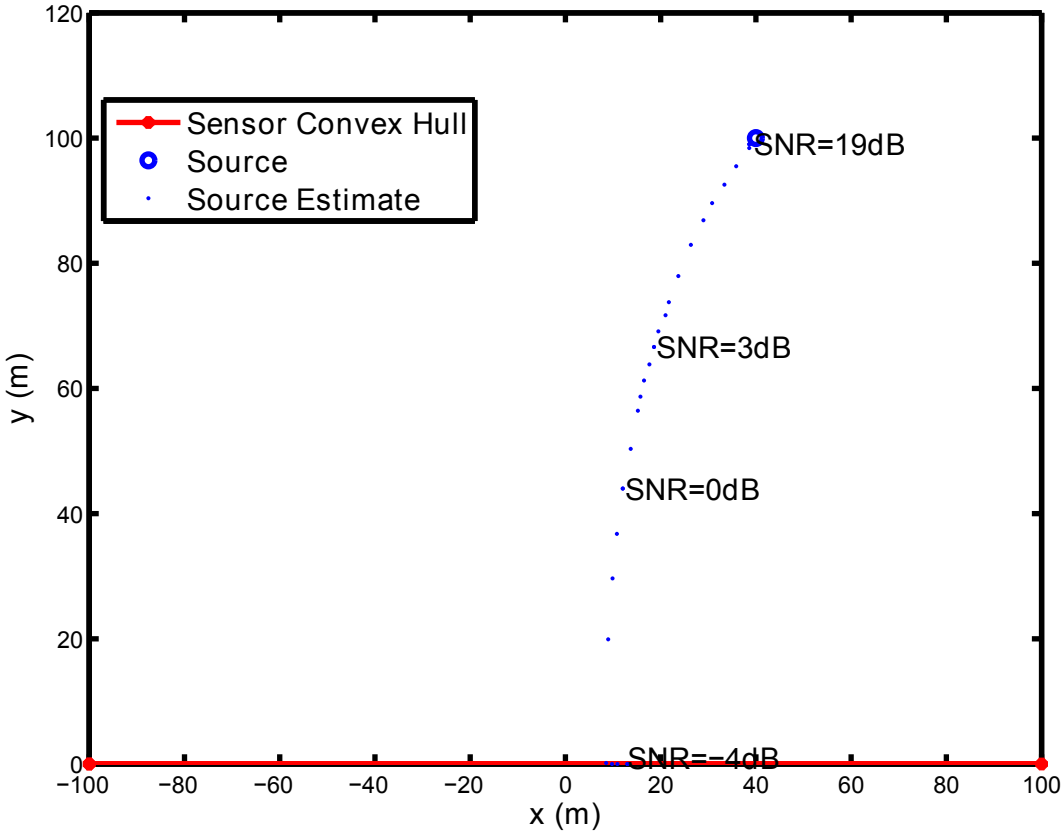

Figure 2.9: The map of the average source location estimate for various SNRs and the true source location.

Consider arbitrary $N \geq 2$ and a fairly general observation model that in the noise free case obeys

$$z_i = h(\nu_i), \nu_i = \frac{d_i}{d_1}, i \in \{2, \cdots, N+1\} \tag{2.32}$$

with d_i and d_1 as in (2.1). In the sequel, the $h(\nu_i)$ will satisfy the following assumption.

Assumption 2.5.1. *For $\nu_i > 0$, $i \in \{2, \cdots, n\}$, $h(\nu_i)$ is strictly decreasing and analytic. Further for every $\rho_1, \rho_2 > 0$, there exists $M(\rho_1, \rho_2)$ such that the $h(\nu_i)$*

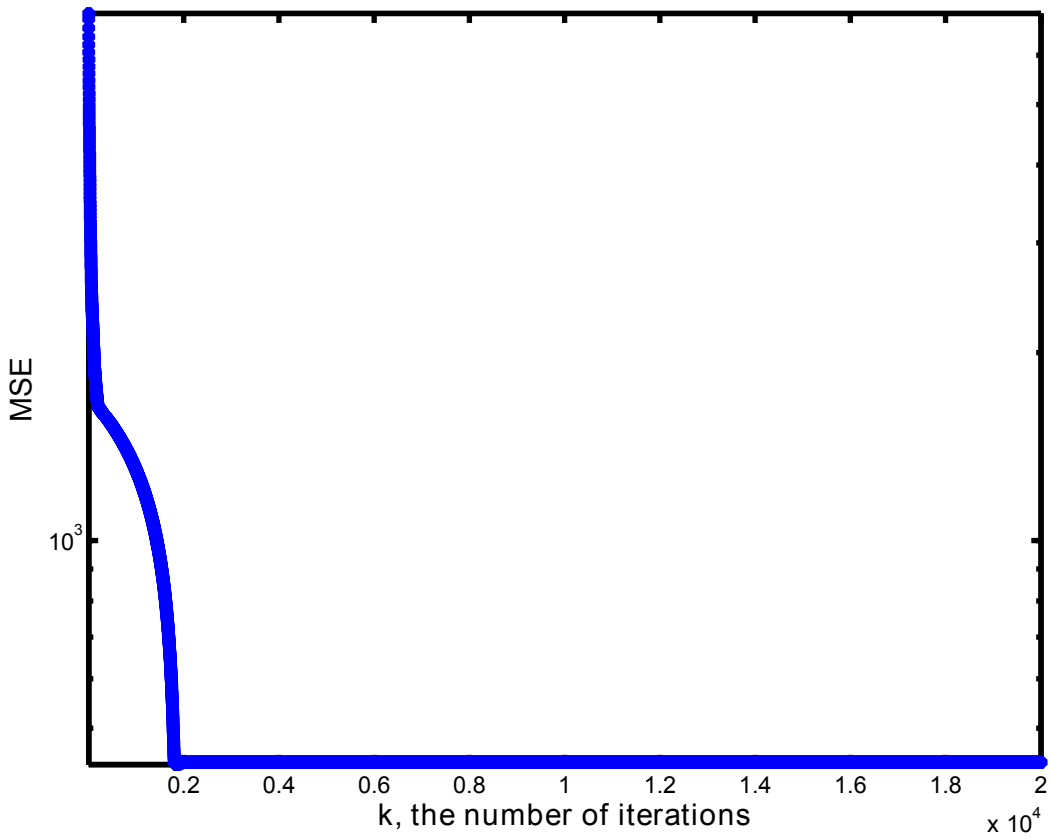

Figure 2.10: MSE vs k for SNR 6 dB.

and their first two derivatives are all bounded in magnitude by $M(\rho_1, \rho_2)$ *whenever* $\rho_1 \leq \nu_i \leq \rho_2$.

It is readily seen that with $\alpha > 0$,

$$h(\nu_i) = \frac{s_i}{s_1} = \nu_i^{-2} e^{-\alpha d_1(\nu_i - 1)} \tag{2.33}$$

obeys Assumption 2.5.1, as does the standard RSS model where $\alpha = 0$. Observe that the gradient of (2.33) is:

$$h'(\nu_i) = -h(\nu_i)\left(\frac{2}{\nu_i} + \alpha d_1\right) \tag{2.34}$$

which is non positive for $\alpha \geq 0$. Therefore $h(\nu_i)$ is strictly decreasing for $\alpha \geq 0, i \in \{2, \cdots, N+1\}$.

Now consider the cost function:

$$J(y) = \sum_{i=2}^{n} (z_i - h(\nu_i))^2 \tag{2.35}$$

Suppose the $x_i \in \mathbb{R}^N$ avoid an $(N-1)$-dimensional hyperplane. Then clearly the global minima of (2.35) is a finite set including $y = y^*$. Consequently, the gradient descent minimization of (2.35) is a candidate localization algorithm and can be implemented using (2.7). The knowledge of α and z_i in (2.33) ensures that (2.7) is implementable. Whether we can get $y = y^*$ uniquely is the subject of our main results in section 2.5.1. Observe:

$$\frac{\partial J(y)}{\partial y} = \frac{2}{d_1^2} \sum_{i=2}^{n} (z_i - h(\nu_i))\, h'(\nu_i) \left(\frac{1}{\nu_i}(x_i - y) - \nu_i(x_1 - y)\right) \tag{2.36}$$

We also note that with $h(\nu_i)$ as in (2.33), the estimate minimizing (2.35) would be the maximum likelihood estimate, if w_i in (2.2) were Gaussian and $\frac{\lambda_1}{w_i} \gg 1$. For $\frac{\lambda_1}{w_i} \gg 1$:

$$z_i = \left(\frac{\lambda_i + w_i}{\lambda_1}\right)\left(1 + \sum_{n=0}^{\infty}\left(-\frac{w_1}{\lambda_1}\right)^{n+1}\right) \approx \frac{\lambda_i}{\lambda_1} + \frac{w_i}{\lambda_1}. \tag{2.37}$$

Though in practice w_i is modeled as Poisson, high variance Poisson distributions are well approximated by Gaussian ones. In the event Theorem 2.1 applies.

2.5.1 The main result

We begin with a lemma.

Lemma 2.6. *Suppose* $\{y, y^*, x_1\} \in \mathbb{R}^N$ *obeys: (a)* $y \neq y^*$ *and (b)* $\{y, y^*\} \neq x_1$.

(I) If $\|x_1 - y\| \neq \|x_1 - y^*\|$, *then* $S = \left\{\eta \in \mathbb{R}^N \,\middle|\, \|\eta - y\| \leq \frac{\|x_1 - y\|}{\|x_1 - y^*\|}\|\eta - y^*\|\right\}$ *is an N-dimensional hypersphere.*

(II) If $\|x_1 - y\| = \|x_1 - y^*\|$, *then* $S = \left\{\eta \in \mathbb{R}^N \,\middle|\, \|\eta - y\| \leq \frac{\|x_1 - y\|}{\|x_1 - y^*\|}\|\eta - y^*\|\right\}$ *is an N- dimensional open half plane with a separating hyperplane*

$$\mathcal{H} = \left\{\eta \in \mathbb{R}^N \,\middle|\, \|\eta - y\| = \frac{\|x_1 - y\|}{\|x_1 - y^*\|}\|\eta - y^*\|\right\}.$$

Proof. Without loss of generality, suppose $x_1 = 0$. This can be attained through translation and rotation because distance measurements are invariant under translation and rotation. We abuse notation and maintain the variables y and y^* to preserve clarity. $\Leftrightarrow$

$$\begin{aligned}
(\eta - y)^T(\eta - y) &\leq \frac{\|y\|^2}{\|y^*\|^2}(\eta - y^*)^T(\eta - y^*) \\
\eta^T\eta\left(1 - \frac{\|y\|^2}{\|y^*\|^2}\right) - 2\eta^T\left(y - \frac{\|y\|^2}{\|y^*\|^2}y^*\right) &\leq -\left(\|y\|^2 - \frac{\|y\|^2}{\|y^*\|^2}\|y^*\|^2\right) \qquad (2.38) \\
\eta^T\eta\left(1 - \frac{\|y\|^2}{\|y^*\|^2}\right) - 2\eta^T\left(y - \frac{\|y\|^2}{\|y^*\|^2}y^*\right) &\leq 0 \Leftrightarrow
\end{aligned}$$

Case I: Suppose $\|y\| \neq \|y^*\|$ and without loss of generality $\|y\| < \|y^*\|$, then from (2.38)

$$\eta^T\eta\underbrace{\left(1 - \frac{\|y\|^2}{\|y^*\|^2}\right)}_{\beta^2, \beta > 0} - 2\eta^T\underbrace{\left(y - \frac{\|y\|^2}{\|y^*\|^2}y^*\right)}_{z} \leq 0 \Leftrightarrow$$

$$\eta^T\eta - 2\frac{\eta^T z}{\beta^2} + \frac{z^T z}{\beta^4} \leq \frac{z^T z}{\beta^4}$$

$$\left(\eta - \frac{z}{\beta^2}\right)^T \left(\eta - \frac{z}{\beta^2}\right) \leq \frac{z^T z}{\beta^4} \tag{2.39}$$

(2.39) is an N-dimensional hypersphere. This proves (I).

Case II: Suppose $\|y\| = \|y^*\|$, then from (2.38)

$$\eta^T \eta \left(1 - \frac{\|y\|^2}{\|y^*\|^2}\right) - 2\eta^T \left(y - \frac{\|y\|^2}{\|y^*\|^2} y^*\right) \leq 0$$

$$\eta^T (y^* - y) \leq 0 \tag{2.40}$$

(2.40) is an N-dimensional open half plane with a separating (N-1)-Dimensional hyperplane of $\eta^T (y^* - y) = 0$. This proves (II). □

Theorem 2.7. *Suppose* $\{y, y^*\} \in \mathbb{R}^N$ *obeys:*

(a) $y \neq y^*$

(b) $S = \left\{\eta \in \mathbb{R}^N \,\middle|\, \|\eta - y\| \leq \frac{\|x_1 - y\|}{\|x_1 - y^*\|} \|\eta - y^*\|\right\}$ *and*

(c) $y \in S$.

Then $y^* \notin S$.

Proof. Suppose $y^* \in S$. Chose $\eta = y^* \in S \Leftrightarrow$

$$\|y^* - y\| \leq \frac{\|x_1 - y\|}{\|x_1 - y^*\|} \|y^* - y^*\|$$

$$\|y^* - y\| \leq 0 \Leftrightarrow \tag{2.41}$$

$$y = y^*$$

This is an obvious contradiction and completes the proof. □

Lemma 2.8. *Under Assumption 2.3.2, suppose* $\{y, y^*, x_i\} \in \mathbb{R}^N, i \in \{1, \cdots, N+1\}$ *obeys:*

(a) $y \neq y^*$

(b) $\nu_i = \nu_i^*$

(c) $S = \left\{ \eta \in \mathbb{R}^N \,\middle|\, \|\eta - y\| \leq \frac{\|x_1 - y\|}{\|x_1 - y^*\|} \|\eta - y^*\| \right\}$.

Then S *is strictly an N-Dimensional hypersphere. Further* $co\{x_1, \cdots, x_{N+1}\} \subset S$.

Proof. From Assumption 2.3.2 and (b), the x_i's form an N-polytope with (N+1) vertices. The vertices of the N-polytope are the x_i's which lie on the boundary of S. Since an N-polytope cannot be formed on an (N-1) hyperplane, the x_i's cannot lie on (2.40). The x_i's lie on (2.39) which is a hypersphere. It also follows that since $co\{x_1, \cdots, x_{N+1}\}$ is a polytope with the x_i's on the boundary of the hypersphere S, the $co\{x_1, \cdots, x_{N+1}\} \subset S$. This concludes the proof. □

Theorem 2.9. *Under Assumptions 2.3.2 and 2.3.3, suppose* $\{y, y^*, x_i\} \in \mathbb{R}^N, i \in \{1, \cdots, N+1\}$ *obeys:*

(a) $\{y, y^*\} \in co\{x_1, \cdots, x_{N+1}\}$

(b) $\nu_i = \nu_i^*$ *and*

(c) $S = \left\{ \eta \in \mathbb{R}^N \,\middle|\, \|\eta - y\| \leq \frac{\|x_1 - y\|}{\|x_1 - y^*\|} \|\eta - y^*\| \right\}$.

Then $y = y^*$.

Proof. From Theorem 2.7, if $y \neq y^*$ and $y^* \in S$, then $y \notin S$. However from Lemma 2.8, S is a hypersphere and $co\{x_1, \cdots, x_{N+1}\} \subset S$ meaning if $y \neq y^*$, $y^* \notin S \Leftrightarrow y^* \notin co\{x_1, \cdots, x_{N+1}\}$. Therefore $\{y, y^*\} \in co\{x_1, \cdots, x_{N+1}\}$ if and only if $y = y^*$. This concludes the proof. □

We now complete our results by showing that $N+1$ measurements in N-Dimensions is enough to localize a source in the convex hull of N+1 sensors even if A is unknown.

Our final result shows that should the source lie in the open convex hull of the sensors, and should there be precisely the minimum number of sensors required to estimate the source, then the open convex hull of the sensors is bereft of false stationary points. Further there is exactly 1 optimum in the convex hull.

Theorem 2.10. *Consider (2.35) under assumptions 2.5.1, 2.3.2 and 2.3.3. Consider* $y \in co\{x_1, \cdots, x_{N+1}\}$. *Then there holds:*

$$\frac{\partial J(y)}{\partial y} = 0 \Leftrightarrow J(y) = 0.$$

Proof. From (2.15) and (2.16) we obtain:

$$\sum_{i=1}^{N+1} \beta_i x_i = \left(\sum_{i=1}^{N+1} \beta_i\right) y \Leftrightarrow \sum_{i=1}^{N+1} \beta_i (x_i - y) = 0.$$

In other words $\beta = [\beta_1, \cdots, \beta_{N+1}]^\top$ is in the right nullspace of the matrix: $\mathcal{X}(y) = \begin{bmatrix} x_1 - y & \cdots & x_{N+1} - y \end{bmatrix}$. As the x_i's do not lie on an $(N-1)$-dimensional hyperplane $\mathcal{X}(y)$ has rank N for all $y \in \mathbb{R}^N$. Thus its nullspace has dimension 1, and as $\beta_i > 0$, all its non-zero null vectors have elements that are either all positive, or are all negative. Now suppose

$$\frac{\partial J(y)}{\partial y} = 0. \tag{2.42}$$

Notice that (2.34) can be re-written as:

$$\frac{\partial J(y)}{\partial y} = \frac{2}{d_1^2} \sum_{i=2}^{n} \left(z_i - h(\nu_i)\right) h'(\nu_i) \frac{1}{\nu_i} \left((x_i - y) - \nu_i^2 (x_1 - y)\right) \tag{2.43}$$

Define:

$$\xi_i = \frac{2}{d_1^2} \sum_{i=2}^{n} \left(z_i - h(\nu_i)\right) h'(\nu_i) \frac{1}{\nu_i} \tag{2.44}$$

and

$$\xi_1 = -\sum_{i=2}^{n} \xi_i \nu_i^2 \tag{2.45}$$

and notice that we can substitute (2.44) and (2.45) in (2.43) to obtain

$$\frac{\partial J(y)}{\partial y} = \frac{2}{d_1^2} \sum_{i=1}^{N+1} \xi_i (x_i - y) \tag{2.46}$$

From (2.46) , $\xi = [\xi_1, \cdots, \xi_{N+1}]^\top$ is in the right null space of $\mathcal{X}(y)$ if $\frac{\partial J(y)}{\partial y} = 0$. Now suppose $\xi \neq 0$. Then every ξ_i is either positive or every one of them is negative. Suppose $\xi_i > 0, i \in \{2, \cdots, N+1\}$.Then $\xi_1 < 0$ from (2.45). Similarly suppose $\xi_i < 0, i \in \{2, \cdots, N+1\}$.Then $\xi_1 > 0$ from (2.45). This is an obvious contradiction. Therefore $\xi_i = 0, i \in \{1, \cdots, N+1\}$.

From Assumption 2.5.1, $\{h'(\nu_i), h'(\nu_i^*)\} < 0$ for all i. Thus, the strict monotonicity of the $h(\nu_i)$ ensures that for all $i \in \{2, \cdots, N+1\}$, $z_i = h(\nu_i)$ using (2.44). Since $z_i = h(\nu_i^*)$ in the noise free case, $h(\nu_i^*) = h(\nu_i) \Rightarrow$

$$\nu_i = \nu_i^*, i \in \{1, \cdots, N+1\} \tag{2.47}$$

As both y and y^* are in $co\{x_1, \cdots, x_{N+1}\}$, Theorem 2.9 precludes the possibility of (2.47) if $y \neq y^*$.

Thus $\xi = 0$, $y = y^*$, and from (2.44), (2.45) and (2.35), $J(y) = 0$. On the other hand if $J(y) = 0$, then clearly from (2.7), (2.42) holds. □

Remark 2.3. The result is counter intuitive; that we can still estimate the radioactive source with precisely $N+1$ having an additional unknown variable A. We can show this result to be true in the 1-D case for the conventional RSS model where path loss coefficient $\alpha = 0$ in (2.2). In this case, two sensor measurements is sufficient to localize the source even though there is an additional unknown parameter A. Consider Figure 2.11. With $\alpha = 0$, the ratio of the measurements at the two sensor measurements

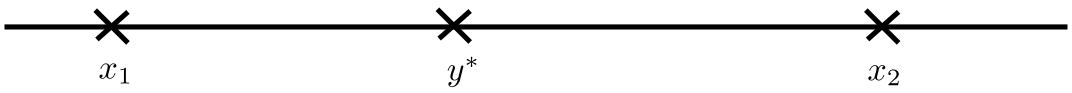

Figure 2.11: Illustration of a source in the convex hull of two sensors

will result in one equation:

$$z_2 = \frac{1}{\nu_2^2} \tag{2.48}$$

Suppose $z_2 = c^2$ for some $c > 0$. Then any solution y must satisfy

$$(y - x_1)^2 = c^2(y - x_2)^2. \tag{2.49}$$

Also, with the knowledge that the source lies in the convex hull of x_1 and x_2, $\exists \beta_i > 0, i \in \{1, 2\}$ such that

$$\sum_{i=1}^{2} \beta_i (y - x_i) = 0$$

$$\beta_1(y - x_1) + \beta_2(y - x_2) = 0$$

$$y = \frac{\beta_1}{\beta_1 + \beta_2} x_1 + \left(1 - \frac{\beta_1}{\beta_1 + \beta_2}\right) x_2. \tag{2.50}$$

Let $\frac{\beta_1}{\beta_1+\beta_2} = \beta$ where $0 < \beta < 1$. (2.50) can now be written as

$$y = \beta x_1 + (1-\beta)\, x_2. \tag{2.51}$$

We can now solve (2.49) and (2.51) for β.

$$((\beta-1)x_1 + (1-\beta)x_2)^2 = c^2(\beta x_1 - \beta x_2)^2$$

$$(1-\beta)^2(x_2-x_1)^2 = \beta^2 c^2 (x_1-x_2)^2$$

$$\left(\frac{1}{\beta} - 1\right)^2 = c^2$$

$$\left(\frac{1}{\beta} - 1 - c\right)\left(\frac{1}{\beta} - 1 + c\right) = 0 \tag{2.52}$$

From (2.52), either $c = \frac{1}{\beta} - 1$ or $c = 1 - \frac{1}{\beta}$. Since $1 - \frac{1}{\beta} < 0$ and $c > 0$ because $0 < \beta < 1$, there is only one unique solution of β: $\beta = \frac{1}{1+c}$. Notice that, this confirms theorem 2.10 for the 1-dimensional conventional RSS model. There are **two** solutions but only **one** is in the convex hull of x_1 and x_2 and for this solution $y = y^*$.

Remark 2.4. We observe that theorem 2.10 also holds if the strictly decreasing nature of all the $h(\nu_i)$ is replaced by their being strictly increasing.

Thus should the source be in the open convex hull of $N+1$ sensors avoiding any $N-1$-dimensional hyperplane, there is only 1 optimum in the convex hull and the convex hull is also devoid of any false mimima. Localization is therefore guaranteed provided the location estimate never leaves the convex hull.

In practice however, it may leave the convex hull, even if the initial estimate is in the convex hull. To combat this, consider the following augmented gradient descent algorithm. If in (2.7), $y[k+1] \notin co\{x_1, \cdots, x_{N+1}\}$, then choose $y[k+1]$ to

be a randomly chosen point inside the open convex hull. We now argue that such a projection based algorithm will converge in probability as long as the source is inside the open convex hull. Define $\bar{J}$ to be minimum value of $J(y)$ at the boundary of $co\{x_1, \cdots, x_{N+1}\}$, and

$$S = \left\{ y \in \mathbb{R}^N \,\middle|\, J(y) < \bar{J} \right\} \bigcap co\{x_1, \cdots, x_{N+1}\}.$$

This set has nontrivial extent as $y^* \in co\{x_1, \cdots, x_{N+1}\}$, and $J(y^*) = 0$. Thus with probability 1, there exists k_1 such that a projected estimate at k_1 will enter this set. As $S \subset co\{x_1, \cdots, x_{N+1}\}$ in view of Theorem 2.10, S satisfies (I) and (II) of Theorem 2.1 and convergence in probability follows. In practice, simulations presented in the next section show, that estimates leave the convex hull very rarely, and that too only at very low SNR values.

2.5.2 Simulation results

We consider two simulation examples; one with $N = 2$, the other with $N = 3$. In both cases we use $n = N + 1$. The received signal at sensor i is: $s_i \sim$ poisson $\left(\frac{A}{d_i^2} e^{-\alpha d_i} + w \right)$ and w is the background noise. The SNR is computed as:

$$SNR = 10 \log_{10} \left(\frac{\sum_{i=1}^{N+1} \frac{A e^{-\alpha d_i}}{d_i^2}}{\sum_{i=1}^{N+1} w} \right) = 10 \log_{10} \left(\frac{\sum_{i=1}^{N+1} \frac{A e^{-\alpha d_i}}{w d_i^2}}{N+1} \right).$$

In all cases $\alpha = 0.0068$, $A = 2 \times 10^7$. $\mu = 20$ for $N = 2$ and $\mu = 12$ for $N = 3$. The mean squared error (MSE) is averaged over 5000 random initial start points all within the convex hull of the sensors. The algorithm runs for 1000 iterations for both $N = 2$ and $N = 3$. Also, for each iteration of each run, the s_i's are Poisson and

generated independently. A projection augmented gradient descent minimization of (2.35) under (2.33) is performed. The fact that the actual s_i differ from the value used in generating the gradient, confirms the robustness of the algorithm to uncertainties in the s_i with unknown A.

Figure 2.12 depicts performance when $N = 2$. The sensors are at (-100,-100), (100,-100) and (-50,100), the source is at (20,-40),$\in co\{x_1, \cdots, x_{N+1}\}$. Figure 2.13 presents the map of the average location estimate provided by our algorithm for various SNR values, as well as the actual source location. Figure 2.14 is for gauging the convergence speed. For an SNR of 6dB it plots the MSE as a function of the iteration index k. The MSE at each value of k is obtained by averaging over the 5000 random runs described above. The fast rate of convergence is self-evident.

The 3-dimensional counterpart of Figure 2.12 is depicted in Figure 2.15. The sensors are at (-100,-100,0), (100,-100,0), (-50,100,0) and (0,100,100) and the source is at (20,-40,5). The performance is depicted in figure 2.15.

A noteworthy fact about all these simulations is that except in low SNR regimes, the estimates do not leave the convex hull. Even with low SNRs they leave the convex hull only about 1% of the time. Further, the expectation of the signal at the sensors in the absence of noise are very small. For $N = 2$ the received signals devoid of noise are $[446, 1013, 281]^T$ whiles those for $N = 3$ are $[445, 1010, 281, 216]^T$. The simulations show the robustness of our algorithm.

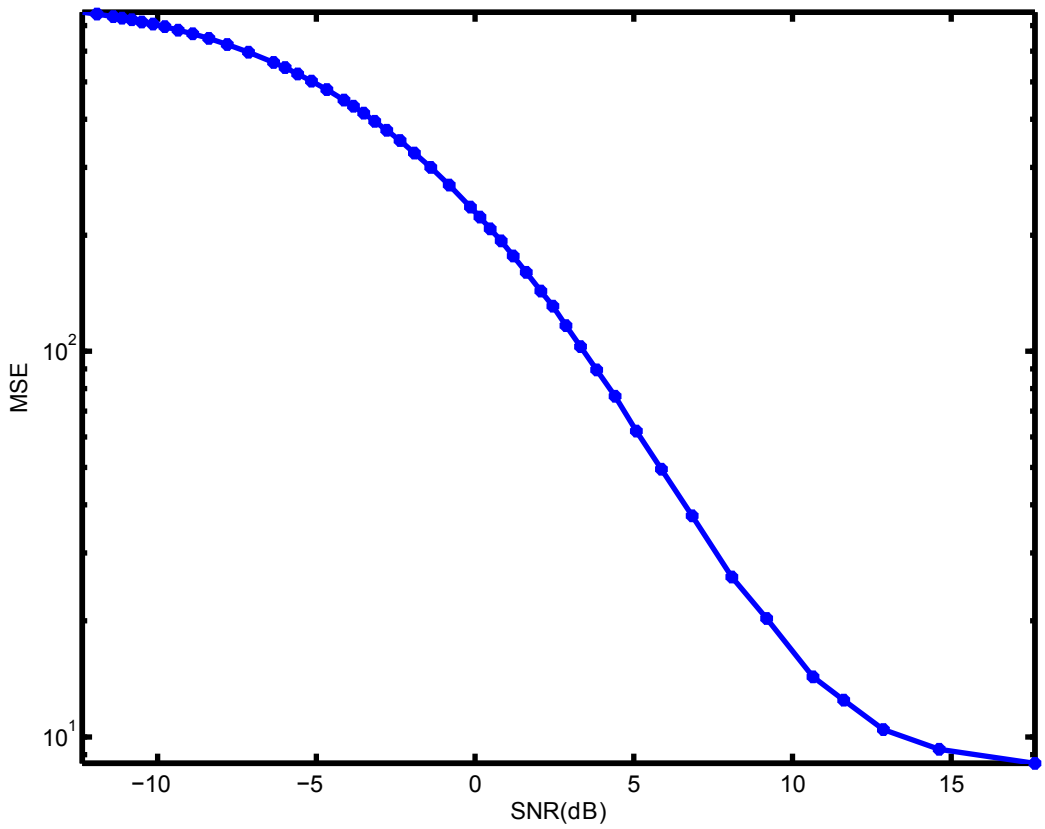

Figure 2.12: MSE against SNR with $N = 2$.

2.6 Conclusion

We have considered projection based gradient descent estimation of known and unknown radioactive sources from gamma ray counts using the smallest number of measurement sensors under three general assumptions. Our algorithms are all devoid of false stationary points and achieve global uniform asymptotic convergence in probability. Simulations demonstrate robustness of our algorithms. Our results in this chapter apply to a much wider class of signal models than just (2.2). In Chapter 3, we consider tracking of radioactive sources using cheap binary proximity

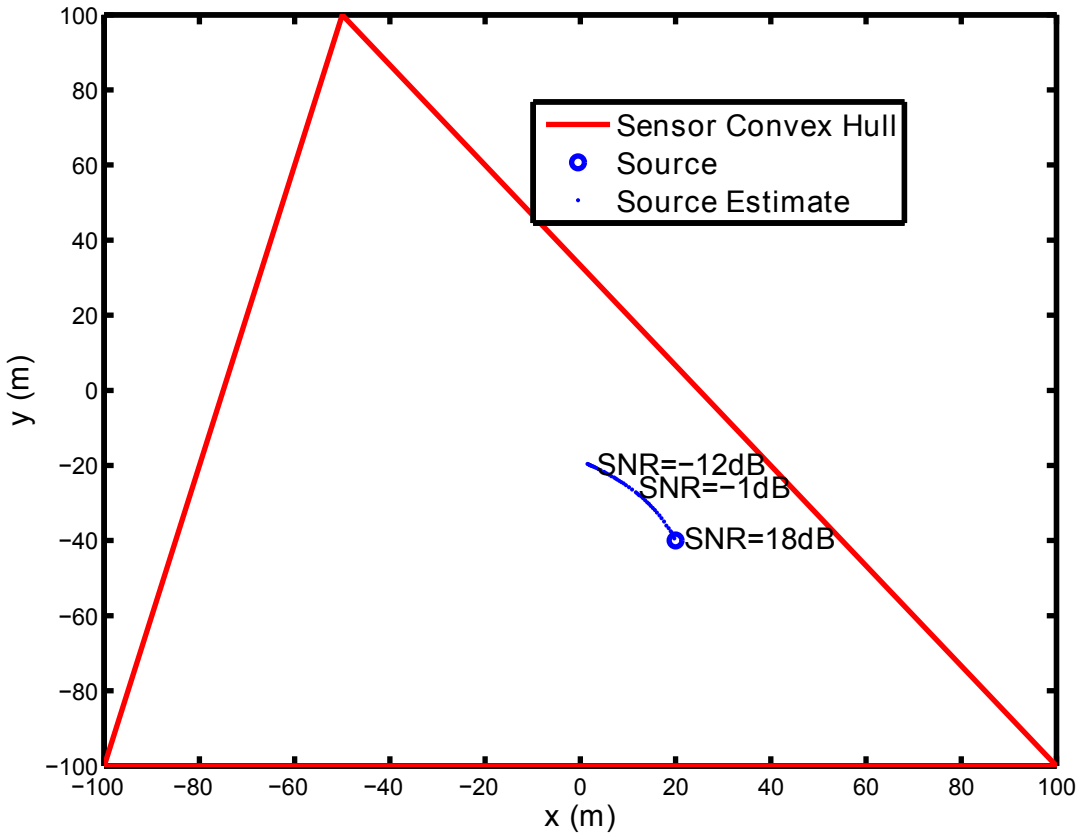

Figure 2.13: The map of the average source location estimate for various SNRs and the true source location.

sensors. We are interested in tracking radioactive sources moving on piece-wise linear trajectories.

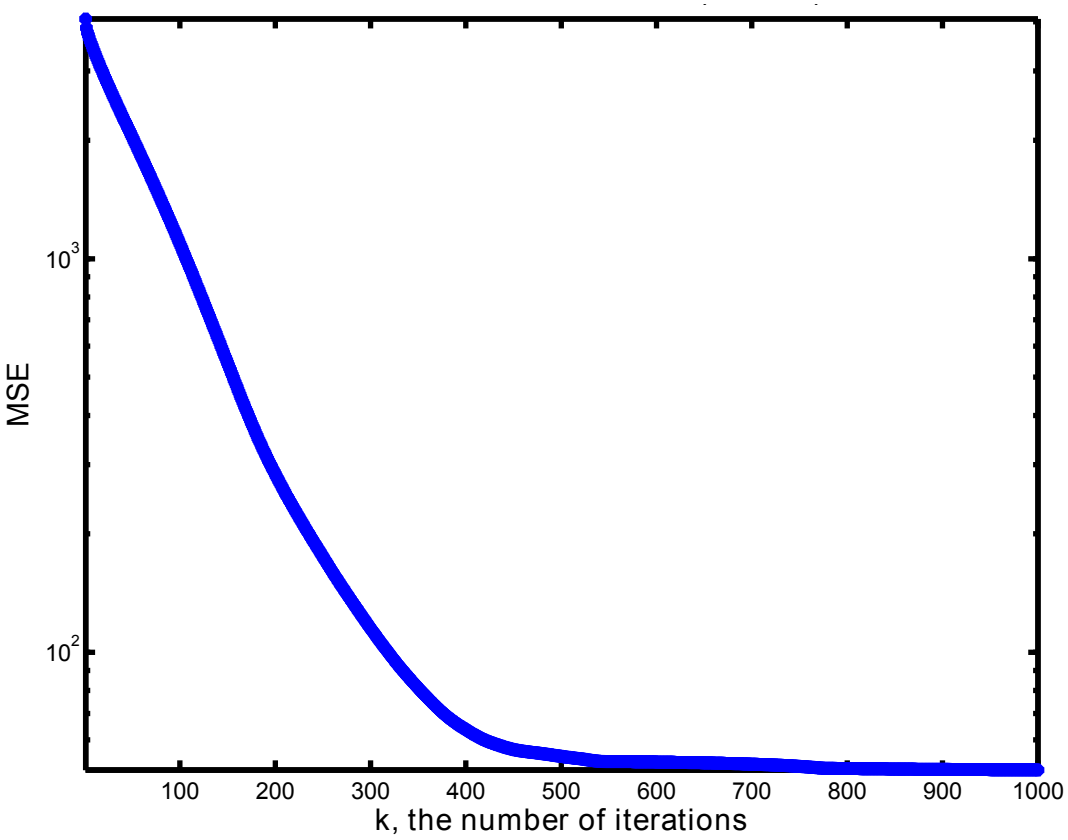

Figure 2.14: MSE vs k for SNR 6 dB.

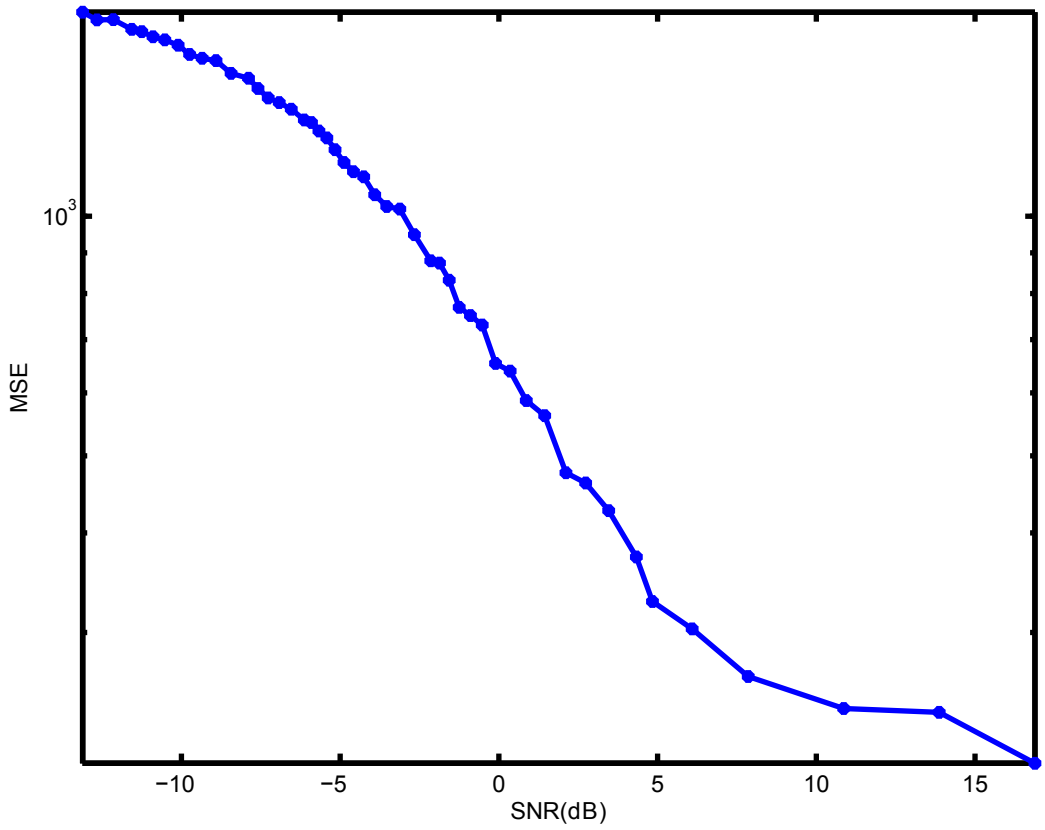

Figure 2.15: MSE against SNR with $N = 3$.

CHAPTER 3
TRACKING OF RADIOACTIVE SOURCES WITH CHEAP BINARY PROXIMITY SENSORS

3.1 Introduction

In this chapter, we describe and provide novel approaches to tracking radioactive sources on piecewise linear trajectories through a network of binary proximity sensors.

We consider a network of inexpensive and simple binary proximity sensors as a way to handle this fundamental issue. This is in keeping with the basic philosophy of large-scale sensor networks [30] that favors distributed networks of simple, inexpensive, disposable sensors to a small number of complex, expensive ones. We allow individual sensors to be simple, inaccurate and vulnerable to drift and calibration errors, and rely on statistical robustness by combining the observations of many sensors. With noisy sensors, it is also possible to radically quantize observations [31] with little sacrifice in performance.

We ask the following fundamental question: How many binary sensors are needed to track an object moving on an unknown piece-wise linear trajectory *with unknown speed?* We are motivated by the observation that inertial and other dynamical constraints restrict most trajectories to be smooth; and smooth trajectories can be arbitrarily well approximated by piece-wise linear trajectory joins. We assume that all sensors have the same sensing range and know their neighbor's location.

In the first major result, we show that three generically placed sensors can

uniquely determine almost all linear trajectories that intersect with their sensing range, if the nominal sensing range is known, simply by observing the times at which the target enters and leaves these sensing ranges. In the second major result, we show that four generically placed sensors can uniquely determine almost all linear trajectories that intersect with their sensing range, even if the nominal sensing range is not known, simply by observing the times at which the target enters and leaves these ranges. We do not require these sensors to have overlapping sensing ranges in both results. This naturally extends to piece-wise linear trajectories. We also show that under the assumption of uniformly distributed sensors, vanishingly small densities can uniquely determine a straight line trajectory with vanishingly small error probability. Thus, the sensor density required to almost surely track an arbitrary trajectory with a prescribed error is determined only by the number of straight lines needed to approximate that trajectory to that error level. This contrasts with say [22] where straight line trajectories are approximated by averaging the locations of the sensors whose sensing ranges they cross. Consequently, even in the zero noise case, achieving a prescribed level of accuracy in tracking a linear trajectory cannot be thus limited. Even though, the problem of determining the points of intersection of a straight-line trajectory with the coverage area of a binary sensor is non-linear, our first result, the case of known nominal sensing range, presents a linear reformulation of the tracking problem that allows a simple least-squares solution. Based on the linear reformulation, we present a practical, computationally efficient algorithm to solve the piecewise linear trajectory estimation problem. We present an extensive

set of simulations to illustrate the performance of our proposed approach and its robustness to sensor errors and uncertainties. Our second result also leads to a Newton based iterative algorithm which relies solely on the "*on*" and "*off*" times denoting a radioactive source entering and leaving the unknown sensing range of a sensor respectively.

Consider a stationary source located at $y^* \in \mathbb{R}^2$, and binary proximity sensors located at $x_i \in \mathbb{R}^2$. Define $d_i = \|x_i - y^*\|$ where $\|\cdot\|$ denotes the 2-norm. The sensors themselves can be a number of portable and non-portable gamma-ray spectrometers [6] which produce an indicator signal I_i, dependent on the total gamma-ray counts received [5]:

$$I_i = \begin{cases} 1, & \text{if } Poisson\left(\frac{Ae^{-\alpha d_i}}{d_i^2} + w_i\right) \geq T_d \\ 0, & \text{if } Poisson\left(\frac{Ae^{-\alpha d_i}}{d_i^2} + w_i\right) < T_d \end{cases} \tag{3.1}$$

A, α and w_i are as defined in Chapter 2. T_d is a predetermined threshold above the background noise to trigger sensor measurements. We are interested in using the transitions, 0-1 and 1-0, which define the "on" and "off" times of the binary proximity sensor to localize the trajectory of the source.

In principle knowledge of the A (or of their mean), α and the "*on*" and "*off*" time measurements provide a noisy estimate of d_i's at those points which is an estimate of the sensing range $r + \Delta_r$ of the sensor where r is the nominal range in the absence of noise. It is obvious that the sensing range is a function of the statistics of the source even in the absence of noise. We consider two cases; a priori knowledge of r and otherwise for a given source and threshold T_d. This brings us to our key

contributions.

3.2 Summary of our contributions

First, we translate a highly nonlinear problem, for a known nominal sensing range of sensors, of finding the parameters of a line which intersects the sensing range of a number of sensors into a finite set of linear equations. Infact, we reduce the problem to a tangent finding problem. We also show that three sensors are enough to uniquely localize a portion of the linear trajectory with probability one. We finally show that a line passing through a uniformly distributed sensor network with common sensing range will intersect with three sensors with probability one.

Second we tackle tracking of a source with unknown nominal sensing range of sensors. We consider a class of natural, non-convex cost functions, applicable to observation models much more general than (3.1). We show that when $n = 4$ in 2-Dimension space, i.e. a minimum number of sensors is deployed, an iterative descent minimization of such cost functions converges to the true trajectory with probability 1 for a source moving on a piecewise linear trajectory with constant but unknown speed and nominal sensing range r.

3.3 Tracking of radioactive sources with known nominal sensing range r

Consider a region of interest $\mathcal{D} \subset \mathbb{R}^2$ over which we would like to track a moving object, and a binary sensor network of N sensors which are deployed over the region. Let (x_i, y_i)'s, $i = \{1, 2, ..., N\}$ denote the locations of the sensors. Each sensor continuously monitors the received signal strength of the object of interest and

compares it with a prescribed threshold as shown in (3.1). The entire measurement history of a binary sensor can be fully summarized as a set of time-stamps of the instants when the object enters or leaves the sensing region of the sensor.

We assume here that all sensors are homogeneous, i.e. that all sensors have the same nominal sensing range $r > 0$. This is of course an ideal case; in practice each sensor has a sensing range $r + \Delta_i$, $i = \{1, 2, ..., N\}$ that deviates from the nominal range because of calibration errors or model uncertainties. We initially consider ideal sensors and subsequently generalize to more realistic models manifested with uncertainties.

3.3.1 Tracking with known constant speed s

Consider an object that moves on a straight line L in the Cartesian coordinate system with a known speed s. Suppose the object passes through the sensing ranges of three binary sensors (small circles) with "on" and "off" times (i.e. the timestamps of the entry and exit time instants) τ_{i1} and τ_{i2}, $i = \{1, 2, 3\}$ respectively. Since the time interval $\tau_{i2} - \tau_{i1}$ and the speed s are available, the chord lengths produced by the line in the three small circles can be calculated as $2d_i = s(\tau_{i2} - \tau_{i1}), i = \{1, 2, 3\}$. The following fact is self-evident.

Lemma 3.1. *A line intersects a circle of radius r with the chord lengths $2d$, if and only if the line is a tangent to the concentric circle of radius $\sqrt{r^2 - d^2}$.*

Next we consider a lemma that appeals to the notion of *homothetic centers*. Specifically, the homothetic centers of two similar geometric figures are defined as

points from which both the figures can be seen as a dilation/contraction of one another [32]. Thus, the internal and external homothetic centers for two circles are as shown in Figure 3.1 (a) as the points of intersection of the internal and external tangents respectively.

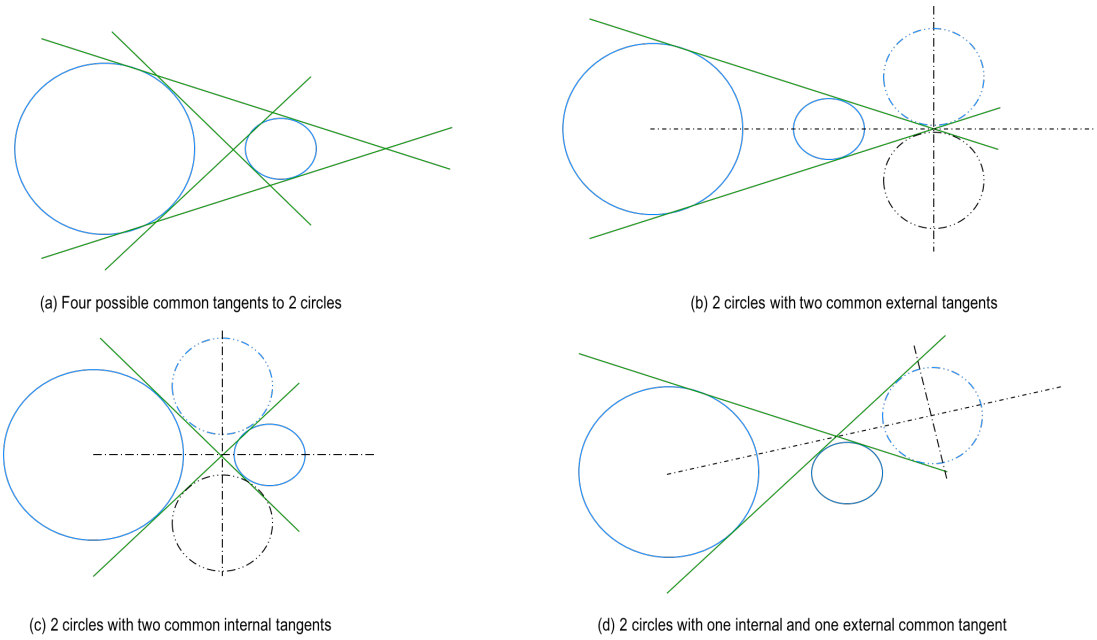

Figure 3.1: Scenarios that will present non unique tangent to three circles

Lemma 3.2. *Consider three non-overlapping circles with noncollinear centers. Suppose there are two distinct lines that are tangents to all three circles. Then the center of one of the circles must be on a line that is perpendicular to the line connecting the other centers of the other two circles and passes through one of their homothetic centers.*

Proof. For two non-overlapping circles, there are four possible shared tangent lines as shown in Figure 3.1(a). We have three possibilities where the third circle is non-collinear and shares two tangent lines with both the first two circles. The shared tangent lines could be one of the following:

1. Two external tangents as in Figure 3.1 (b) if the first two circles have different radii.

2. Two internal tangent lines as in Figure 3.1 (c)

3. A pair of lines, one external tangent and one internal tangent as in Figure 3.1 (d). Note, however, that this case is exactly the same as in Figure 3.1(c) by swapping two circles.

In view of the last point only the first two cases need be considered. In both cases consider the circle depicted by dashed lines. As it is tangent to both external tangent lines, the center of this circle is on the line that is perpendicular to the line connecting the centers of the first two circles. Also the same line has to pass through the homothetic center [32]. This completes the proof. □

Using this result, we now consider the question of whether the line representing the object trajectory is generically, uniquely determined by a set of three chord lengths, $2d_i$, $i = \{1, 2, 3\}$, from three sensors.

Theorem 3.3. *Consider a straight line L, and a set of three points (x_i, y_i), $i \in \{1, 2, 3\}$ that obey the following:*

(i) The (x_i, y_i), $i \in \{1, 2, 3\}$ *are mutually independent and uniformly distributed in* $\mathcal{D} \subset \mathbb{R}^2$.

(ii) The circles with radius r *centered on* (x_i, y_i) *are non-overlapping.*

(iii) The straight line L *intersects these three circles with chord lengths* $2d_i$.

Then the (x_i, y_i), r *and* d_i *uniquely determine the line* L, *with probability 1.*

Proof. Because of Lemma 3.1, the chord lengths $2d_i$ define three circles of radii $\sqrt{r^2 - d_i^2}$, respectively centered at the points (x_i, y_i), to which the line is simultaneously tangent. Conditioned on (i-iii), with probability 1, these circles will have non-collinear centers and the center of no circle will be on the line that (a) is perpendicular to the line connecting the centers of other two circles and (b) passes through a homothetic center of the latter. Then from Lemma 3.2 this line is uniquely determined from (x_i, y_i), r and d_i with probability 1. □

If an object travels with known speed on a straight line that intersects the sensing ranges of three generically placed circles, then the chord lengths $2d_i$ can be determined from $s(\tau_{i2} - \tau_{i1})$. Thus, Theorem 3.3 proves that such a line can be uniquely determined for with probability 1.

3.3.1.1 Efficient numerical solution for tracking with known speed s

Theorem 3.3 shows that given the measurements of three binary sensors, a straight line trajectory can be uniquely determined with high probability. We now consider the problem of designing an algorithm to estimate the trajectory from the

measurements. One obvious possibility is to calculate the intersecting points of the line and circles by directly solving $ax + by + c = 0$ jointly with

$$(x - x_i)^2 + (y - y_i)^2 = r^2, \ \ \forall\, i \in \{1, 2, 3\}.$$

Note that this is a nonlinear (quadratic) equation in the a, b, c coefficients. More importantly, this direct procedure is not easily generalizable to the case of unknown speed s, or unknown sensing ranges. We present here an alternative method that is accurate yet practical and efficient, and which is also easily generalized to more realistic sensing models tackled in subsequent sections.

We start by noting that the trajectory estimation problem can be reduced to the problem of finding a shared tangent line to three circles of radius $\sqrt{r^2 - d_i^2}$ centered at (x_i, y_i), $i = \{1, 2, 3\}$ respectively, where $2d_i = (\tau_{i2} - \tau_{i1})s$. Observe the distance of the line $ax + by + c = 0$ to the centers (x_i, y_i) are $\frac{|ax_i + by_i + c|}{\sqrt{a^2+b^2}} = \sqrt{r^2 - d_i^2}$, $i = \{1, 2, 3\}$, or in matrix form, for particular sign choices:

$$\underbrace{\begin{pmatrix} x_1 & y_1 & 1 \\ x_2 & y_2 & 1 \\ x_3 & y_3 & 1 \end{pmatrix}}_{A_3} \begin{pmatrix} \alpha \\ \beta \\ \gamma \end{pmatrix} = \underbrace{\begin{pmatrix} \pm\sqrt{r^2 - d_1^2} \\ \pm\sqrt{r^2 - d_2^2} \\ \pm\sqrt{r^2 - d_3^2} \end{pmatrix}}_{e_3} \tag{3.2}$$

subject to $\alpha^2 + \beta^2 = \frac{a^2}{a^2+b^2} + \frac{b^2}{a^2+b^2} = 1$.

Notice that (3.2) can be derived alternately. Define $\alpha = \frac{a}{\sqrt{a^2+b^2}}, \beta = \frac{b}{\sqrt{a^2+b^2}}$ and $\gamma = \frac{c}{\sqrt{a^2+b^2}}$, then the line $ax + by + c = 0$ can be written as $\alpha x + \beta y + \gamma = 0$. The points of intersection of this line and a circle centered at (x_i, y_i) and radius r is

given by

$$\{x_{(1)}, x_{(2)}\} = \frac{2x_i - 2\frac{\alpha}{\beta}\left(\frac{\alpha}{\beta} + y_i\right) \pm \sqrt{\left(2x_i - 2\frac{\alpha}{\beta}\left(y_i + \frac{\gamma}{\beta}\right)\right)^2 - \frac{4}{\beta^2}\left(x_i^2 + \left(y_i + \frac{\gamma}{\beta}\right)^2 - r^2\right)}}{\frac{2}{\beta^2}} \tag{3.3}$$

which reduces to

$$\{x_{(1)}, x_{(2)}\} = \frac{2x_i - 2\frac{\alpha}{\beta}\left(\frac{\alpha}{\beta} + y_i\right) \pm \frac{2}{\beta}\sqrt{r^2 - (\alpha x_i + \beta y_i + \gamma)^2}}{\frac{2}{\beta^2}} \tag{3.4}$$

A chord length $2d_i$ with intersections as in (3.4) is equivalent to $\frac{\|x_{(1)} - x_2\|}{\beta}$ and leads to

$$d_i = \sqrt{r^2 - (\alpha x_i + \beta y_i + \gamma)^2} \tag{3.5}$$

from which (3.2) is obtained. The solution can be easily calculated by for instance the least squares solution

$$\begin{pmatrix} \alpha \\ \beta \\ \gamma \end{pmatrix} = (A_3^T A_3)^{-1} A_3^T e_3 \tag{3.6}$$

$$\text{subject to } \alpha^2 + \beta^2 = 1. \tag{3.7}$$

Note that as stated the expression in (3.6) is more complicated than it needs to be; since for 3 sensors A_3 is a square matrix, its pseudo-inverse in (3.6) can be replaced with an inverse, i.e. (3.6) can be simplified to

$$\begin{pmatrix} \alpha \\ \beta \\ \gamma \end{pmatrix} = A_3^{-1} e_3 \tag{3.8}$$

We will, however, work with the expression in (3.6) which unlike (3.8) generalizes in a straight-forward way to arbitrary number of sensors.

There are four solutions (there are eight total possible combinations of the $\pm$ signs in (3.2) from which we obtain four distinct sets of equations of the form (3.6)). Under the conditions of Theorem 3.3 we know that with probability 1, only one solution exists, i.e., only one of the four possible equations combinations satisfies $\alpha^2 + \beta^2 = 1$. A natural algorithm thus emerges.

By the results in the previous section, with probability one only one solution exists, i.e., only one solution satisfies $\alpha^2 + \beta^2 = 1$ which gives rise to the line $\alpha x + \beta y + \gamma = 0$ as summarized in the following theorem.

Theorem 3.4. *Let the centers (x_i, y_i)'s be iid uniformly distributed in $\mathcal{D} \in R^2$. Consider the 4 estimates given by (3.6) (the other 4 are symmetric). With probability 1, there is only one satisfying $\alpha^2+\beta^2 = 1$ which gives rise to the line $\alpha x+\beta y+\gamma = 0$.*

3.3.1.2 Path direction change

If the unknown object moves along a line and triggers three or more binary sensors, the sensor on-off times together with the available speed provided can be used to determine the path of the object uniquely from (3.6) and (3.7). Note however that the path is assumed to be a combination of line segments and thus the object may change its direction. A consequence is that there does not exist a line passing through the sensing range of the most recently triggered sensor and the sensing ranges of the previous two consecutively triggered sensors. In short, equations (3.6) and (3.7) do

not have any solution. On the other hand, however, it provides an indication that the object changes its movement direction. Now we are in a position to state the detection algorithm.

Algorithm 3.1 Least squares iterative search algorithm:

Step 0: Wait until the path triggers three sensors.

Step 1: Calculate d_i and $\sqrt{r^2 - d_i^2}$. Determine if a solution of (3.6) and (3.7) exists.

- If such a solution exist, the line $\alpha x + \beta y + \gamma = 0$ is uniquely determined. Find the intersecting points of the line and three circles and connect these points by a line segment. Go to Step 2.
- If such a solution does not exists, connect the center of the most recent triggered sensor with the end point of the previously calculated line segment. Go to Step 2.

Step 2: Wait until the path triggers another sensor. Combine the on-off times of the sensor with the information provided by two previously consecutively triggered sensors. Go to Step 1.

3.3.2 Tracking with unknown constant speed s

The preceding, assumes that the speed of the object is known at all times which permits us to determine chord lengths from time-stamps. In addition, it also assumes

that the sensing ranges of different sensors are non-overlapping. We now show how our approach can be extended to relax these assumptions. The basic idea is to work with *ratios* of chord length over short distances where the constant *(though unknown)* speed approximation holds. The chord ratios under constant speed assumption have to be equal to the corresponding ratios of time durations, which can be calculated from the time-stamp measurements of the binary sensors.

We start by noting that from Theorem 3.3, even when the object speed is unknown, if we know that a line L is tangent to three circles of known radii, then barring pathologies, this line will be unique. So in the following, we may assume that the line will produce at least one non-zero chord, say $(\tau_{12} - \tau_{11})s \neq 0$. Secondly, even without knowing the speed, the time intervals $\tau_{i2} - \tau_{i1}$ and the chord length *ratios*,

$$\frac{l_i}{l_1} = \begin{cases} \frac{(\tau_{21}-\tau_{12})s}{(\tau_{12}-\tau_{11})s} = \frac{\tau_{21}-\tau_{12}}{\tau_{12}-\tau_{11}}, \ i = 2 \\ \frac{(\tau_{22}-\tau_{21})s}{(\tau_{12}-\tau_{11})s} = \frac{\tau_{22}-\tau_{21}}{\tau_{12}-\tau_{11}}, \ i = 3 \\ \frac{(\tau_{31}-\tau_{22})s}{(\tau_{12}-\tau_{11})s} = \frac{\tau_{31}-\tau_{22}}{\tau_{12}-\tau_{11}}, \ i = 4 \\ \frac{(\tau_{32}-\tau_{31})s}{(\tau_{12}-\tau_{11})s} = \frac{\tau_{32}-\tau_{31}}{\tau_{12}-\tau_{11}}, \ i = 5 \end{cases} \tag{3.9}$$

are available. Here as shown in Figure 3.2 for odd i, l_i is the length of the chord length within the range of a given sensor, and for even i it is the chord length between successive sensors.

Theorem 3.5. *Consider a straight line L, and a set of three points (x_i, y_i), $i \in \{1, 2, 3\}$ that obey the following:*

(i) The (x_i, y_i), $i \in \{1, 2, 3\}$ are mutually independent and uniformly distributed in $\mathcal{D} \subset \mathbb{R}^2$.

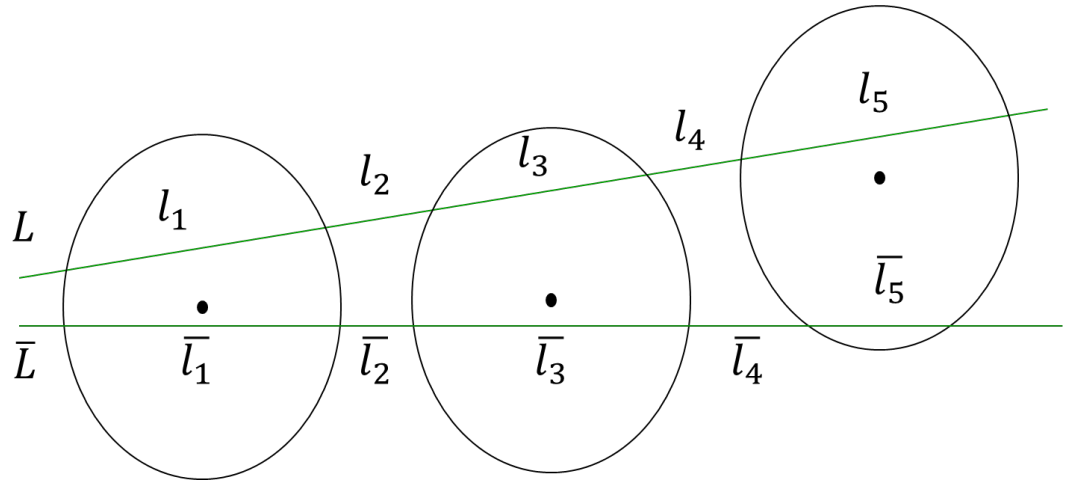

Figure 3.2: Illustration of chord lengths l_i.

(ii) They are distinct.

(iii) The straight line L intersects the three circles, each of radius r, centered on (x_i, y_i), with $l_i \neq 0$, $i \in \{1, \cdots, 5\}$, depicted in Figure 3.2.

Then the (x_i, y_i), r and the ratios

$$\frac{l_i}{l_1},\ i = \{2, 3, 4, 5\}$$

uniquely determine the line L, with probability 1.

Before presenting the proof, we first provide 2 lemmas. Notice that through a rotation and translation, if need be, it is always possible to assume without loss of generality that the (unknown) line coincides with the horizontal axis and the first circle intersects the line at $(l_1, 0)$ as shown in Figure 3(A).

Lemma 3.6. *Given an (unknown) line $y = kx + b$ which intersects 3 circles of radius r as described before, suppose the centers of the circles are mutually independently and uniformly distributed in $\mathcal{D} \subset \mathbb{R}^2$. Then, with probability one (with respect to the uniform distribution), the chord length*

$$l_i \neq l_j, \ \ for \ i \neq j, i, j = \{1, 2, ..., 5\}$$

Proof. We only show that $l_i \neq l_j, \ i, j = \{1, 2, 3\}$. The proof of the rest is identical. For $l_2 = l_1$, the center of the second circle has to be on the dashed circle with radius r centered at $(2l_1, 0)$ as shown in Figure 3.2 (A), i.e, on a one dimensional manifold in a 2-dimensional space. For $l_3 = l_1$, the center of the second circle has to be on the lines of $y = \pm\sqrt{r^2 - \left(\frac{l_1}{2}\right)^2}$ which are again two 1-dimensional manifolds in a 2-dimensional space as shown in Figure 3.2 (B). For $l_3 = l_2$, the center of the second circle has to satisfy

$$\begin{aligned} x &= l_1 + l_2 + \frac{l_2}{2} = f_x(l_2) \\ y &= \pm\sqrt{r^2 - \left(\frac{l_2}{2}\right)^2} = \pm f_y(l_2) \end{aligned}$$

which are two line segments, $0 \leq l_2 \leq 2r$, in a 2-dimensional space as in Figure 3.2 (C). Since the centers are independently and uniformly distributed, the probability that the second center lies on any of the above 1-dimensional manifolds in a 2-dimensional space is zero. This completes the proof. □

We note that the main result remains valid even if the conditions of this lemma are violated. It is just that the proof is greatly simplified by using this lemma. We

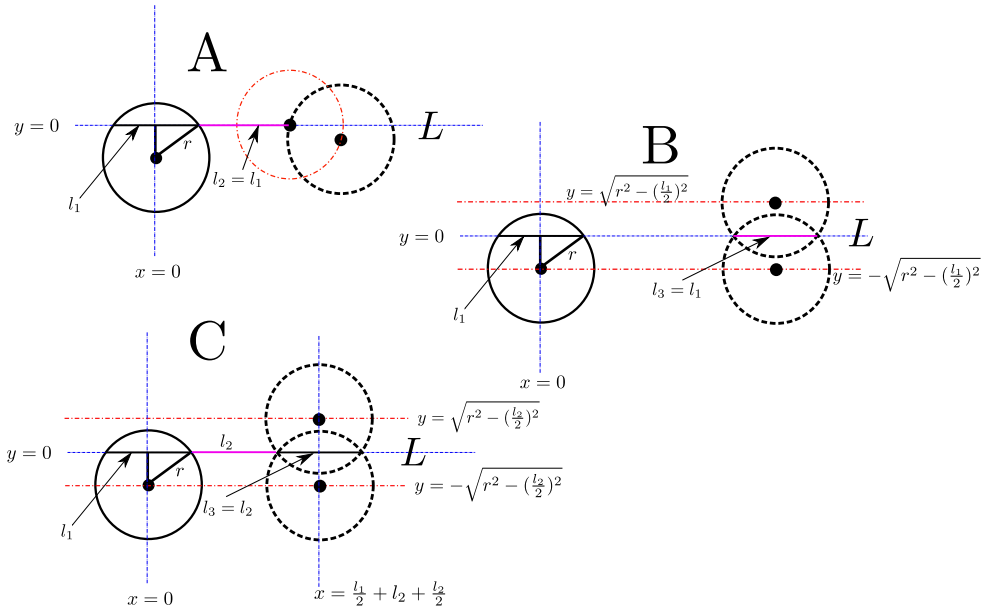

Figure 3.3: The chord length.

now provide the second lemma. For this lemma again without loss of generality, we may assume that the centers of the first two circles are at the origin and $(x_2, 0)$ for some $x_2 > 0$ respectively.

Lemma 3.7. *Consider the setting depicted in Fig. 3.2. Suppose all circles have radius r, the first two are centered at $(0,0)$ and $(x_2,0)$ respectively, and the line in the figure is labeled as $L : y = kx + b$. Then, there exist only a finite number of lines that could intersect the first two circles with the same length ratios l_i/l_1, $i = \{2, 3\}$.*

Proof. Consider a line $\bar{L}$ that intersects the first two circles. For the moment, assume that the line has the form $y = kx + b$ for some k and b. We will find necessary conditions for k and b so that the line could intersect these two circles with the given length ratios. Suppose the points of intersection of the line $\bar{L}$ and the circles, moving

from left to right in ascending order of i are $(\bar{v}_i, \bar{u}_i)$. For $i \in \{i, 2, 3, 4\}$ these obey:

$$\bar{v_i}^2 + (k\bar{v}_i + b)^2 = r^2,\ (\bar{v}_i - x_2)^2 + (k\bar{v}_i + b)^2 = r^2.$$

This implies that with $\delta = (1 + k^2)(b^2 - r^2)$,

$$\bar{v}_1 = \frac{-kb - \sqrt{b^2k^2 - \delta}}{1 + k^2},$$

$$\bar{u}_1 = k\bar{v}_1 + b,$$

$$\bar{v}_2 = \frac{-kb + \sqrt{b^2k^2 - \delta}}{1 + k^2},$$

$$\bar{u}_2 = k\bar{v}_2 + b$$

and

$$\bar{v}_3 = \frac{-(kb - x_2) - \sqrt{(bk - x_2)^2 - \delta}}{1 + k^2},$$

$$\bar{u}_3 = k\bar{v}_3 + b,$$

$$\bar{v}_4 = \frac{-(kb - x_2) + \sqrt{(bk - x_2)^2 - \delta}}{1 + k^2},$$

$$\bar{u}_4 = k\bar{v}_4 + b$$

Define, as also depicted in Figure 3.4,

$$\bar{l}_i = \left\| \begin{pmatrix} \bar{u}_{i+1} \\ \\ \bar{v}_{i+1} \end{pmatrix} - \begin{pmatrix} \bar{u}_i \\ \\ \bar{v}_i \end{pmatrix} \right\|,\ i = \{1, 2, 3\}.$$

If $\bar{L}$ intersects the first two circles with the same length ratios as L, it follows that

$$\frac{l_2}{l_1} = \frac{\bar{l}_2}{\bar{l}_1},\ \frac{l_3}{l_1} = \frac{\bar{l}_3}{\bar{l}_1}$$

Note that

$$\bar{l}_1^2 = (\bar{u}_2 - \bar{u}_1)^2 + (\bar{v}_2 - \bar{v}_1)^2 = (1+k^2)(\bar{v}_2 - \bar{v}_1)^2$$
$$= \frac{4(b^2k^2 - (1+k^2)(b^2 - r^2))}{(1+k^2)}$$

$$\bar{l}_3^2 = (\bar{u}_4 - \bar{u}_3)^2 + (\bar{v}_4 - \bar{v}_3)^2$$
$$= \frac{4((bk - x_2)^2 - (1+k^2)(b^2 - r^2))}{(1+k^2)}$$

So $\left(\frac{l_3}{l_1}\right)^2 = \left(\frac{\bar{l}_3}{\bar{l}_1}\right)^2$ and $\left(\frac{l_2}{l_1}\right)^2 = \left(\frac{\bar{l}_2}{\bar{l}_1}\right)^2$ lead to

$$b^2 - (1+k^2)r^2 + \frac{2bkx_2 - x_2^2}{(1 - \frac{l_3^2}{l_1^2})} = 0$$

$$b^2 - (1+k^2)r^2 + \frac{2bkx_2 - x_2^2}{(1 - \frac{l_2^2}{l_1^2})} = 0$$

The denominators of equations are non-zero with probability one as shown in the previous lemma. By subtracting these two equations and the assumption that $x_2 \neq 0$,

$$bk = \frac{1}{2}x_2$$

By plugging $bk = \frac{1}{2}x_2$ back into any one of the equations, we have

$$b^2 - r^2(1+k^2) = 0 \Rightarrow b = \pm r\sqrt{1+k^2}$$

and by $bk = \frac{1}{2}x_2$

$$(\frac{1}{2}x_2)^2 = (\pm rk\sqrt{1+k^2})^2$$

which is a polynomial equation in k and has finite number of solutions by the fundamental theorem of algebra [33]. Consequently from $bk = \frac{1}{2}x_2$ so is b. This completes the proof. □

We now turn to the proof of Theorem 3.5.

Proof of Theorem 3.5: First, an arbitrary line $\alpha x + \beta y + \gamma = 0$ can take two forms, $x = c$ or $y = kx + b$. However, to show the uniqueness, the proofs for the cases $x = c$ and $y = b$ are the same by rotating the coordinate by 90°. So we focus on the line $y = kx + b$ as described in the previous two lemmas. Suppose that a line $\bar{L}$ intersects three circles. Then, from the previous lemmas, both L and $\bar{L}$ must be from the set of finite candidate lines intersecting the first two circles described in the previous lemma with the fixed length ratios. Let L and $\bar{L}$ intersect the third circle at $\begin{pmatrix} v_i \\ u_i \end{pmatrix}$ and $\begin{pmatrix} \bar{v}_i \\ \bar{u}_i \end{pmatrix}$, $i \in \{5, 6\}$ respectively. Further, for $i \in \{4, 5\}$, suppose

$$l_i = \left\| \begin{pmatrix} v_{i+1} \\ u_{i+1} \end{pmatrix} - \begin{pmatrix} v_i \\ u_i \end{pmatrix} \right\|, \ \bar{l}_i = \left\| \begin{pmatrix} \bar{v}_{i+1} \\ \bar{u}_{i+1} \end{pmatrix} - \begin{pmatrix} \bar{v}_i \\ \bar{u}_i \end{pmatrix} \right\|.$$

as shown in Figure 2. For each $\bar{L}$ from the (finite) candidate set, the slope and intercept (k_i, b_i) are given. To satisfy the additional length ratios, if the line intersects the third circle,

$$\frac{l_4}{l_1} = \frac{\bar{l}_4}{\bar{l}_1}, \ \frac{l_5}{l_1} = \frac{\bar{l}_5}{\bar{l}_1} \tag{3.10}$$

the center of the third circle (x_3, y_3) cannot be arbitrary but must satisfy the above fixed ratios (3.10). By the exact arguments as in the previous lemma, one can show that this results in a finite order polynomial equation in one of the unknowns x_3 or y_3. Again by the fundamental theorem of algebra that a finite order non-constant single variable polynomial equation has finite solutions [33], there are only a finite number of solutions x_3 for each candidate $\bar{L}$ line. Therefore, for given first two centers and

the length ratios, there are only a finite number of the third centers that would allow a line $\bar{L}$ to have the same length ratios as the line L. Generically placed sensors will preclude the third center from coinciding exactly with these finitely many isolated points. This completes the proof.

Unsurprisingly, the above results can be extended if the line L intersects more than 3 circles with known length ratios.

3.3.2.1 Algorithm for tracking with unknown constant speed s

To apply Algorithm 5.1 in the previous section, estimates of the unknown speed s and the chord length d_i have to be calculated. Since the speed s is unknown, we may replace $\sqrt{r^2 - d_i^2}$ by $\sqrt{r^2 - \hat{d}_i^2(\hat{s})}$ where $\hat{s}$ is an estimate of s and the $\hat{d}_i(\hat{s})$ are the estimates of d_i,

$$\hat{d}_i = \frac{\tau_{i2} - \tau_{i1}}{2}\hat{s}$$

Clearly, if $\hat{s} = s$, one of four solutions from

$$\begin{pmatrix} x_1 & y_1 & 1 \\ x_2 & y_2 & 1 \\ x_3 & y_3 & 1 \end{pmatrix} \begin{pmatrix} \alpha \\ \beta \\ \gamma \end{pmatrix} = \begin{pmatrix} \pm\sqrt{r^2 - \hat{d}_1^2} \\ \pm\sqrt{r^2 - \hat{d}_2^2} \\ \pm\sqrt{r^2 - \hat{d}_3^2} \end{pmatrix} \tag{3.11}$$

satisfies $\alpha^2(\hat{s}) + \beta^2(\hat{s}) = 1$. However, there is a fundamental difference between the cases of known and unknown speed. In the case of known speed, the length ratios l_i/l_1 do not play any role in ensuring the uniqueness of the line while in the unknown speed case, these ratios are necessary. These ratios can be divided into two types, the chord ratios $\frac{\tau_{i2}-\tau_{i1}}{\tau_{12}-\tau_{11}}$, and the outer length ratios $\frac{\tau_{(i+1)1}-\tau_{i2}}{\tau_{12}-\tau_{11}}$. The chord ratios are

taken care of automatically in (3.11) because $\frac{\hat{d}_i}{\hat{d}_1} = \frac{\tau_{(i+1)1}-\tau_{i2}}{\tau_{12}-\tau_{11}}$. So the algorithm has to account for the outer length ratios. The algorithm can now be summarized as follows.

Algorithm 3.2 Detection algorithm for unknown speed:

Step 0: Calculate $\frac{\bar{l}_i}{\bar{l}_1} = \frac{l_i}{l_1}$ as defined in (3.9).

Step 1: Apply Algorithm 5.1 but replacing (3.6) and (3.7) by

$$\begin{aligned} &\min_{\hat{s}>0}(\alpha^2(\hat{s}) + \beta^2(\hat{s}) - 1)^2 \\ s.t. &\begin{pmatrix} x_1 & y_1 & 1 \\ x_2 & y_2 & 1 \\ x_3 & y_3 & 1 \end{pmatrix} \begin{pmatrix} \alpha \\ \beta \\ \gamma \end{pmatrix} = \begin{pmatrix} \pm\sqrt{r^2 - \hat{d}_1^2} \\ \pm\sqrt{r^2 - \hat{d}_2^2} \\ \pm\sqrt{r^2 - \hat{d}_3^2} \end{pmatrix} \end{aligned} \tag{3.12}$$

$$\frac{l_{2i}}{l_1} = \frac{\bar{l}_{2i}}{\bar{l}_1}, \ i = 2, 4 \tag{3.13}$$

and

$$\hat{d}_i(\hat{s}) = \frac{(\tau_{i2} - \tau_{i1})\hat{s}}{2}, \ i = 1, 2, 3. \tag{3.14}$$

By the previous analysis, the line $\alpha x + \beta y + \gamma = 0$ can be uniquely determined for generic sensor placements.

3.3.3 Uncertainty in the sensing range

So far, we have assumed that the sensing range of binary sensors are all exactly r. In practice because of calibration uncertainties, device-to-device variations, system noise due to Poisson nature of received signals and measurement noise, the sensing

range r is only approximately known.We now show how this can be accommodated in our approach.

Assumption 3.3.1. *The sensing range of the i-th sensor is*

$$r_i = r + \Delta_i,\ |\Delta_i| \leq \Delta < r$$

where the Δ_i *are iid random variables distributed in* $-\Delta \leq \Delta_i \leq \Delta$ *for some* $\Delta \geq 0$.

Assume $\Delta = \alpha r$ depending on the quality of the sensors. For example, $\Delta = 0.1r$ which implies the uncertainty level 2Δ is about 20% of the nominal value r. Now, let us reconsider (3.12). Clearly, if the sensing range r is accurate and s is available, for generic sensor locations, only one solution of

$$A_3 \begin{pmatrix} \alpha \\ \beta \\ \gamma \end{pmatrix} = e_3$$

i.e.

$$\begin{pmatrix} \hat{\alpha} \\ \hat{\beta} \\ \hat{\gamma} \end{pmatrix} = (A_3^T A_3)^{-1} A_3^T e_3$$

would satisfy $\hat{\alpha}^2 + \hat{\beta}^2 = 1$ obeyed by the line. With uncertainty, this is no longer valid. Since the actual radius $r_i = r + \Delta_i$ is unknown, the resultant chord length $\hat{d}_i$ could be larger than the assumed radius r or equivalently $\sqrt{r^2 - \hat{d}_i^2}$ could be a complex number. In such a case, the equation in solving (α, β, γ) is rendered meaningless. Thus in the presence of uncertainty, not every sensor provides useful information.

To this end, we only use data from the i-th sensor if $r - \Delta > \hat{d}_i$ which guarantees $(r + \Delta_i)^2 - \hat{d}_i^2 > 0$. Define

$$A_m = \begin{pmatrix} x_1 & y_1 & 1 \\ x_2 & y_2 & 1 \\ \vdots & \vdots & \vdots \\ x_m & y_m & 1 \end{pmatrix} \tag{3.15}$$

$$\hat{e}_m(\hat{s}, \Delta_i) = \begin{pmatrix} \pm\sqrt{r^2 - \hat{d}_1^2} \\ \pm\sqrt{r^2 - \hat{d}_2^2} \\ \vdots \\ \pm\sqrt{r^2 - \hat{d}_m^2} \end{pmatrix} \tag{3.16}$$

and

$$r - \Delta > \hat{d}_i, \ i = 1, 2, ..., m \geq 3 \tag{3.17}$$

Now consider

$$\begin{pmatrix} x_1 & y_1 & 1 \\ x_2 & y_2 & 1 \\ \vdots & \vdots & \vdots \\ x_m & y_m & 1 \end{pmatrix} \begin{pmatrix} \alpha \\ \beta \\ \gamma \end{pmatrix} = \begin{pmatrix} \pm\sqrt{r^2 - \hat{d}_1^2} \\ \pm\sqrt{r^2 - \hat{d}_2^2} \\ \vdots \\ \pm\sqrt{r^2 - \hat{d}_m^2} \end{pmatrix} \Rightarrow \tag{3.18}$$

$$A_m \begin{pmatrix} \alpha \\ \beta \\ \gamma \end{pmatrix} = \underbrace{\begin{pmatrix} \pm\sqrt{(r+\Delta_1)^2 - \hat{d}_1^2} \\ \pm\sqrt{(r+\Delta_2)^2 - \hat{d}_2^2} \\ \vdots \\ \pm\sqrt{(r+\Delta_i)^2 - \hat{d}_m^2} \end{pmatrix}}_{e_m(\hat{s},\Delta_i)} + \underbrace{\begin{pmatrix} \pm\sqrt{r^2 - \hat{d}_1^2} \\ \pm\sqrt{r^2 - \hat{d}_2^2} \\ \vdots \\ \pm\sqrt{r^2 - \hat{d}_m^2} \end{pmatrix} - \begin{pmatrix} \pm\sqrt{(r+\Delta_1)^2 - \hat{d}_1^2} \\ \pm\sqrt{(r+\Delta_2)^2 - \hat{d}_2^2} \\ \vdots \\ \pm\sqrt{(r+\Delta_i)^2 - \hat{d}_m^2} \end{pmatrix}}_{\Delta e_m(\hat{s},\Delta_i)} \tag{3.19}$$

Obviously, the first part

$$A_m \begin{pmatrix} \alpha \\ \beta \\ \gamma \end{pmatrix} = e_m(\hat{s}, \Delta_i) \tag{3.20}$$

is the relevant equation if the uncertainties Δ_i were available and the solution

$$\begin{pmatrix} \bar{\alpha} \\ \bar{\beta} \\ \bar{\gamma} \end{pmatrix} = (A_m^T A_m)^{-1} A_m^T e_m(\hat{s}, \Delta_i)$$

leads to the line $\bar{\alpha}x+\bar{\beta}y+\bar{\gamma} = 0$ provided that $\bar{\alpha}^2+\bar{\beta}^2 = 1$ and the length ratios $\frac{l_i}{l_1} = \frac{\bar{l}_i}{\bar{l}_1}$ are satisfied as in (3.12). The problem is that the Δ_i are unknown. To study the effect of the uncertainty $\Delta e_m(\hat{s}, \Delta_i)$, note that under the assumption that $r - \Delta > \hat{d}_i$,

it is easily verified that $\sqrt{r^2 - \hat{d}_i^2} - \sqrt{(r+\Delta_i)^2 - \hat{d}_i^2} = -\Delta_i(1 + \frac{1}{2}(\frac{\hat{d}_i}{r})^2) + h.o.t.$ where h.o.t. refers to higher order terms in Δ_i. Obviously, if we consider the dominant term, i.e., the first order term, the effect of the uncertainty

$$(A_m^T A_m)^{-1} A_m^T \begin{pmatrix} -\Delta_1(1 + \frac{1}{2}(\frac{\hat{d}_1}{r})^2) \\ \vdots \\ -\Delta_m(1 + \frac{1}{2}(\frac{\hat{d}_m}{r})^2) \end{pmatrix}$$

goes to zero as m increases provided that only the good information $r - \Delta > \hat{d}_i$'s, $i = 1, 2, ..., m$ are used and Δ_i are zero mean. To summarize, we have

Theorem 3.8. *Suppose the conditions of Theorem 3.5 hold except that the circles have radii $r + \Delta_i$. With the various quantities defined as above, suppose* $\begin{pmatrix} \bar{\alpha} \\ \bar{\beta} \\ \bar{\gamma} \end{pmatrix}$ *is the true solution and* $\begin{pmatrix} \hat{\alpha} \\ \hat{\beta} \\ \hat{\gamma} \end{pmatrix}$ *denote the estimate generated by the algorithm outlined above. Then the following hold.*

- *Assume $r - \Delta > \hat{d}_i$, $i = 1, 2, ..., m$ and Δ_i is iid of zero mean. Then as m*

increases

$$\begin{pmatrix} \bar{\alpha} \\ \bar{\beta} \\ \bar{\gamma} \end{pmatrix} - \begin{pmatrix} \hat{\alpha} \\ \hat{\beta} \\ \hat{\gamma} \end{pmatrix} = (A_m^T A_m)^{-1} A_m^T \times$$

$$\begin{pmatrix} -\Delta_1(1 + \frac{1}{2}(\frac{\hat{d}_1}{r})^2) \\ \vdots \\ -\Delta_m(1 + \frac{1}{2}(\frac{\hat{d}_m}{r})^2) \end{pmatrix} + h.o.t.$$

$$\rightarrow h.o.t.$$

- *Further if the center coordinates x_i and y_i are iid uniformly distributed of zero mean, then as m increases*

$$\begin{pmatrix} \bar{\alpha} \\ \bar{\beta} \\ \bar{\gamma} \end{pmatrix} - \begin{pmatrix} \hat{\alpha} \\ \hat{\beta} \\ \hat{\gamma} \end{pmatrix} \rightarrow \begin{pmatrix} 0 \\ 0 \\ h.o.t. \end{pmatrix}$$

Proof. The first part is a direct consequence of the discussion preceding the theorem statement. To show the second part, note

$$(A_m^T A_m)^{-1} A_m^T \rightarrow \text{ diag } \left\{ \frac{1}{\sigma_x^2}, \frac{1}{\sigma_y^2}, 1 \right\} \times$$

$$\frac{1}{m} \begin{pmatrix} x_1 & x_2 & \cdots & x_m \\ y_1 & y_2 & \cdots & y_m \\ 1 & 1 & \cdots & 1 \end{pmatrix} \Delta e_m(\hat{s}, \Delta_i)$$

where σ_x^2 and σ_y^2 are the variances of x_i and y_i. The conclusion follows from the fact that x_i and y_i are iid and zero mean. This completes the proof. □

3.3.4 Asymptotic results for sensor density required for tracking

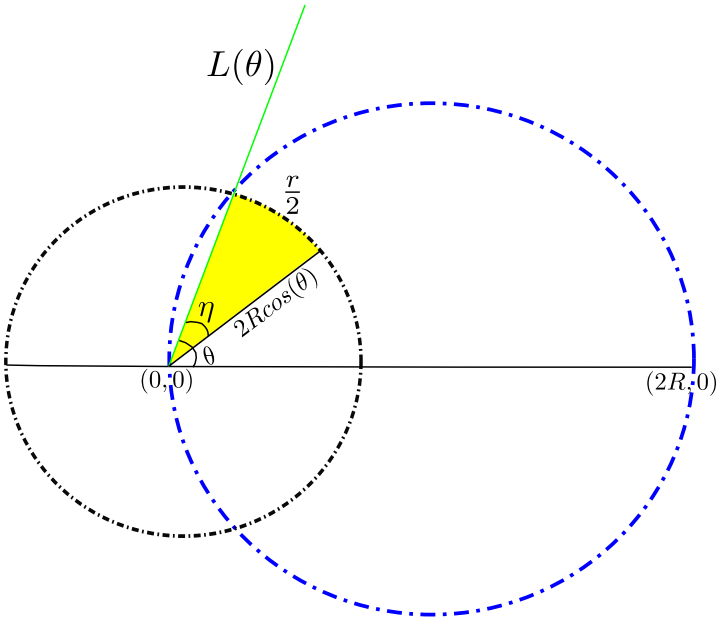

Figure 3.4: General representation of a line through a disc of radius R

We now address the following question: Should the trajectory be a single straight line passing through $\mathcal{D}$, does its estimation require a high density of sensors in $\mathcal{D}$? We will show in this section that a high density is unnecessary, and that in fact vanishingly small densities also suffice. It is evident from the previous sections that should a line intersect the sensing ranges of three generically placed sensors, then it can be uniquely determined from the time stamps delineating entrance into and departure from these sensing ranges.

Thus we ask the following related question. Suppose the coverage area of the

sensor network $\mathcal{D}$ is large compared to the sensing range of a sensor. Specifically suppose $\mathcal{D} \subset \mathbb{R}^2$ is a large disk with radius $R \gg r$. Asymptotically, what sensor density guarantees that this line intersects the sensing region of at least one of the sensors? Asymptotically, this density will be of the same order as that guaranteeing intersection with the sensing ranges of at least three sensors. We observe that the results we present extend readily to $\mathcal{D}$ that is rectangular or has other shapes.

We choose the origin and the coordinate axes so that the center of the disk $\mathcal{D}$ is at $(R, 0)$ as shown in Fig. 3.4. Consider a line passing through the origin with an angle θ with respect to the horizontal axis, $L(\theta)$. Note that because of the circular symmetry of the problem, there is no loss of generality in our choice of line $L(\theta)$ to represent the trajectory of the object to be tracked.

Let the sensing range of the binary sensor i be a circle of radius r centered at (x_i, y_i) uniformly distributed in $\mathcal{D}$. Let N be the number of the binary sensors in $\mathcal{D}$ and $P(N, R, r, L(\theta))$ be the probability that the line $L(\theta)$ does not intersect any small circle of radius r in $\mathcal{D}$. The probability is with respect to the uniform distribution defining sensor locations. What we are interested is the asymptotic dependence of $P(N, R, r, L(\theta))$ on R. As will be evident in the sequel this allows us to draw conclusions about sensor densities.

Theorem 3.9. *Let the centers (x_i, y_i) be i.i.d uniformly distributed in*

$$\mathcal{D} = \left\{ z \in \mathbb{R}^2 \middle| \left\| z - [R, 0]^\top \right\| \leq R \right\}.$$

Define $L(\theta)$ to be the line passing through the origin, making an angle θ with the

x-axis. Assume $\theta \in (-\pi/2, \pi/2)$ *and*

$$\frac{R}{r} = c_1 N^{1-\delta} \tag{3.21}$$

for some $c_1 > 0$ *and* $0 < \delta < 1$. *Then,*

$$\lim_{N\to\infty} P(N, R, r, L(\theta)) = 0.$$

Proof. The chord length of the line $L(\theta)$ for $\theta \in (-\pi/2, \pi/2)$ is $d = 2Rcos(\theta)$. Define the circle centered at the origin with radius d. Make an arc of the arc length $\frac{r}{2}$ along the circle toward the positive horizonal axis as shown in Fig. 4. The angle η and the area of the small fan-like sector in Fig. 4 are

$$\eta = \frac{r}{2}\frac{1}{2\pi d}2\pi = \frac{1}{4cos(\theta)}\frac{r}{R},$$
$$A(\theta, \eta) = \frac{\eta}{2\pi}\pi d^2 = \frac{cos(\theta)}{2} rR$$

respectively. Clearly, if any of the N sensors is placed in the fan-like sector, the circle intersects the line $L(\theta)$. Because of the uniform distribution and the fact that the fan-like sector is completely inside the big disk, the probability that the center of the ith small circle (x_i, y_i), $1 \le i \le N$, is in the fan-like sector is the ratio of the areas of the fan-like sector and the big disk

$$\frac{cos(\theta)}{2} rR\frac{1}{\pi R^2} = \frac{cos(\theta)}{2\pi}\frac{r}{R} = c_2\frac{r}{R}$$

So the probability that none of the centers of N small circles lies in the fan-like sector

is for some c_3, and any $x \leq c_3 N^{\delta}$

$$P(N, R, r, L(\theta)) \leq \left(1 - c_2 \frac{r}{R}\right)^N = \left(1 - c_3 \frac{N^{\delta}}{N}\right)^N$$
$$\leq \left(1 - \frac{x}{N}\right)^N.$$

As

$$\lim_{N \to \infty} \left(1 - \frac{x}{N}\right)^N = e^{-x},$$

and $x > 0$ can be arbitrarily large as $N \to \infty$, it follows that

$$\lim_{N \to \infty} P(N, R, r, L(\theta)) = 0.$$

□

The following corollary that addresses the simultaneous intersection with m sensing ranges, follows easily.

Corollary 3.3.1. *Let m be any fixed positive number and $P_m(N, R, r, L(\theta))$ the probability that the line $L(\theta)$ does not intersect m or more small circles. Then, under the conditions of Theorem 3.9,*

$$\lim_{N \to \infty} P_m(N, R, r, L(\theta)) = 0.$$

Let us now address the implication of theorem 3.9 and corollary 3.3.1 to the density of measurement sensors. Suppose δ in Theorem 3.9 is less than 0.5. Then the sensor density

$$\rho = \frac{N}{\pi R^2} = O\left(\frac{1}{N^{1-2\delta}}\right)$$

declines to zero as N goes to infinity. Thus the probability that a line $L(\theta)$ intersects at least one sensors sensing range approaches one *even with vanishingly small densities.* Some other remarks are in order

Remark 3.1. The following remarks are intuitive.

- At first blush the problem we are considering appears to be related to the disk covering problem for finding the least number of small circles of radius r for covering a disk of radius R. For small enough r, the least number N of sensors whose sensing ranges collectively cover $\mathcal{D}$, satisfies [34]

$$\frac{N\pi r^2}{\pi R^2} = \frac{2\pi}{3\sqrt{3}}.$$

  According to this the total area covered by the sensors $N\pi r^2$ has to be larger than the area of the big disk πR^2 by a factor of $\frac{2\pi}{3\sqrt{3}}$. This result effectively demands that the sensing ranges be overlapping. By contrast our results do not require any such overlap, see e.g. Theorem 3.9. In fact suppose again that $0 < \delta < 0.5$. Then

$$\frac{N\pi r^2}{\pi R^2} = \frac{1}{c_1^2} \cdot \frac{1}{N^{1-2\delta}}$$

  approaches zero as N approaches infinity. Thus, sensing ranges do not have to cover $\mathcal{D}$ and in fact the ratio of the total area covered by the N sensors and the area of $\mathcal{D}$ can approach zero.

- Again almost all results in the binary sensor literature assume a very high density of sensors so that the whole area is completely covered by binary sensors. With a very high density, every point in the region lies in the sensing range of

several sensors. The object position and trajectory can be pinned down with a higher degree of accuracy because the intersection is much smaller than the sensing area of any single sensor. Clearly, a higher density implies that more sensing ranges overlap resulting in a smaller area of intersection and thus a more accurate estimate. In fact, as shown in [14] the estimation accuracy is in the order of $1/\rho r$. The estimation error goes to zero only when $\rho \to \infty$. If the density $\rho \to 0$, the estimation error goes to infinity. By contrast in our method, ρ does not have to go to infinity to have an accurate estimate and can in fact be vanishingly small.

3.3.4.1 Simulation results

1. We first consider the case with no uncertainty in r. Let $\mathcal{D} \in R^2$ be rectangular of dimension 20 meters by 20 meters centered at the origin. The sensing radius of the binary sensors is $r = 1$ meter. 35 sensors are uniformly distributed in $\mathcal{D}$. Note the area covered by the sensors is about 27% of the total area of $\mathcal{D}$ and so the density is not very high and in fact 73% of the area is not covered. The unknown path of the object consists of 4 line segments with 4 different unknown speeds $s_1 = 0.72, s_2 = 1.31, s_3 = 10.6$ and $s_4 = 0.96$ (meter/second) in each segment as shown in Figure 3.5. The unknown paths are shown in bold lines and smaller black line is the estimate of the path by applying the algorithm in (3.12) based on three circles. Clearly, the unknown path is accurately estimated even if it changes the direction and speed a number of times.

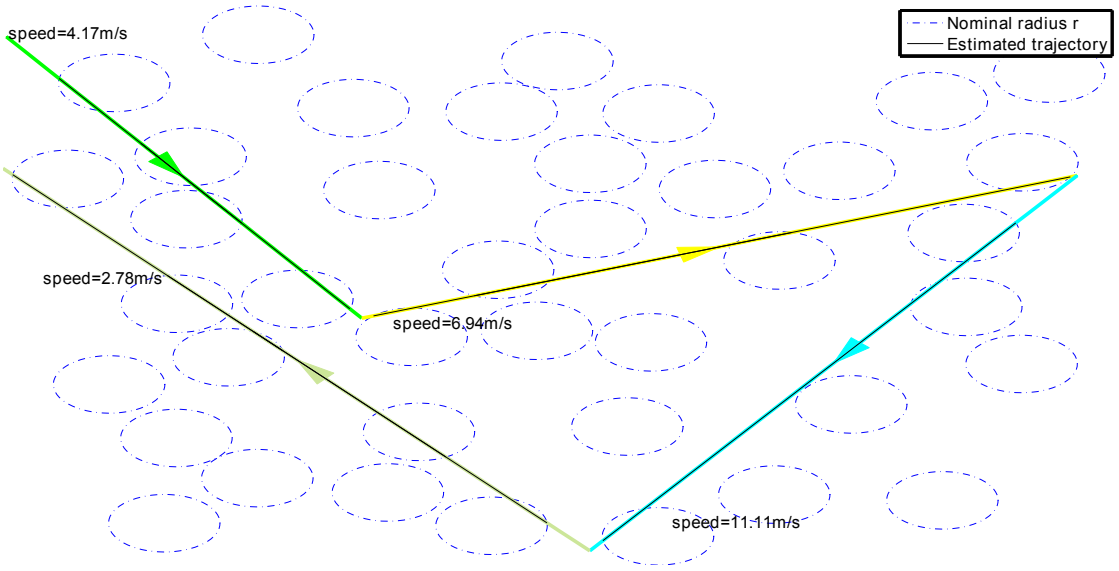

Figure 3.5: Noise-free tracking

2. We consider the case with 30% uncertainty in r. Using the same settings as in 1 above, the unknown paths are shown in bold lines and smaller black line is the estimate of the path by applying the algorithm in (3.12) based on four circles. Clearly, the unknown path estimated is close to the true path even if it changes the direction and speed a number of times as shown in Figure 3.6.

3. We consider the case where there is noise in the sensing range. The sensing range of the ith sensor therefore becomes $r + \Delta_i, \Delta_i \sim U[-\Delta, \Delta]$. We then use differing number of sensors to do the estimation of the parameters of the line. For the simulation described below the nominal sensing radius r=100m, the region $D \in R^2$ containing the sensors is a 2km by 2km square grid centered at the origin. The centers of the sensors are iid uniformly in D. We consider three cases of $\Delta \in \{\frac{5r}{100}, \frac{10r}{100}, \frac{15r}{100}\}$. The density of the sensors used in all simulations is

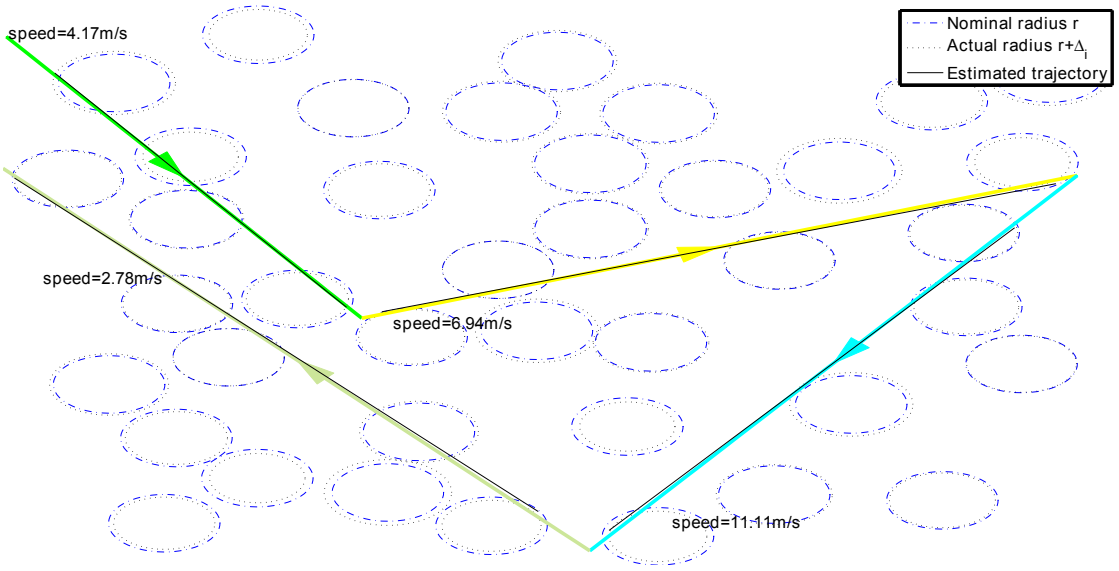

Figure 3.6: Tracking with 30% uncertainty in sensing radius

$\frac{422}{2000^2} = 1.055e^{-}4$ sensors/m^2. 1000 Monte Carlo simulations are done for each noise level in the sensing radius r.

Figure 3.7 depicts the line to be estimated with corresponding intersecting sensors, Figure 3.8 depicts the RMSE using $\sqrt[2]{\frac{1}{t_f - t_0}\int_{t_0}^{t_f}(x(t)-\hat{x}(t))^2 + (y(t)-\hat{y}(t))^2 dt}$, whiles Figure 3.9 depicts the NMSE using $\frac{(\alpha-\hat{\alpha})^2+(\beta-\hat{\beta})^2+(\gamma-\hat{\gamma})^2}{\alpha^2+\beta^2+\gamma^2}$.

For k sensors, there are 2^{n-1} distinct solutions. In the noisy scenario, thus $r_i = r + \Delta_i$, the solution will not exactly satisfy $\alpha^2 + \beta^2 = 1$. The simulations therefore employ a two stage selection criteria.

In the first stage, lines which satisfy $1 - \epsilon \leq \alpha^2 + \beta^2 \leq 1 + \epsilon$, $0 \leq \epsilon < 1$, are chosen. If only one line is returned, then that is the solution. If $m \geq 2$ solution are returned, the m solutions are used in stage two. If no solution is returned

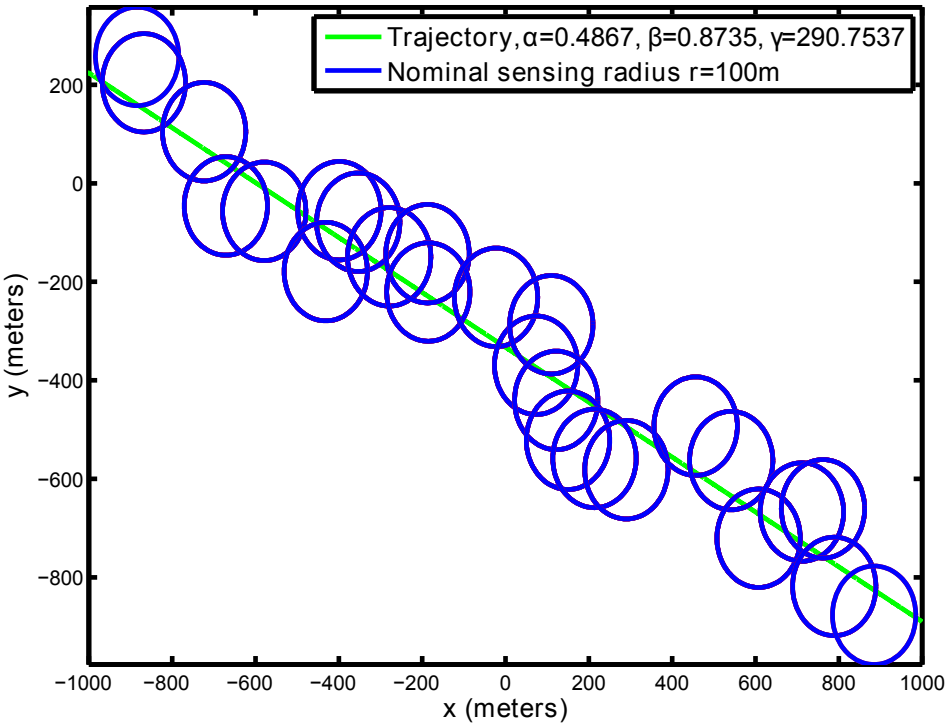

Figure 3.7: Line to be estimated

from stage 1, all the possible solutions are used in stage 2. In the simulations, $\epsilon = 0.1$ for all noise levels.

In the second stage, the lines which passed stage one are tested using the criteria $(1-\lambda)\|\alpha^2+\beta^2-1\| + \lambda(\|l_2 - \hat{l}_2, l_4 - \hat{l}_4, ..., l_{2n-2} - \hat{l}_{2n-2}\|)$. In the simulations, $\lambda = 0.5$ for all noise levels.

3.4 Tracking of radioactive sources with unknown nominal sensing range r

In section 3.3 we considered the problem of tracking radioactive sources on piece-wise linear trajectories with the nominal sensing radii of the measurement sen-

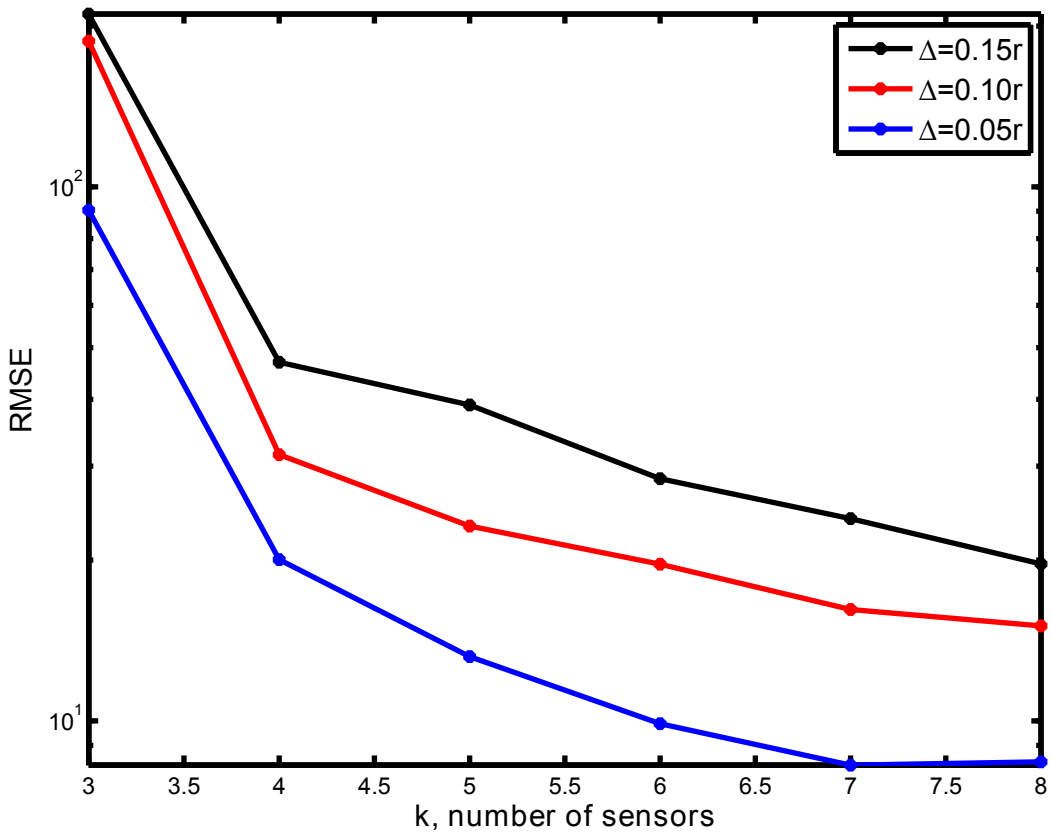

Figure 3.8: RMSE against k, number of sensors

sors known. We now relax that assumption, and now assume that even though the nominal sensing radii r is constant and homogeneous across the measurement sensors, the value of r is however unknown a priori. We develop a robust algorithm which localizes the trajectory of the radioactive source.

Suppose that a source moves on a linear trajectory $L : y = ax + b$ in the cartesian coordinate with unknown constant speed s. Suppose L interesects four binary sensors of unknown detecting sensing radii r with on and off intersecting time stamps τ_{2i-1} and τ_{2i} respectively $\forall i \in \{1, 2, 3, 4\}$. The within sensor chord lengths

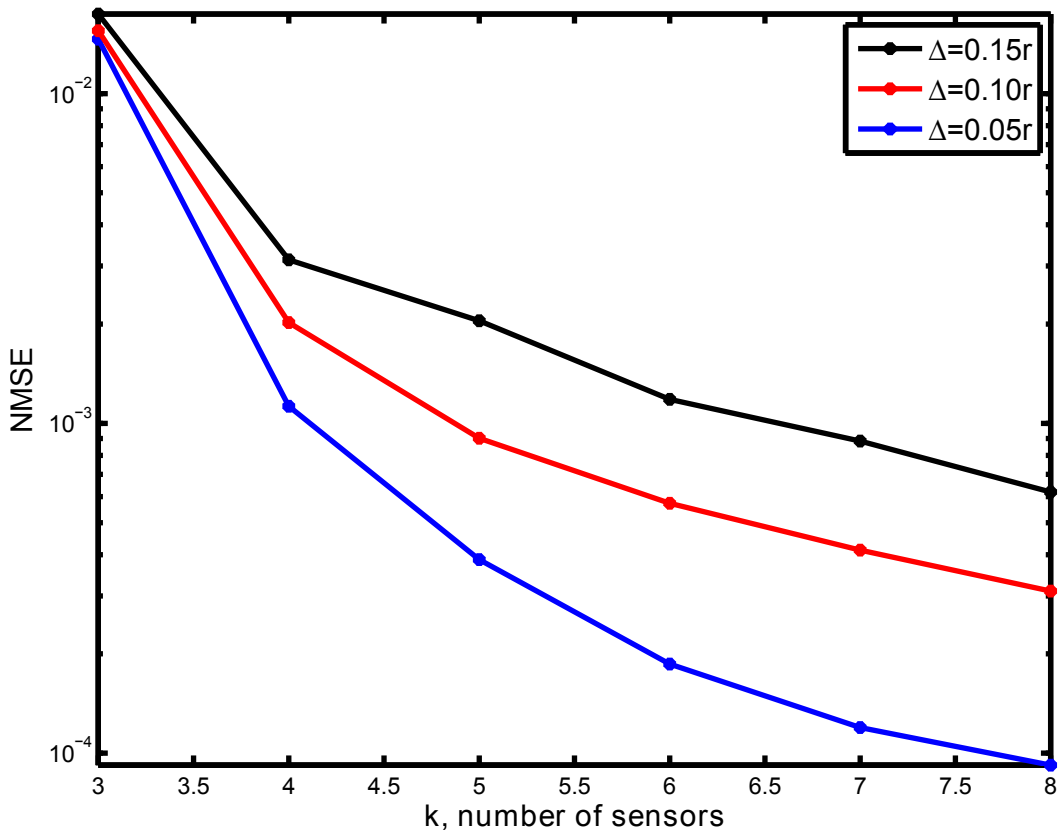

Figure 3.9: Parameter NMSE against k, number of sensors

$l_{2i-1} = s(\tau_{2i} - \tau_{2i-1}) = s\Delta\tau_{2i-1}$ and between sensor lengths $l_{2i} = s(\tau_{2i+1} - \tau_{2i}) = s\Delta\tau_{2i}$ are thus available.

Given that L intersects with a sensor ,S_i, centered at (m_i, n_i), then the x-coordinates of the points of intersection are

$$x = \frac{m_i - a(b - n_i) \pm \sqrt{(1 + a^2)r^2 - (am_i + b - n_i)^2}}{1 + a^2} \tag{3.22}$$

From (3.22), the chord lengths and between sensor lengths on the four sensors,$l_i =$

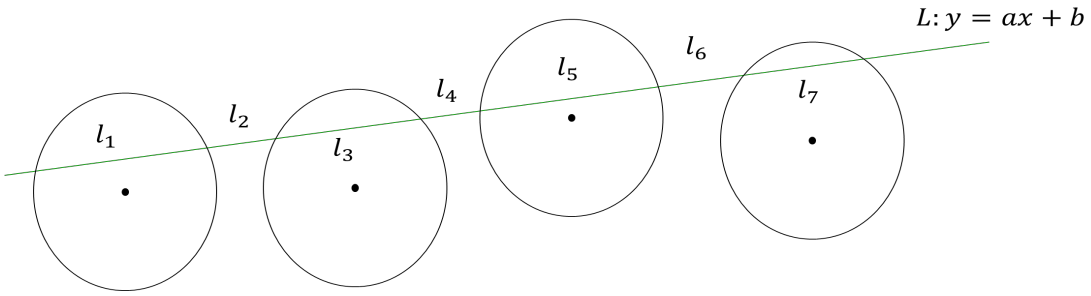

Figure 3.10: Four sensors intersecting a line.

$s\Delta\tau_i, i \in \{1, 2, ..., 7\}$,are therefore given by

$$l_i = 2\sqrt{r^2 - \frac{\left(am_{\frac{i+1}{2}} + b - n_{\frac{i+1}{2}}\right)^2}{1+a^2}}, i \in \{1, 3, 5, 7\} \tag{3.23}$$

and

$$l_i = \frac{m_{\frac{i}{2}+1} - m_{\frac{i}{2}} + a\left(n_{\frac{i}{2}+1} - n_{\frac{i}{2}}\right)}{\sqrt{1+a^2}} - \sqrt{r^2 - \frac{\left(am_{\frac{i}{2}+1} + b - n_{\frac{i}{2}+1}\right)^2}{1+a^2}} - \sqrt{r^2 - \frac{\left(am_{\frac{i}{2}} + b - n_{\frac{i}{2}}\right)^2}{1+a^2}},$$

$$i \in \{2, 4, 6\} \tag{3.24}$$

3.4.1 Determination of unique trajectory using four sensors with s and r unknown

3.4.1.1 Within sensor measurements

Using the four chord lengths from (3.23) and normalizing by l_1 provides three equations thus

$$\frac{\Delta\tau_{2i-1}^2}{\Delta\tau_1^2} = \frac{r^2 - \frac{(am_i + b - n_i)^2}{1+a^2}}{r^2 - \frac{(am_1 + b - n_1)^2}{1+a^2}}, i \in \{2, 3, 4\} \Rightarrow$$

$$r^2 = \frac{\Delta\tau_{2i-1}^2}{\Delta\tau_{2i-1}^2 - \Delta\tau_1^2} \frac{(am_1 + b - n_1)^2}{1+a^2} - \frac{\Delta\tau_1^2}{\Delta\tau_{2i-1}^2 - \Delta\tau_1^2} \frac{(am_i + b - n_i)^2}{1+a^2} \tag{3.25}$$

where $i \in \{2,3,4\}, \Delta\tau_{2i-1} \neq \Delta\tau_1$

The three resulting equations from (3.25) can then be used to eliminate r by choosing pairs of two. This gives three new equations devoid of r thus;

$$\left(\frac{\Delta\tau_{2i-1}^2}{\Delta\tau_{2i-1}^2 - \Delta\tau_1^2} - \frac{\Delta\tau_{2j-1}^2}{\Delta\tau_{2j-1}^2 - \Delta\tau_1^2}\right)(am_1 + b - n_1)^2 - \frac{\Delta\tau_1^2(am_i + b - n_i)^2}{\Delta\tau_{2i-1}^2 - \Delta\tau_1^2} + \frac{\Delta\tau_1^2(am_j + b - n_j)^2}{\Delta\tau_{2j-1}^2 - \Delta\tau_1^2} = 0 \tag{3.26}$$

where $\{i \neq j\} \in \{2,3,4\}, \Delta\tau_{2i-1} \neq \Delta\tau_1, \Delta\tau_{2j-1} \neq \Delta\tau_1$

3.4.1.2 Between sensor measurements

From (3.24), we can form 3 equations using the between sensor measurements normalized by the preceding chord length to remove the unknown speed s.

$$\frac{\Delta\tau_{2i}}{\Delta\tau_{2i-1}} = \frac{m_{i+1} - m_i + a(n_{i+1} - n_i) - \sqrt{(1+a^2)r^2 - (am_{i+1} + b - n_{i+1})^2}}{2\sqrt{(1+a^2)r^2 - (am_i + b - n_i)^2}} - \frac{1}{2} \tag{3.27}$$

where $i \in \{1,2,3\}$.

We further eliminate r using (3.28) by leveraging the within sensor chord lengths.

$$r^2 = \frac{\Delta\tau_{2i+1}^2(am_i + b - n_i)^2 - \Delta\tau_{2i-1}^2(am_{i+1} + b - n_{i+1})^2}{(\Delta\tau_{2i+1}^2 - \Delta\tau_{2i-1}^2)(1+a^2)} \tag{3.28}$$

where $i \in \{1,2,3\}$ and $\Delta\tau_{2i-1} \neq \Delta\tau_{2i+1}$. Substituting (3.28) in (3.27) and rearranging terms leads to three new equations in (3.29) devoid of s and r.

$$\frac{(am_i + b - n_i)^2 - (am_{i+1} + b - n_{i+1})^2}{\Delta\tau_{2i+1}^2 - \Delta\tau_{2i-1}^2} - \frac{(m_{i+1} - m_i + a(n_{i+1} - n_i))^2}{(2\Delta\tau_{2i} + \Delta\tau_{2i-1} + \Delta\tau_{2i+1})^2} = 0 \tag{3.29}$$

where $i \in \{1,2,3\}$ and $\Delta\tau_{2i-1} \neq \Delta\tau_{2i+1}$.

3.4.1.3 Finding unique trajectory

Theorem 3.10. *Suppose an object moves on a straight line $L : y = ax + b$, with unknown constant speed s and intersects with four sensors whose centers $(m_i, n_i), i \in \{1, 2, 3, 4\}$ are i.i.d uniformly distributed and all sensors have unknown range r. Suppose the "on" an "off" intersecting time-stamps τ_{2i-1} and τ_{2i} are known, then with probability being one L is uniquely determined.*

Proof. Using the first three sensors, three equations can be realized. Define $\Delta\tau_i = \tau_{i+1} - \tau_i$. Then the three resulting equations are as shown in (3.30)-(3.32).

$$\left(\frac{\Delta\tau_3^2}{\Delta\tau_3^2-\Delta\tau_1^2} - \frac{\Delta\tau_5^2}{\Delta\tau_5^2-\Delta\tau_1^2}\right)(am_1 + b - n_1)^2 - \frac{\Delta\tau_1^2(am_2+b-n_2)^2}{\Delta\tau_3^2-\Delta\tau_1^2} + \frac{\Delta\tau_1^2(am_3+b-n_3)^2}{\Delta\tau_5^2-\Delta\tau_1^2} = 0 \tag{3.30}$$

$$\frac{(2\Delta\tau_2+\Delta\tau_1+\Delta\tau_3)^2}{\Delta\tau_3^2-\Delta\tau_1^2}((am_1 + b - n_1)^2 - (am_2 + b - n_2)^2) = (m_2 - m_1 + a(n_2 - n_1))^2 \tag{3.31}$$

$$\frac{(2\Delta\tau_4+\Delta\tau_3+\Delta\tau_5)^2}{\Delta\tau_5^2-\Delta\tau_3^2}((am_2 + b - n_2)^2 - (am_3 + b - n_3)^2) = (m_3 - m_2 + a(n_3 - n_2))^2. \tag{3.32}$$

Without loss of generality assume $m_1 = n1 = n2 = 0$. This can be achieved by rotation and translation of the centers in the Cartesian plane. We however retain all variables to preserve clarity. The following Lemmas, 3.11 and 3.12, will be required to continue the proof of Theorem 3.10.

Lemma 3.11. *Suppose an object moves in a straight line $L : y = ax + b$, with constant speed s and intersects with four sensors whose centers $(m_i, n_i), i \in \{1, 2, 3, 4\}$*

are i.i.d uniformly, and all sensors have sensing range r. Suppose the "on" an "off" intersecting time-stamps τ_{2i-1} and τ_{2i} are known such that the within sensor transition times are $\Delta\tau_{2i-1} = \tau_{2i} - \tau_{2i-1}, i \in \{1,2,3,4\}$. Then with probability one the transition times $\Delta\tau_{2i-1} - \Delta\tau_{2j-1} \neq 0, i \neq j, i, j \in \{1,2,3,4\}$.

Proof. Without loss of generality, assume the line L is coincident with the horizontal axis and the first sensor is centered at $(0, n_1)$. This is easily attained by rotation and translation. With this assumption, $n_1 = \pm\sqrt{r^2 - s^2\frac{\Delta\tau_1^2}{4}}$. For $\Delta\tau_1 = \Delta\tau_3$ the second sensor has to have its center on a line $y = \pm\sqrt{r^2 - s^2\frac{\Delta\tau_1^2}{4}}$ which is two 1-dimensional manifolds in a 2-dimensional space. Since the centers are i.i.d uniformly, the probability that the second sensor lies on any of these two 1-dimensional manifolds is zero. See Figure 3.11 for illustration. The argument holds for any two pairs of sensors i and j, i $\neq j, i, j \in \{1,2,3,4\}$. This completes the proof. □

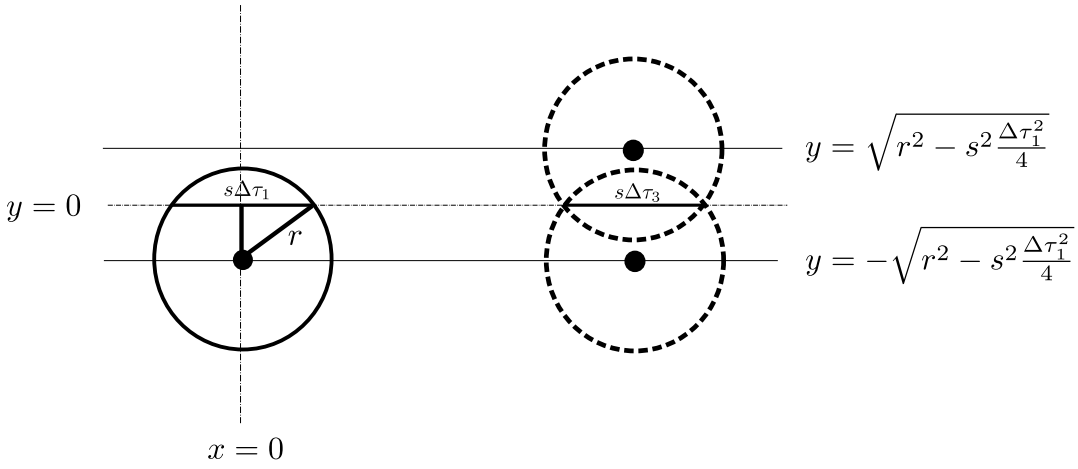

Figure 3.11: Illustration for Lemma 3.12.

Lemma 3.12. *Suppose an object moves on a straight line $L : y = ax + b$, with unknown constant speed s and intersects with three sensors whose centers $(0,0), (0,n_2)$ and $(m_3,n_3), \{n_2, m_3, n_3\} \notin \{0\}$, and all sensors have unknown range r. Suppose the "on" an "off" intersecting timestamps τ_{2i-1} and τ_{2i} are known, then with probability one only finite number of lines could satisfy (3.30)-(3.32).*

Proof. From Lemma 3.11, with probability one, (3.30)-(3.32) can be realized if L intersects 3 sensors. Taking (3.30) produces;

$$\left(\frac{\Delta\tau_3^2}{\Delta\tau_3^2-\Delta\tau_1^2} - \frac{\Delta\tau_5^2}{\Delta\tau_5^2-\Delta\tau_1^2}\right)\frac{b^2}{\Delta\tau_1^2} = \frac{(b-n_2)^2}{\Delta\tau_3^2-\Delta\tau_1^2} + \frac{(am_3+b-n_3)^2}{\Delta\tau_5^2-\Delta\tau_1^2}$$

$$\left(\frac{2n_2}{\Delta\tau_3^2-\Delta\tau_1^2} + \frac{2(am_3-n_3)}{\Delta\tau_5^2-\Delta\tau_1^2}\right)b = \frac{n_2^2}{\Delta\tau_3^2-\Delta\tau_1^2} + \frac{(am_3-n_3)^2}{\Delta\tau_5^2-\Delta\tau_1^2}.$$

$$\Rightarrow b = \frac{n_2^2(\Delta\tau_5^2-\Delta\tau_1^2) - (am_3-n_3)^2(\Delta\tau_3^2-\Delta\tau_1^2)}{2n_2(\Delta\tau_5^2-\Delta\tau_1^2) + 2(am_3-n_3)(\Delta\tau_3^2-\Delta\tau_1^2)} \tag{3.33}$$

Similarly, taking (3.31) produces;

$$\begin{aligned}\frac{(2\Delta\tau_2+\Delta\tau_1+\Delta\tau_3)^2}{\Delta\tau_3^2-\Delta\tau_1^2}(b^2-(b-n_2)^2) - (an_2)^2 &= 0\\ \frac{(2\Delta\tau_2+\Delta\tau_1+\Delta\tau_3)^2}{\Delta\tau_3^2-\Delta\tau_1^2}(2b-n_2) - a^2n_2 &= 0.\end{aligned}$$

$$\Rightarrow b = \frac{a^2n_2}{2}\frac{\Delta\tau_3^2-\Delta\tau_1^2}{(2\Delta\tau_2+\Delta\tau_1+\Delta\tau_3)^2} + \frac{n_2}{2}. \tag{3.34}$$

Solving (3.33) and (3.34) results in

$$a^3\frac{(\Delta\tau_3^2-\Delta\tau_1^2)}{(2\Delta\tau_2+\Delta\tau_1+\Delta\tau_3)^2} + a^2\left(\frac{n_2(\Delta\tau_5^2-\Delta\tau_1^2)-n_3(\Delta\tau_3^2-\Delta\tau_1^2)}{m_3(2\Delta\tau_2+\Delta\tau_1+\Delta\tau_3)^2} + \frac{m_3}{n_2}\right) - a = 0. \tag{3.35}$$

Notice that (3.35) is a polynomial equation in a and has finite number of solutions by the fundamental theorem of algebra [33]. Consequently, b also has finite number of solutions resulting in a finite pairing of $\{a,b\}$. This concludes the proof. □

Remark 3.2. We note that (3.35) is cubic in "a" even though (3.33) and (3.34) are quadratic. This is because any line L and 3 sensor placement that accepts 3 other lines $\hat{L}$ will have two of the feasible lines being parallel. Rotating and translating the first two senors to $(0,0)$ and $(0,n_2)$ will ensure that those two lines have $a=0$.

We now continue the proof of Theorem 3.10. Suppose that line $\hat{L}$ satisfies (3.30)- (3.32) using three sensors then $\hat{L}$, as well as L must be from the finite set of lines described in Lemma 3.11. With a fourth sensor, $\hat{L}$ and L must satisfy both (3.30)-(3.32) as well as (3.36)-(3.38) below:

$$\left(\frac{\Delta\tau_3^2}{\Delta\tau_3^2-\Delta\tau_1^2}-\frac{\Delta\tau_7^2}{\Delta\tau_7^2-\Delta\tau_1^2}\right)(am_1+b-n_1)^2-\frac{\Delta\tau_1^2(am_2+b-n_2)^2}{\Delta\tau_3^2-\Delta\tau_1^2}+\frac{\Delta\tau_1^2(am_4+b-n_4)^2}{\Delta\tau_7^2-\Delta\tau_1^2} = 0 \tag{3.36}$$

$$\left(\frac{\Delta\tau_5^2}{\Delta\tau_5^2-\Delta\tau_1^2}-\frac{\Delta\tau_7^2}{\Delta\tau_7^2-\Delta\tau_1^2}\right)(am_1+b-n_1)^2-\frac{\Delta\tau_1^2(am_3+b-n_3)^2}{\Delta\tau_5^2-\Delta\tau_1^2}+\frac{\Delta\tau_1^2(am_4+b-n_4)^2}{\Delta\tau_7^2-\Delta\tau_1^2} = 0 \tag{3.37}$$

$$\frac{(2\Delta\tau_6+\Delta\tau_5+\Delta\tau_7)^2}{\Delta\tau_7^2-\Delta\tau_5^2}((am_3+b-n_3)^2-(am_4+b-n_4)^2)=(m_4-m_3+a(n_4-n_3))^2. \tag{3.38}$$

With three sensors resulting in a finite number of candidate lines with probability one, the center of the fourth circle (m_4,n_4) cannot be arbitrary. By the exact argument used in Lemma 3.11, one can show that this results in a finite order polynomial equation in either m_4 or n_4. Hence by the fundamental theorem of algebra [33], this results in finite number of pairs (m_4,n_4) for each candidate line $\hat{L}$. Therefore, for any given three centers and resultant equations from (3.30)-(3.32), there are finite number fourth sensor centers that would result in $\hat{L}$ having the same resultant

equations from (3.36)-(3.38). With the centers of the four sensors i.i.d uniformly, the probability of one of these *finite set of centers* being the center of the fourth circle is zero. This concludes the proof of Theorem 3.10. □

3.4.2 Algorithm with s and r unknown

With four sensors, the full set of realizable equations devoid of s and r is as shown in (3.39) and (3.40) below.

$$g_{i,j}(a,b) = \alpha_{i,j}(am_1 + b - n_1)^2 - \beta_{i,j}(am_2 + b - n_2)^2 + \gamma_{i,j}(am_3 + b - n_3)^2 \quad (3.39)$$

where $g_{i,j}(a,b) = 0 \forall \{i,j\} \in \{2,3,4\}$,

$i \neq j, i < j$,

$\alpha_{i,j} = \frac{\Delta\tau_i^2}{\Delta\tau_i^2 - \Delta\tau_1^2} - \frac{\Delta\tau_j^2}{\Delta\tau_j^2 - \Delta\tau_1^2}$, $\beta_{i,j} = \frac{\Delta\tau_1^2}{\Delta\tau_i^2 - \Delta\tau_1^2}$, and $\gamma_{i,j} = \frac{\Delta\tau_1^2}{\Delta\tau_j^2 - \Delta\tau_1^2}$

$$h_k(a,b) = \delta_k((am_k + b - n_k)^2 - (am_{k+1} + b - n_{k+1})^2) - (m_{k+1} - m_k + a(n_{k+1} - n_k))^2 \quad (3.40)$$

where $k \in \{1,2,3\}$, and $\delta_k = \frac{(2\Delta\tau_{2k} + \Delta\tau_{2k-1} + \Delta\tau_{2k+1})^2}{\Delta\tau_{2k+1}^2 - \Delta\tau_{2k-1}^2}$.

We propose a Newton based least squares iterative search algorithm for determination of $X = [a,b]^T$. Define the function J, a 6×1 vector, as

$$J = [g_{2,3}(a,b), g_{2,4}(a,b), g_{3,4}(a,b), h_1(a,b), h_2(a,b), h_3(a,b)]^T \quad (3.41)$$

where $g_{i,j}(a,b)$ and $h_k(a,b)$ are as defined in (3.39) and (3.40) respectively. Also define the derivative of J as $\dot{J}$, a 6×2 matrix as

$$\dot{J} = \left[\frac{\partial J}{\partial a}, \frac{\partial J}{\partial b}\right]. \quad (3.42)$$

Then we propose the descent law

$$X[k] = X[k-1] - \left[\dot{J}^T\big|_{X[k-1]}\dot{J}\big|_{X[k-1]}\right]^{-1}\dot{J}^T\big|_{X[k-1]}J\big|_{X[k-1]} \tag{3.43}$$

where ^{T} denotes transpose. Of course this algorithm stems from the first order Taylor series expansion of $J\big|_{X[k]} = J\big|_{X[k-1]} + \dot{J}\big|_{X[k-1]}(X[k]-X[k-1]) + h.o.t.$ For $X[k]$ close to $X[k-1]$ the $h.o.t \approx 0$.This leads to a requirement of the initial estimate being close to the solution. We deal with this by setting $X[0]$ as the gradient and intercept from least squares line fit to the centers $\{m_i, n_i\}, i \in \{1,2,3,4\}$. From Theorem 3.10, we know with probability 1, there exist 1 real root close to $X[0]$, guaranteeing convergence of the algorithm to the solution. The pseudo-code of our algorithm is summarized in Algorithm 6.1.

Algorithm 3.3 Newton based least squares iterative search algorithm:

1. $X[0] \leftarrow \begin{bmatrix} \frac{4\sum_{i=1}^4 m_i n_i - \sum_{i=1}^4 m_i \sum_{i=1}^4 n_i}{\sum_{i=1}^4 m_i^2 - (\sum_{i=1}^4 m_i)^2} \\ \frac{4\sum_{i=1}^4 m_i^2 \sum_{i=1}^4 n_i - \sum_{i=1}^4 m_i \sum_{i=1}^4 m_i n_i}{\sum_{i=1}^4 m_i^2 - (\sum_{i=1}^4 m_i)^2} \end{bmatrix}$
2. $X[1] \leftarrow X[0] - \left[\dot{J}^T\big|_{X[0]}\dot{J}\big|_{X[0]}\right]^{-1}\dot{J}^T\big|_{X[0]}J\big|_{X[0]}$
3. $k \leftarrow 2$
4. **while** $\|X[k] - X[k-1]\| \geq tol$ and $k \leq k_{max}$

   $X[k] \leftarrow X[k-1] - \left[\dot{J}^T\big|_{X[k-1]}\dot{J}\big|_{X[k-1]}\right]^{-1}\dot{J}^T\big|_{X[k-1]}J\big|_{X[k-1]}$

   $k \leftarrow k+1$

   end

We model the effects of the background noise and measurement noise as Δ_r, an uncertainty in the sensing range. Thus the sensing range of sensor i becomes $r_i = r + \Delta_i$, where $\Delta_i \sim \mathcal{U}[-\Delta_r, \Delta_r]$.

3.4.3 Simulation results

Simulations were performed on a piecewise linear trajectory with different unknown constant speeds on each line segment. The nominal radius r and the speed s are unknown. Figure 3.12 shows simulation with $\Delta_r = 0$ whilst Figure 3.13 shows simulations with $\Delta_r = 0.15r$.

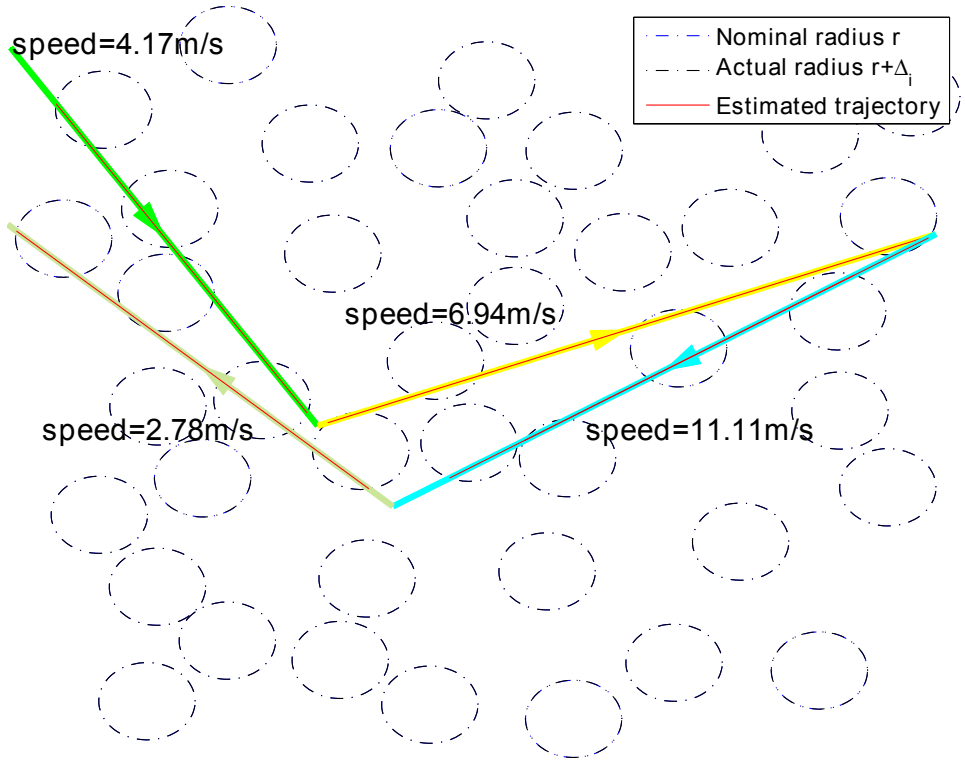

Figure 3.12: Trajectory with no uncertainty in r.

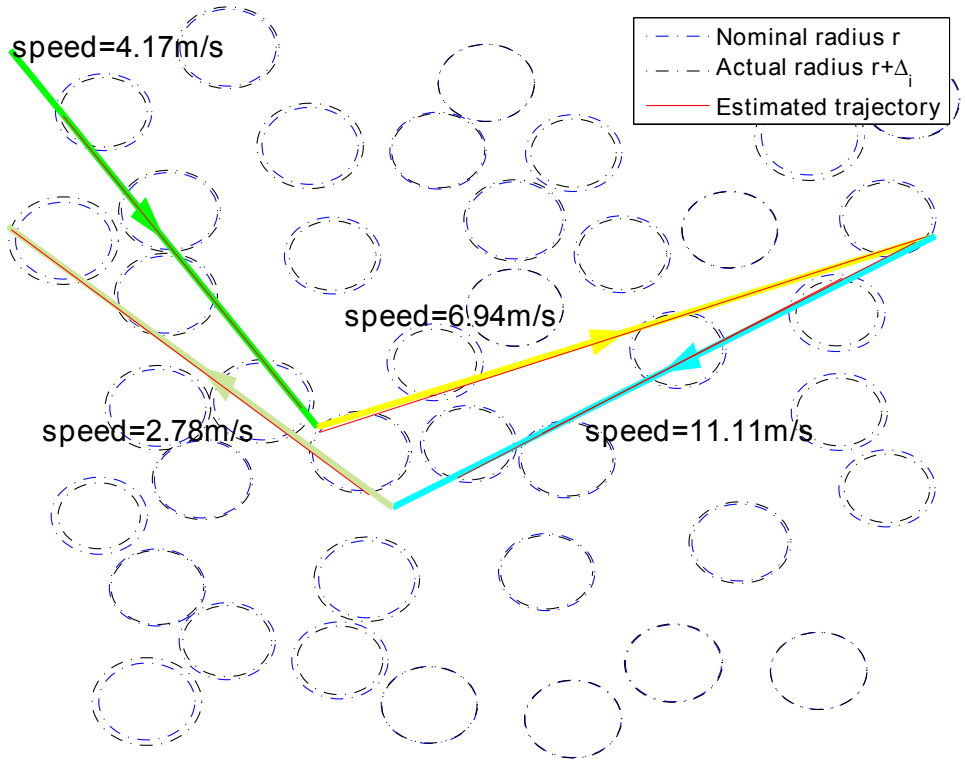

Figure 3.13: Trajectory with $\Delta_r = 0.15r$.

Figure 3.14 shows the results of 5000 Monte Carlo simulations for $\Delta_r \in [0.01r, 0.15r]$.

3.5 Conclusion

We have considered tracking of radioactive sources using binary proximity sensors with two general assumptions. The first assumption is that the source moves on a piecewise linear trajectory. The second assumption is that over each section of the piecewise linear trajectory, the source moves with a constant speed. We show that under these two general assumptions, the nonlinear source tracking problem can

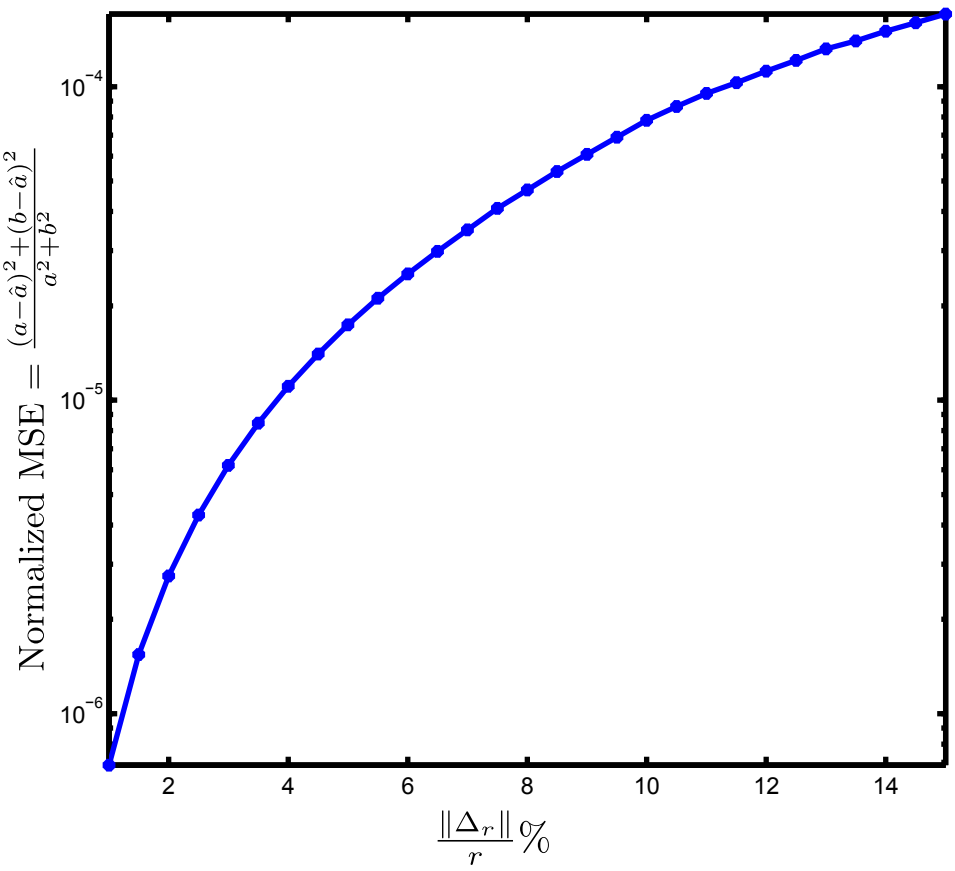

Figure 3.14: 5000 Monte Carlo simulations for $\Delta_r \in [0.01r, 0.15r]$

be converted into a linear parameter estimation problem if the nominal sensing range is known. We show that using three sensor measurements of "*on*" and "*off*" time stamps, the trajectory can be uniquely determined with probability 1. Simulations demonstrate robustness of our algorithm. We also show a newton based least squares iterative descent tracking of radioactive sources for the case where the nominal sensing range is unknown but homogeneous among the measurement sensors. Finally we show that using four sensor measurements of "*on*" and "*off*" time-stamps, the trajectory

can be uniquely determined with probability 1. Simulations demonstrate robustness.

CHAPTER 4
PERFORMANCE BOUNDS ON ESTIMATION ACCURACY OF RADIOACTIVE SOURCES USING IDEAL MOBILE SENSORS

The technical challenges of estimating radioactive sources have already been motivated in Chapter 1. Even beyond these challenges, a theoretical limitation arises from the fact that the radiation from a radioactive source is a fundamentally probabilistic physical process, resulting in an irreducible amount of randomness and uncertainty associated with its measurements. Radiation comprises discrete emissions of particles, and likewise detection of radiation fundamentally consists of a sequence of events involving the absorption of discrete particles. These emission and detection events are modeled statistically as Poisson arrival processes [35, 36].

While the variability of radiation measurements because of this random Poisson statistics is well-known and routinely taken into account in the literature [3] on radioactive source detection and estimation, the effect of this randomness has never been studied separately from other uncertainties like background radiation and modeling errors. While the latter effects are often larger in real-world radiation source detection and estimation applications, the variability of the Poisson process itself can have non-negligible effects, especially with weak sources, inexpensive detectors and fast-moving sources and/or detectors [4] that may limit observation intervals to be short. Indeed, to our knowledge, the only previous work to study the effect of the randomness in the radiation source detection and estimation process separately is [37] which looks at the probability of detection error and false alarm resulting from the

randomness of the emissions.

We examine the theoretical limits on the achievable accuracy of estimation of radioactive sources imposed by the inherent randomness of gamma particle emission and detection process itself, even in the absence of any other external impairments in the detection or estimation process such as measurement errors, background noise, modeling uncertainties and so on. This study is intended as a step towards a better understanding of the effect of this randomness. In addition, our theoretical limits with ideal sensors represent upper bounds on the performance achievable with any real-world detector, and provide important benchmarks for practical detection and estimation.

4.1 Problem formulation

We consider first the general problem of estimating the trajectory of a moving radioactive source using the measurements of a mobile, ideal detector. We then specialize to a stationary source and a detector moving in a straight line with uniform speed and a simple square-law signal strength model. While much of our analysis can be extended to the more general problem, we focus on these special cases as they admit elegant closed form expressions that are revealing and insightful. We consider an infinite horizon arrival process generalizable to a finite time horizon case.

4.1.1 The ideal nuclear detector

We define an ideal detector as a device that records the time of arrival of every particle absorbed by its detection hardware. We ignore possible limits on the timing

accuracy of such a detector due to the quantum energy-time uncertainty principle [38].

This ideal device is of course strictly superior to any practical radiation detector in the sense that the observations of any practical device can be represented as a (possibly noisy) function of the measurements of the ideal sensor. For instance, a detector that uses average arrival rates for signal strength measurements can equivalently be represented as averaging inter-arrival times from an ideal sensor. Similarly, a practical sensor that detects particle counts over a set of finite observation intervals can be represented as a device that quantizes an ideal sensor's time-stamp measurements. Designs for practical sensors with detection time bins as short as 150 ms have been reported [39]. As detection intervals become shorter, such practical detectors can approach the performance of an ideal sensor.

4.1.2 General problem statement

Consider a radioactive source moving along a trajectory

$$\mathbf{z}_\theta(t) \equiv [x_\theta(t), y_\theta(t)] \tag{4.1}$$

parameterized by an arbitrary set of unknown variables θ, and a detector moving along the known trajectory $\mathbf{z}(t)$. The distance of the detector from the source at time t is

$$d(t) = \|\mathbf{z}_\theta(t) - \mathbf{z}(t)\| \tag{4.2}$$

where $\|\cdot\|$ denotes the 2-norm representing the usual Euclidean distance.

In the sequel, we assume that the mean arrival rate of gamma particles from

the source depend only on the distance from the source. In other words, we do not consider directional detectors such as CZT Compton scattering devices [40] and limit ourselves to scintillation-type devices [41] and isotropic media. However, our analysis is not limited to this case, and can be easily extended. Accordingly, in our formulation, particles from the source are absorbed by the detector at discrete times representing an instance of an inhomogeneous Poisson process [42] with the mean arrival rate

$$\lambda(t) = f(d(t)) \tag{4.3}$$

where $f(d(t))$ is a decreasing function of distance representing the attenuation of the source strength over space.

The general problem of radioactive source estimation can be stated as the problem of finding the source strength and trajectory by estimating the set of unknown parameters θ, given a (possibly countably infinite) set of observed arrival times $\tau_m, m \in \{1, \cdots, n\}$ at the ideal detector over some (possibly infinite) observation interval (T_1, T_2). This problem is readily generalized to a network of many sensors.

4.1.3 Special case: Stationary source with uniform speed mobile detector on a straight line

As stated earlier, we mostly focus on a special case of the problem in 4.1.2. In this special case, the source is stationary at an unknown location

$$\mathbf{z}_\theta(t) = [x_0, y_0] \tag{4.4}$$

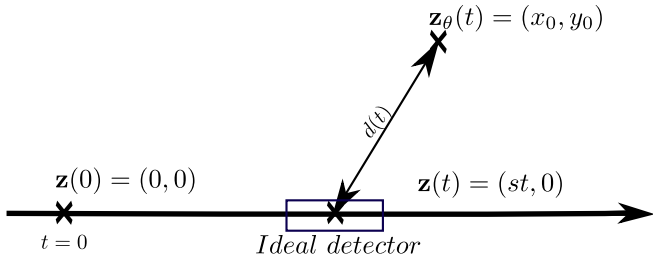

Figure 4.1: Ideal detector moving on a straight line with constant speed.

and the detector is moving with a constant speed s on a straight line that without loss of generality can be taken to be the abscissa of the Cartesian plane. Furthermore, we choose our coordinates so that the detector's position at time $t = 0$ is chosen as the origin. Then the detector's trajectory is

$$\mathcal{L} : \mathbf{z}(t) = [st, 0] \tag{4.5}$$

and the corresponding distance from the source is

$$d(t) = \sqrt{y_0^2 + (x_0 - st)^2} \tag{4.6}$$

As observations are from a detector confined to a line, to remove the flip ambiguity in localization this engenders, we assume that $y_0 > 0$.

In this special case, we also assume that the signal attenuation follows a simple inverse square law

$$f(d(t)) = \frac{A}{d^2(t)} \tag{4.7}$$

which gives for the mean arrival rate at the detector

$$\lambda(t) = \frac{A}{y_0^2 + (x_0 - st)^2}, \tag{4.8}$$

where A is a source strength parameter that depends on the type, shape and total volume of the nuclear source as well as the detector characteristics.This setup is depicted in Figure 4.1.

The unknown parameters for this case consists of the triplet

$$\theta = [A,\ x_0,\ y_0]^T \tag{4.9}$$

The total number of arrival times recorded by an ideal detector is a Poisson random variable N with mean equal to the area under the curve generated by $\lambda(t) = f(d(t))$, which turns out to be finite even for an infinite time horizon for the inverse-square law attenuation model in (4.8):

$$E\big[N\big] = \int_{-\infty}^{\infty} \frac{A}{y_0^2 + (x_0 - st)^2}\ \mathrm{dt} = \frac{\pi A}{s y_0} \tag{4.10}$$

The nuclear source localization problem in this special case, is then the problem of estimating the triplet $\theta = [A, x_0, y_0]$ given a set of measured time-stamps representing the arrivals of radiation particles $\tau_m, m \in \{1, \cdots, n\}$ over the infinite time horizon $t \in (-\infty, \infty)$. One realization of the random arrival process is shown in Fig. 4.2.

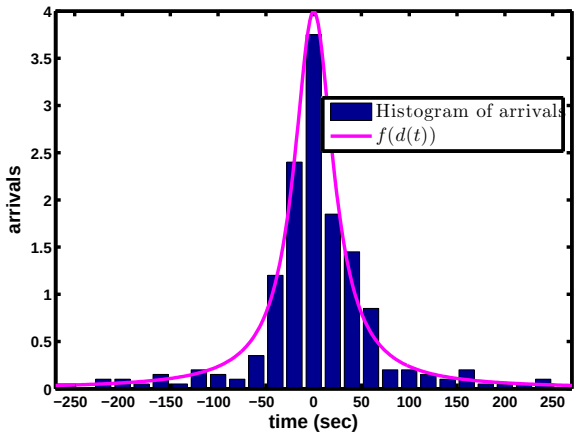

Figure 4.2: One instance of the Poisson arrival process at the ideal detector.

4.2 Maximum likelihood estimation of nuclear source location and strength

We now derive the likelihood function for the general estimation problem presented in Section 4.1.2. We will then specialize this likelihood function for the special case in Section 4.1.3 and derive the maximum likelihood solution.

4.2.1 Likelihood function

Let $\tau \equiv [\tau_1,\ \tau_2,\ \ldots,\ \tau_n]$ represent the vector with the observations at the detector i.e. the time-stamps. Assume that the time-stamps are sorted so that $\tau_1 < \tau_2 < \tau_3 \ldots < \tau_n$. The likelihood function is simply the joint conditional density of τ given the parameters θ, i.e.

$$l(\theta) = f_{\tau|\theta}(\tau|\theta) \tag{4.11}$$

We will now use well-known properties of Poisson processes [42] to derive a general expression for the corresponding log-likelihood function $L(\theta) = \log(l(\theta))$. We start by dividing the time-line into short intervals $\mathcal{I}_k = \{t \in (t_k,\ t_{k+1} = t_k + \Delta t]\},\ k \in (-\infty, \infty)$ each of duration Δt as shown in Fig. 4.3. Let λ_k be the mean arrival rate in $\mathcal{I}_k$:

$$\lambda_k = \frac{1}{\Delta t} \int_{t_k}^{t_{k+1}} \lambda(t) dt \tag{4.12}$$

Then, the expected number of arrivals in $\mathcal{I}_k$ is $n_k = \lambda_k \Delta t$. Note that (4.12) implies $\lim_{\Delta t \to 0} \lambda_k = \lambda(t_k)$. The probability of receiving m arrivals in the interval $\mathcal{I}_k$ follows the Poisson distribution: $p(m) = \frac{n_k^m e^{-n_k}}{m!}$. Assuming that Δt is chosen small enough, each of the intervals $\mathcal{I}_k$ contain either $m = 0$ or $m = 1$ arrivals. Furthermore, the number of arrivals in each interval are all independent random variables. Let n_i denote the interval which contains the i'th arrival τ_i i.e. $\tau_i \in \mathcal{I}_{n_i}$. Let $\mathcal{N}$ denote the set of intervals in which $m = 1$ arrivals occurred i.e. $\mathcal{N} = \{k : \exists i \text{ such that } n_i = k\}$. Let $\mathcal{N}^c$ be the complementary set of intervals in which $m = 0$ arrivals occurred. Finally, note that (4.12) implies $\lim_{\Delta t \to 0} \lambda_{n_i} = \lambda(\tau_i)$. We then have for the likelihood function

$$l(\theta) = f_{\tau|\theta}(\tau|\theta) = \prod_{k \in \mathcal{N}} \lambda_k \Delta t e^{-\lambda_k \Delta t} \prod_{k \in \mathcal{N}^c} e^{-\lambda_k \Delta t} \tag{4.13}$$

$$= (\Delta t)^N \left(\prod_{k \in \mathcal{N}} \lambda_k \right) \left(e^{-\sum_{k=-\infty}^{\infty} \lambda_k \Delta t} \right) \tag{4.14}$$

Noting that $(\Delta t)^N$ does not depend on the unknown parameters θ, and taking limits as $\Delta t \to 0$ on the remaining terms, we can now write down a modified log-

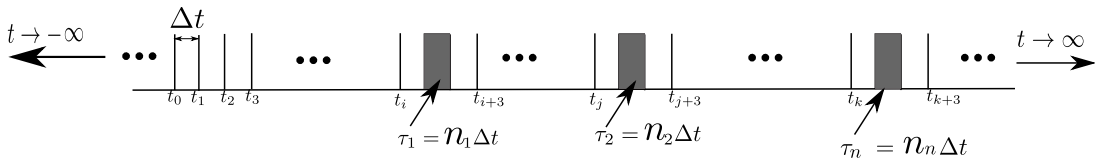

Figure 4.3: Illustration of arrival times over infinite time horizon.

likelihood function

$$L(\theta) = -\int_{-\infty}^{\infty} \lambda(t)dt + \sum_{i=1}^{n} \log\left(\lambda(\tau_i)\right) \tag{4.15}$$

Specializing (4.15) to the case of Section 4.1.3 gives:

$$L(A, x_0, y_0) \;\; = -\tfrac{\pi A}{s y_0} + n \log A - \textstyle\sum_{i=1}^{n} \log\left(y_0^2 + (x_0 - s\tau_i)^2\right) \tag{4.16}$$

For the finite time horizon, (4.16) generalizes to:

$$L(A, x_0, y_0) \;\; = -\tfrac{A}{s y_0}\kappa(T_1, T_2, x_0, y_0) + n \log A - \textstyle\sum_{i=1}^{n} \log\left(y_0^2 + (x_0 - s\tau_i)^2\right) \tag{4.17}$$

where $\kappa(T_1, T_2, x_0, y_0) = \arctan(\frac{x_0 - sT_1}{y_0}) - \arctan(\frac{x_0 - sT_2}{y_0})$.

4.2.2 The maximum likelihood estimate

For a given set of observations by the detector τ_i, the maximum likelihood estimates are defined as $[\hat{A}, \hat{x}_s, \hat{y}_s] = \arg\max_{A,x_0,y_0} L(A, x_0, y_0)$.

Proposition 1. The log-likelihood function in (4.16) has a unique critical point and this point is the global maximum for $L(A, x_0, y_0)$.

Define the set of n functions $\alpha_i(x, y),\ i = 1 \ldots n$ as:

$$\alpha_i(x, y) = \frac{1}{y^2 + (x - s\tau_i)^2} \tag{4.18}$$

Differentiating $L(A, x_0, y_0)$ with respect to $A,\ x_0,\ y_0$ and equating to zero immediately gives for the ML estimates:

$$\begin{aligned}
\hat{A} &= \frac{ns\hat{y}}{\kappa(T_1, T_2, \hat{x}, \hat{y})} \\
\sum_{i=1}^{n} \alpha_i(\hat{x}, \hat{y})\big(\hat{x} - s\tau_i\big) &= \frac{n\hat{y}\left(\frac{1}{\hat{y}^2-(\hat{x}-sT_2)^2} - \frac{1}{\hat{y}^2-(\hat{x}-sT_1)^2}\right)}{2\kappa(T_1, T_2, \hat{x}, \hat{y})} \\
\sum_{i=1}^{n} \alpha_i(\hat{x}, \hat{y}) &= \frac{n}{2\hat{y}^2} - \frac{n\left(\frac{\hat{x}-sT_2}{\hat{y}^2-(\hat{x}-sT_2)^2} - \frac{\hat{x}-sT_1}{\hat{y}^2-(\hat{x}-sT_1)^2}\right)}{2\hat{y}\kappa(T_1, T_2, \hat{x}, \hat{y})}
\end{aligned} \tag{4.19}$$

(4.19) generalizes for the infinite horizon case to:

$$\hat{A} = \frac{ns\hat{y}}{\pi},\ \sum_{i=1}^{n} \alpha_i(\hat{x}, \hat{y})\big(\hat{x} - s\tau_i\big) = 0,\ \sum_{i=1}^{n} \alpha_i(\hat{x}, \hat{y}) = \frac{n}{2\hat{y}^2} \tag{4.20}$$

Equation (4.20) provides an explicit expression for $\hat{A}$, and a pair of equations that implicitly determine $\hat{x},\ \hat{y}$. Now given constant a, define

$$Q(y) \doteq y^2 \sum_{i=1}^{n} \alpha_i(a, y) - \frac{n}{2} \equiv \sum_{i=1}^{n} \frac{y^2}{y^2 + (a - s\tau_i)^2} - \frac{n}{2} \tag{4.21}$$

Clearly, $Q(0) = -\frac{n}{2}$, and $\lim_{y\to\infty} Q(y) = \frac{n}{2}$. Since $Q(y)$ is a strictly monotonic function of y for $y > 0$, it follows then that there is a unique positive solution to $Q(y) = 0$. Let us denote this solution $y = f_1(a)$.

Proposition 2. The sequence $y[m]$ defined by the recursion $y[m+1] = \sqrt{\frac{n}{2\sum_{i=1}^{n} \alpha_i(a, y[m])}}$ converges to $f_1(a)$.

Proof. From (4.20) define Q(x,y) $\doteq y^2 \sum_{i=1}^{n} \alpha_i(x, y) - \frac{n}{2}$.

$$\frac{\partial Q(x,y)}{\partial y^2} = \sum_{i=1}^{n} \alpha_i(x, y) - y^2 \sum_{i=1}^{n} \alpha_i^2(x, y) = \sum_{i=1}^{n} (x - s\tau_i)^2 \alpha_i^2(x, y) > 0. \tag{4.22}$$

$Q(x, y)$ is a strictly increasing function of y^2. $Q(0, x) = -\frac{n}{2}$ and $Q(\infty, x) = \frac{n}{2}$. Therefore, for a fixed value of x there is a unique $y > 0$ such that $Q(x, y) = 0$. □

Comparing (4.21) with (4.20), we see that the ML solution satisfies $\hat{y} = f_1(\hat{x})$. Thus Proposition 2 provides a simple recursive procedure to calculate $\hat{y}$ given an estimate of $\hat{x}$. Now define

$$f_2(x) \doteq \frac{\sum_{i=1}^{n} s\tau_i \alpha_i\big(x, f_1(x)\big)}{\sum_{i=1}^{n} \alpha_i\big(x, f_1(x)\big)} \tag{4.23}$$

Comparing (4.23) with (4.20), we see that $\hat{x} - f_2(\hat{x}) = 0$. We finally have the following proposition.

Proposition 3. The sequence $x[m]$ defined by the recursion $x[m+1] = f_2\big(x[m]\big)$ converges to $\hat{x}$.

Propositions 3 and 2 along with the expression for $\hat{A}$ in (4.20) provide a complete numerical procedure to calculate the maximum likelihood solution to our localization problem.

4.3 Cramer-Rao bound

Finally, recalling that $y_0 > 0$ we derive the Cramer-Rao lower bounds (crlb) for $\theta = \{A, x_0, y_0\}$. From (4.15) and (4.16),

$$\frac{\partial L(A, x_0, y_0)}{\partial \theta} = \begin{bmatrix} -\frac{\kappa(T_1, T_2, x_0, y_0)}{sy} + \frac{n}{A} \\ \frac{A}{s}\left(\frac{1}{y_0^2 + (x_0 - sT_2)^2} - \frac{1}{y_0^2 + (x_0 - sT_1)^2}\right) - 2\sum_{i=1}^{n} \alpha_i(x_0, y_0)(x_0 - s\tau_i) \\ \frac{\pi A}{s y_0^2} - 2\sum_{i=1}^{n} \alpha_i(x_0, y_0) y_0 \end{bmatrix} \tag{4.24}$$

Define

$$z_i = x_0 - s\tau_i, \tag{4.25}$$

Algorithm 4.1 Algorithm for finding ML estimate

Initialize Algorithm:

[1] $\alpha_i(\hat{x}_{[0]}, \hat{y}_{[0]})_{[0]} \leftarrow \frac{1}{n}$

[2] $\hat{x}_{[0]} \leftarrow \frac{1}{n}\sum_{i=1}^{n} s\tau_i$

[3] $\hat{y}^2_{[0]} \leftarrow \frac{n}{2}$

Iterate till convergence:

while $\left\| \begin{matrix} \hat{x}_{[k]} - \hat{x}_{[k-1]} \\ \hat{y}^2_{[k]} - \hat{y}^2_{[k-1]} \end{matrix} \right\| < Tolerance$

[4] $\alpha_i(\hat{x}_{[k]}, \hat{y}_{[k]})_{[k+1]} \leftarrow \frac{1}{\hat{y}^2_{[k]} + \left(\hat{x}_{[k]} - s\tau_i\right)^2}$

[5] $\hat{x}_{[k+1]} \leftarrow \frac{s\sum_{i=1}^{n} \alpha_i(\hat{x}_{[k]}, \hat{y}_{[k]})_{[k+1]}\tau_i}{\sum_{i=1}^{n} \alpha_i(\hat{x}_{[k]}, \hat{y}_{[k]})_{[k+1]}}$

[6] $\hat{y}^2_{[k+1]} \leftarrow \frac{n}{2\sum_{i=1}^{n} \alpha_i(\hat{x}_{[k]}, \hat{y}_{[k]})_{[k+1]}}$

[7] $k \leftarrow k + 1$

end

$$\alpha_{(T_1,T_2)} = \frac{1}{y_0^2 + (x_0 - sT_2)^2} - \frac{1}{y_0^2 + (x_0 - sT_1)^2}, \tag{4.26}$$

$$\beta_{(T_1,T_2)} = \frac{x_0 - sT_2}{y_0^2 + (x_0 - sT_2)^2} - \frac{x_0 - sT_1}{y_0^2 + (x_0 - sT_1)^2}, \tag{4.27}$$

$$\gamma_{(T_1,T_2)} = \frac{x_0 - sT_2}{(y_0^2 + (x_0 - sT_2)^2)^2} - \frac{x_0 - sT_1}{(y_0^2 + (x_0 - sT_1)^2)^2}. \tag{4.28}$$

and

$$\psi_{(T_1,T_2)} = \frac{1}{(y_0^2 + (x_0 - sT_2)^2)^2} - \frac{1}{(y_0^2 + (x_0 - sT_1)^2)^2}. \tag{4.29}$$

Then the Hessian matrix of the log likelihood function is:

$$\begin{bmatrix} -\frac{n}{A^2} & \frac{\alpha_{(T_1,T_2)}}{s} & \frac{\kappa(T_1,T_2,x_0,y_0)}{sy^2} - \frac{\beta_{(T_1,T_2)}}{sy_0} \\ \frac{\alpha_{(T_1,T_2)}}{s} & -2\sum_{i=1}^{n}\alpha_i^2(x,y)(y^2 - z_i^2) - \frac{2A\gamma_{(T_1,T_2)}}{s} & 4\sum_{i=1}^{n}\alpha_i^2(x,y)yz_i - \frac{2Ay_0\psi_{(T_1,T_2)}}{s} \\ \frac{\kappa(T_1,T_2,x_0,y_0)}{sy^2} - \frac{\beta_{(T_1,T_2)}}{sy_0} & 4\sum_{i=1}^{n}\alpha_i^2(x,y)yz_i - \frac{2Ay_0\psi_{(T_1,T_2)}}{s} & \eta_{(3,3)} \end{bmatrix} \tag{4.30}$$

where $\eta_{(3,3)} = -\frac{2A\kappa(T_1,T_2,x_0,y_0)}{sy_0^3} + 2\sum_{i=1}^{n}\alpha_i^2(x,y)(y^2 - z_i^2) + \frac{A}{s}\left((1 + \frac{1}{y_0^2})\beta_{(T_1,T_2)} + 2\gamma_{(T_1,T_2)}\right)$

The corresponding Fisher information matrix from from (4.30) is:

$$FIM = \begin{bmatrix} \frac{\kappa(T_1,T_2,x_0,y_0)}{sy_0A} & -\frac{\alpha_{(T_1,T_2)}}{s} & -\frac{\kappa(T_1,T_2,x_0,y_0)}{sy^2} + \frac{\beta_{(T_1,T_2)}}{sy_0} \\ -\frac{\alpha_{(T_1,T_2)}}{s} & \frac{A\kappa(T_1,T_2,x_0,y_0)}{2sy_0^3} + \frac{2A\gamma_{(T_1,T_2)}}{s} & \frac{(2A-1)y_0\psi_{(T_1,T_2)}}{s} \\ -\frac{\kappa(T_1,T_2,x_0,y_0)}{sy^2} + \frac{\beta_{(T_1,T_2)}}{sy_0} & \frac{(2A-1)y_0\psi_{(T_1,T_2)}}{s} & \hat{\eta}_{(3,3)} \end{bmatrix} \tag{4.31}$$

where $\hat{\eta}_{(3,3)} = \frac{3A\kappa(T_1,T_2,x_0,y_0)}{2sy_0^3} - \frac{2A}{s}\left(\frac{\beta_{(T_1,T_2)}}{y_0^2} + \gamma_{(T_1,T_2)}\right)$. For the infinite time horizon case, (4.31) reduces to:

$$FIM = \begin{bmatrix} \frac{\pi}{sy_0A} & 0 & -\frac{\pi}{sy_0^2} \\ 0 & \frac{\pi A}{2sy_0^3} & 0 \\ -\frac{\pi}{sy_0^2} & 0 & \frac{3\pi A}{2sy_0^3} \end{bmatrix} \tag{4.32}$$

with a corresponding inverse of:

$$FIM^{-1} = \begin{bmatrix} \frac{3sy_0A}{\pi} & 0 & \frac{2sy_0^2}{\pi} \\ 0 & \frac{2sy_0^3}{\pi A} & 0 \\ \frac{2sy_0^2}{\pi} & 0 & \frac{2sy_0^3}{\pi A} \end{bmatrix}. \tag{4.33}$$

Consequently, the crlb for $\{A, x, y\}$ are $\left\{\frac{3sy_0A}{\pi}, \frac{2sy_0^3}{\pi A}, \frac{2sy_0^3}{\pi A}\right\}$ respectively.

The Cramer-Rao bounds in (4.33) for the infinite time horizon have some interesting properties, some of which are intuitively obvious, while others are somewhat surprising. First note that the bounds are completely independent of x_0 and increase with y_0. This is because the shortest distance of approach between the source and the line on which the detector moves is y_0, independent of x_0. The square law ensures that a shorter distance provides more accurate localization. Likewise, whilst it is intuitively unsurprising that a slower moving detector or stronger source each lead to improved localization accuracy, the bounds in (4.33) allow us to make this intuition more precise: Estimation accuracy improves with a larger A/s. In fact a higher value of s has the same effect on the estimation of all quantities, the Fisher Information Matrix being inversely proportional to s. Finally, the fact that the bounds on the variance of x_0 and y_0 are identical is a mild surprise as there is no obvious symmetry between the two coordinates. In fact the symmetry is lost for the finite horizon case.

4.4 Simulation results

We now present some numerical results where we compare the ML estimate with the Cramer-Rao bounds. The Poisson process in (4.8) is simulated using standard methods [43],[42] with the source location $\mathbf{z}_\theta = [0, 500]^T$ m and the detector speed $s = 20ms^{-1}$. The mean squared error estimation error of the ML estimate is calculated for different values of $A\pi/(sy_0)$; s is kept constant while varying A. The results averaged over 10000 independent independent realizations of the Poisson ar-

rival process is shown in Fig. 4.7. Similar results are obtained if we vary the other parameters s and $x_0,\ y_0$ as predicted by (4.33). The main takeaway from these simulations is that the variance of the ML estimate quickly converges to the CRLB when the expected number of arrivals exceeds 50 or so.

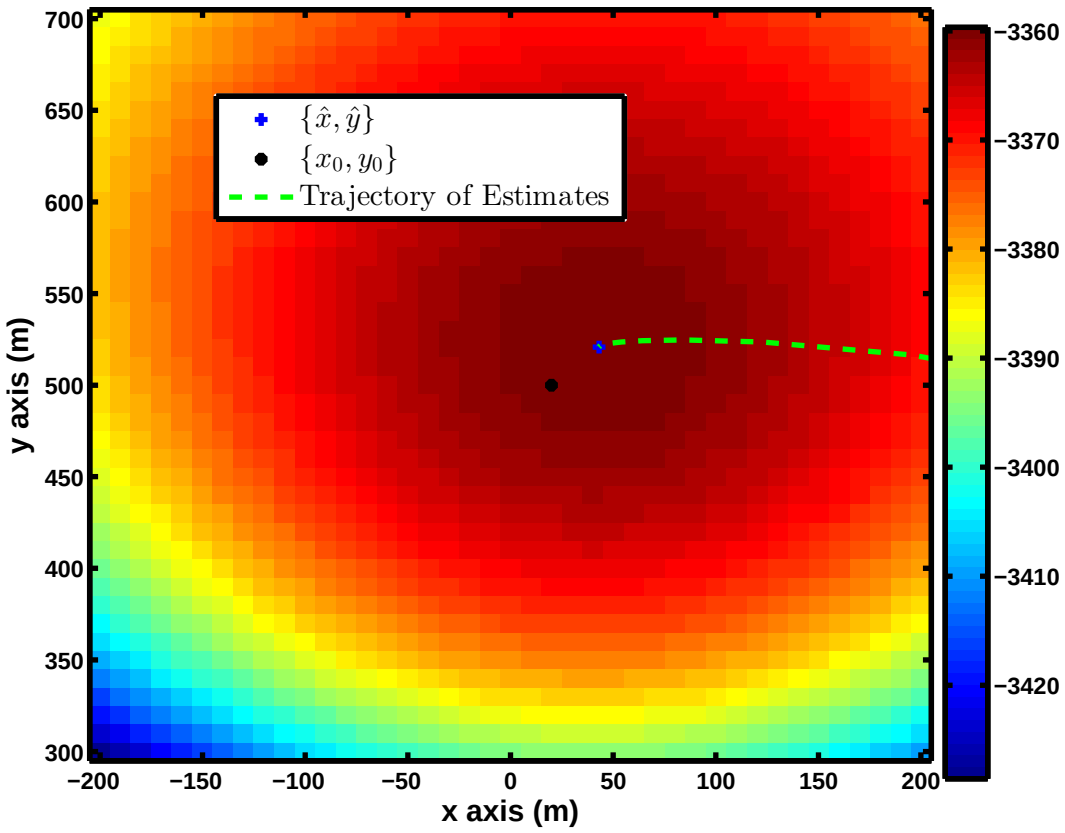

Figure 4.4: Heat map showing algorithm goes to the ML estimate.

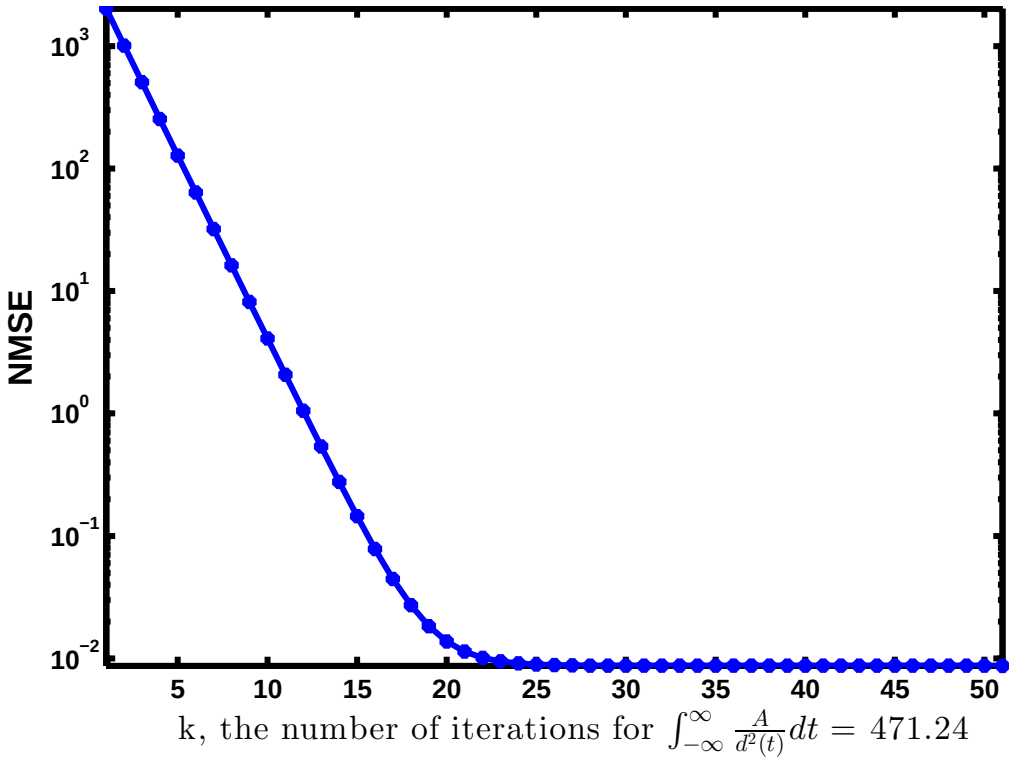

Figure 4.5: Convergence rate of algorithm.

4.5 Conclusion

In this Chapter, we have made a start towards exploring the fundamental limits on the achievable accuracy of localizing nuclear sources because of the inherent randomness of nuclear emission and detection processes. While we considered the special case of a stationary source and an ideal detector moving in a straight line with uniform speed under an inverse square law attenuation model, the analysis can be extended and generalized to tracking moving sources using a network of detectors and taking into account shielding materials as well as practical detector characteristics.

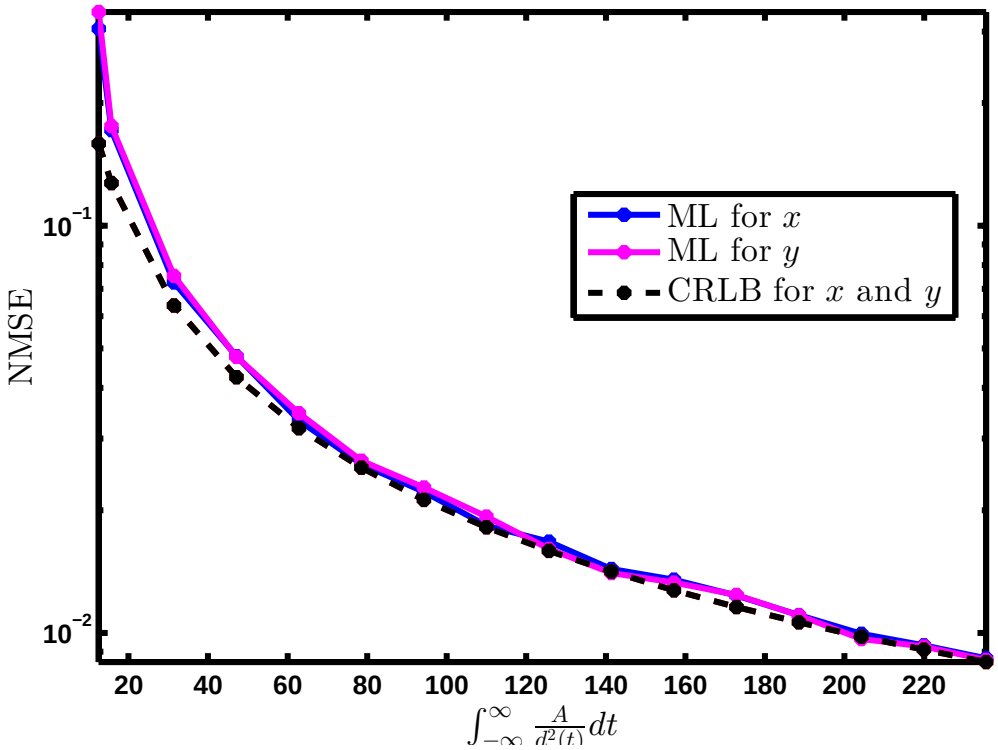

Figure 4.6: Normalized MSE of $\{\hat{x}, \hat{y}\}$ against expected number of detected particles.

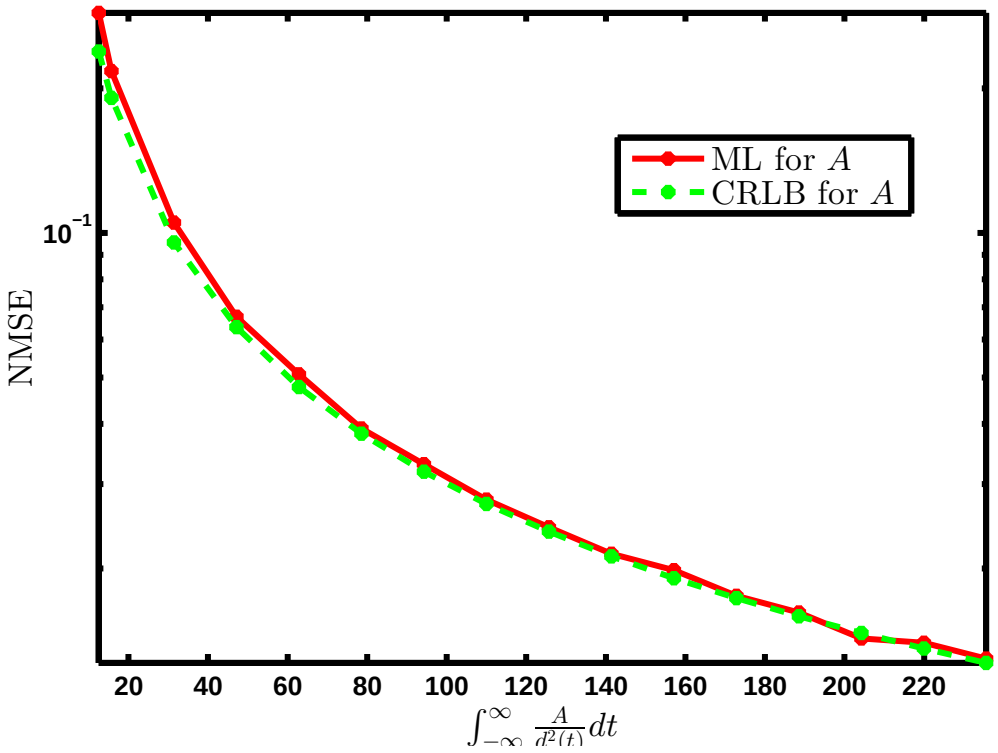

Figure 4.7: Normalized MSE of $\hat{A}$ against expected number of detected particles.

CHAPTER 5
CONCLUSION AND FUTURE RESEARCH

In this thesis, we have presented research which has resulted in novel approaches to the problem of estimation and tracking of radioactive sources under some general conditions that are much more robust than earlier methods in low signal-to-noise ratio regimes. Specifically, we have first considered estimation of radioactive sources with and without knowledge of the expectation of the source signal strength. Our focus has been on using the minimum number of sensors and on conditions to ensure uniqueness and robustness of our algorithms. second, we have considered tracking of radioactive sources under the general assumption that the motion is well approximated with piece-wise linear joins. Under this assumption, we have come up with the minimum number of cheap sensors required to localize each linear trajectory and characterized the robustness of our algorithms. Finally we have looked at the fundamental limits of localization accuracy using a mobile ideal sensor moving on a straight line.

The main challenge for radioactive material detection and estimation is in the fact that the measured signal typically has a large amount of background noise. It is also necessary to achieve coverage over a large area with a limited number of sensors, cheap or otherwise. Further, this problem is characterized by uncertainty and lack of prior knowledge of the signal propagation characteristics. In the model of (2.2), the two parameters , A and α, corresponding to the source strength and the signal absorption in the medium are usually both subject to a great deal of uncertainty.

While it may be reasonable under certain conditions to assume knowledge of the statistics of the background radiation w, and possibly an estimate of the absorption coefficient α based on the building density in urban areas for instance, the source strength can vary over a very wide range depending on the type, size and composition of the material and it is difficult to have any reliable prior knowledge of it.

With all this in mind, we have developed algorithms under general conditions which are robust to signal uncertainties and noise. We have not however solved all the research questions that arise from detection, estimation, localizing and tracking of radioactive sources.

5.1 Open problems

We enumerate some open problems that are logical extensions to this thesis.

1. **Estimation of multiple sources of gamma radiation sources**

   Our results on estimation of radiation sources have centered on a single point radiation source. Suppose there are multiple radioactive sources in $\mathbb{R}^N$, N being the dimension of space, can we robustly localize any or all the sources? In particular, suppose we have $n \geq 1$ sensors with the measurement at the i^{th} sensor, $i \in \{1, \cdots, n\}$ given as

$$S_i \sim Poisson\left(\sum_{m=1}^{M} \frac{A_m e^{-\alpha d_{i_m}}}{d_{i_m}^2} + w_i\right) \tag{5.1}$$

   where $M \geq 1$ is the total number of point radiation sources, A_m is the the signal strength from the m^{th} source at unit distance and zero attenuation coefficient

and no NORM as background, α is the attenuation coefficient due to the channel, w_i is the NORM background noise at the i^{th} sensor and d_{i_m} is the 2-norm defined as

$$d_{i_m} = \|x_i - y_m\| \tag{5.2}$$

with $x_i \in \mathbb{R}^N$ and $y_m \in \mathbb{R}^N$ being the locations of the i^{th} sensor and the m^{th} source respectively. There are two questions that arise: (1) How do we know the number of sources from the sensor measurements? (2) What is the minimum value of n to localize all M sources in $\mathbb{R}^N$?

2. **Tracking of a source on a piece-wise parabolic trajectory**

   In Chapter 3, a general assumption was made that piece-wise linear joins is a good approximation for the source trajectory. However, could we do better than piece-wise linear joins without unnecessarily complicating the problem? The answer is yes. Piece-wise parabolic joins will be a better approximation than piece-wise linear joins.

   Specifically, consider that a radioactive source moves on a parabolic trajectory $P : y = ax^2 + bx + c$ in $\mathbb{R}^N$, where N is the dimension of the search space. Suppose the source moves with a constant speed s and suppose the trajectory of the source intersects n binary sensors of detecting sensing radii r with on and off intersecting time stamps τ_{i_1} and τ_{i_2} respectively $\forall i \in \{1, 2, 3, ..., n\}$. There are two questions that arise: (1) Can we uniquely determine P? (2) What is the lower bound on n?

REFERENCES

[1] Homeland Security. Civil defense and homeland security: a short history of national preparedness efforts. *Homeland Security National Preparedness Task Force*, September 2006.

[2] R. Vilim, R. Klann, et al. Radtrac: A system for detecting, localizing, and tracking radioactive sources in real time. *Nucl. Technol.*, 168(ANL/NE/JA-63415), 2009.

[3] N. S V Rao, M. Shankar, Jren-Chit Chin, D.K.Y. Yau, S. Srivathsan, S.S. Iyengar, Yong Yang, and J.C. Hou. Identification of low-level point radiation sources using a sensor network. In *International Conference on Information Processing in Sensor Networks (IPSN)*, pages 493–504, April 2008.

[4] R.J. Nemzek, J.S. Dreicer, D.C. Torney, and T.T. Warnock. Distributed sensor networks for detection of mobile radioactive sources. *Nuclear Science, IEEE Transactions on*, 51(4):1693–1700, Aug 2004.

[5] H.E. Baidoo-Williams, S. Dasgupta, R. Mudumbai, and E. Bai. On the gradient descent localization of radioactive sources. *Signal Processing Letters, IEEE*, 20(11):1046–1049, Nov 2013.

[6] P. Kump, E. Bai, K. Chan, and W. Eichinger. Detection of shielded radionuclides from weak and poorly resolved spectra using group positive rival. *Radiation Measurements*, 2012.

[7] I. Shames, S. Dasgupta, B. Fidan, and B. D. O. Anderson. Circumnavigation using distance measurements under slow drift. *Automatic Control, IEEE Transactions on*, 57(4):889–903, 2012.

[8] E. Xu, Z. Ding, and S. Dasgupta. Target tracking and mobile sensor navigation in wireless sensor networks. 2009.

[9] J. Chin, D. K.Y. Yau, N. S. V. Rao, Y. Yang, C. Y. T. Ma, and M. Shankar. Accurate localization of low-level radioactive source under noise and measurement errors. In *Proceedings of the 6th ACM conference on Embedded network sensor systems*, SenSys '08, pages 183–196, New York, NY, USA, 2008. ACM.

[10] P.E. Fehlau. Comparing a recursive digital filter with the moving-average and sequential probability-ratio detection methods for snm portal monitors. *Nuclear Science, IEEE Transactions on*, 40(2):143–146, Apr 1993.

[11] B. Deb, J. A F Ross, A Ivan, and M.J. Hartman. Radioactive source estimation using a system of directional and non-directional detectors. *Nuclear Science, IEEE Transactions on*, 58(6):3281–3290, Dec 2011.

[12] R. Mudumbai and U. Madhow. Information theoretic bounds for sensor network localization. In *Information Theory, 2008. ISIT 2008. IEEE International Symposium on*, pages 1602–1606. IEEE, 2008.

[13] P. Kump, E. Bai, K. Chan, B. Eichinger, and K. Li. Variable selection via rival (removing irrelevant variables amidst lasso iterations) and its application to nuclear material detection. *Automatica*, 48(9):2107–2115, 2012.

[14] N. Shrivastava, R. Mudumbai, U. Madhow, and S. Suri. Target tracking with binary proximity sensors. *ACM Transactions on Sensor Networks (TOSN)*, 5(4):30, 2009.

[15] Z. Wang, E. Bulut, and B. K. Szymanski. Distributed energy-efficient target tracking with binary sensor networks. *ACM Transactions on Sensor Networks (TOSN)*, 6(4):32, 2010.

[16] J. Aslam, Z. Butler, F. Constantin, V. Crespi, G. Cybenko, and D. Rus. Tracking a moving object with a binary sensor network. In *Proceedings of the 1st international conference on Embedded networked sensor systems*, pages 150–161. ACM, 2003.

[17] Y. Busnel, L. Querzoni, R. Baldoni, M. Bertier, and A. Kermarrec. On the deterministic tracking of moving objects with a binary sensor network. In *Distributed Computing in Sensor Systems*, pages 46–59. Springer, 2008.

[18] N. Katenka, E. Levina, and G. Michailidis. Robust target localization from binary decisions in wireless sensor networks. *Technometrics*, 50(4):448–461, 2008.

[19] B. F. La Scala, M. R. Morelande, and C. O. Savage. Robust target tracking with unreliable binary proximity sensors. In *Acoustics, Speech and Signal Processing, 2006. ICASSP 2006 Proceedings. 2006 IEEE International Conference on*, volume 4, pages IV–IV. IEEE, 2006.

[20] M. Lázaro, M. Sánchez-Fernández, and A. Artés-Rodríguez. Optimal sensor selection in binary heterogeneous sensor networks. *Signal Processing, IEEE Transactions on*, 57(4):1577–1587, 2009.

[21] Q. Le and L. M. Kaplan. Target localization using proximity binary sensors. In *Aerospace Conference, 2010 IEEE*, pages 1–8. IEEE, 2010.

[22] K. Mechitov, S. Sundresh, Y. Kwon, and G. Agha. Cooperative tracking with binary-detection sensor networks. In *Proceedings of the 1st international conference on Embedded networked sensor systems*, pages 332–333. ACM, 2003.

[23] P. M. Djuric, M. Vemula, and M. F. Bugallo. Target tracking by particle filtering in binary sensor networks. *Signal Processing, IEEE Transactions on*, 56(6):2229–2238, 2008.

[24] T. Nguyen, D. Nguyen, H. Liu, and D. A. Tran. Stochastic binary sensor networks for noisy environments. *International Journal of Sensor Networks*, 2(5):414–427, 2007.

[25] J. Singh, U. Madhow, R. Kumar, S. Suri, and R. Cagley. Tracking multiple targets using binary proximity sensors. In *Proceedings of the 6th international conference on Information processing in sensor networks*, pages 529–538. ACM, 2007.

[26] B. Fidan, S. Dasgupta, and B. D. O. Anderson. Guaranteeing practical convergence in algorithms for sensor and source localization. *Signal Processing, IEEE Transactions on*, 56(9):4458–4469, 2008.

[27] A. H. Sayed, A. Tarighat, and N. Khajehnouri. Network-based wireless location: challenges faced in developing techniques for accurate wireless location information. *Signal Processing Magazine, IEEE*, 22(4):24–40, 2005.

[28] S. Dasgupta and C. R. Johnson. Some comments on the behavior of sign-sign adaptive identifiers. *Systems & control letters*, 7(2):75–82, 1986.

[29] B. D. O. Anderson, R. R. Bitmead, C. R. Johnson, P. V. Kokotovic, R. L. Kosut, I. M. Y. Mareels, L. Praly, and B. D. Riedle. *Stability of adaptive systems: passivity and averaging analysis*. MIT press Cambridge, MA, 1986.

[30] I. F. Akyildiz, W. Su, Y. Sankarasubramaniam, and E.l Cayirci. Wireless sensor networks: a survey. *Computer networks*, 38(4):393–422, 2002.

[31] N. Patwari and A. O. Hero III. Using proximity and quantized rss for sensor localization in wireless networks. In *Proceedings of the 2nd ACM international conference on Wireless sensor networks and applications*, pages 20–29. ACM, 2003.

[32] R. A. Johnson. *Advanced Euclidean geometry: An elementary treatise on the geometry of the triangle and the circle*. Courier Dover Publications, 1960.

[33] B. Fine and G. Rosenberger. *The fundamental theorem of algebra*. Springer, 1997.

[34] R. Kershner. The number of circles covering a set. *American Journal of Mathematics*, 61(3):665–671, 1939.

[35] Glenn F Knoll. *Radiation detection and measurement*. John Wiley & Sons, 2010.

[36] Dimitri Mihalas and Barbara Weibel-Mihalas. *Foundations of radiation hydrodynamics*. Courier Dover Publications, 1999.

[37] C.D. Pahlajani, I Poulakakis, and H.G. Tanner. Decision making in sensor networks observing poisson processes. In *Control Automation (MED), 2013 21st Mediterranean Conference on*, pages 1230–1235, June 2013.

[38] Y Aharonov and D Bohm. Time in the quantum theory and the uncertainty relation for time and energy. *Physical Review*, 122(5):1649, 1961.

[39] Daniel E Archer, Brock R Beauchamp, David A Knapp, G Joseph Mauger, Michael B Mercer, Karl E Nelson, David C Pletcher, Vincent J Riot, and James L Schek. Adaptable radiation monitoring system and method, June 20 2006. US Patent 7,064,336.

[40] FP Doty, HB Barber, FL Augustine, JF Butler, BA Apotovsky, ET Young, and W Hamilton. Pixellated cdznte detector arrays. *Nuclear Instruments and Methods in Physics Research Section A: Accelerators, Spectrometers, Detectors and Associated Equipment*, 353(1):356–360, 1994.

[41] M Barber, RS Bordoli, RD Sedgwick, and AN Tyler. Fast atom bombardment of solids as an ion source in mass spectrometry. *Nature*, 293(5830):270–275, 1981.

[42] Raghu Pasupathy. Generating homogeneous poisson processes. *Wiley Encyclopedia of Operations Research and Management Science*, 2010.

[43] Robert G Gallager. *Stochastic processes: theory for applications*. Cambridge University Press, 2013.